Universität Bremen

Functional Implications of Synaptic Spike Timing Dependent Plasticity and Anti-Hebbian Membrane Potential Dependent Plasticity

Christian Albers

Juni 2015

Functional Implications of Synaptic Spike Timing Dependent Plasticity and Anti-Hebbian Membrane Potential Dependent Plasticity

Vom Fachbereich für Physik und Elektrotechnik

der Universität Bremen

zur Erlangung des akademischen Grades eines

Doktor der Naturwissenschaften (Dr. rer. nat.)

vorgelegte Dissertation

von

Dipl. Phys. Christian Albers

aus Otterstedt

1. Gutachter: Prof. Dr. rer. nat. Klaus Pawelzik

2. Gutachter: Prof. Dr. rer. nat. Stefan Bornholdt

Eingereicht am: 4. Juni 2015

Datum des Kolloquiums: 15. Juni 2015

Contents

Chapter 1

Introduction

In the last 200 years neuroscience made great advances in uncovering the function of the brain. Milestones include the discovery that electric currents applied to nerves can make muscles twitch by Galvani and Volta, the description of the morphology of neurons in the brain by Golgi and Ramon Y Cajal [1], and finding a set of equations that describe the electrical behavior of neurons in great detail by Hodgkin and Huxley [2]. These and other discoveries elucidated the function of neurons, especially their crucial contribution to the computations performed by the brain. Neurons are distinct from other cells in their morphology; they have very long appendages called neurites reaching several millimeters in length that allow neurons to make contact to thousands of other neurons in the brain. In contrast, other cells of the body make only contact to cells directly neighboring them. At the site of contact between neurites of different neurons a physical structure called "synapse" forms. A synapse transmit information from one neuron to the next. The flow of information is unidirectional: The sending neuron is called the "presynaptic neuron", the receiving neuron is called the "postsynaptic neuron".
Apart from the morphology, neurons also differ from other cells in that they are electrically active. A neuron in the brain at rest sustains a gradient of electrical charge across its cellular membrane, which can be measured as a voltage (often called the "membrane potential") between the inside and outside of a neuron. When this equilibrium is tipped sufficiently, instead of relaxing back the perturbation enables a rapid feedback process which leads to a reversement of the voltage. After around one millisecond the neuronal membrane reverses the voltage again back into a state close to the resting state. Because of its short duration and its sharp deviation from the equilibrium state, this event is called a spike. Perturbations of the membrane potential propagate with finite speed. Therefore, a spike is localized within a neuron and from the cell body travels down its neurites, activating synapses to other neurons in the process. An activated synapse perturbs the voltage of the downstream neuron and thereby potentially causes additional spikes there. Because spikes are the basic unit of neuronal activity in the brain, synaptic transmission is equivalent to transmission of information between neurons.
The electrical dynamics of neurons including synaptic transmission and spike timing

can be modelled with high precision by using compact mathematical models with only few parameters. There are competitions held where the goal is to predict the electrical behavior of neuron, and these models reach a very high accuracy in the prediction of neuronal spike times [3]. With modern supercomputer clusters, it is possible to simulate neuronal networks of spiking neurons of enormous size, with the number of neurons in the billions [4]. The human brain is estimated to have between 10 and 100 billion neurons, with each neuron making between 1000 and 10000 connections to other neurons, while a rat brain has around 200 million neurons [5]. Given these numbers, one might wonder why there are no simulations of animal brains yet. To illustrate the problems, let us consider an animal that in principle is perfectly suited for this endeavor: The nematode *C. elegans*. Its anatomy down to the cellular level is almost invariant amongst individuals. Modern techniques allow to slice the nematode in order to digitally reconstruct it [6, 7]. In its far more common hermaphrodite form it is made up of exactly 959 cells, of which 302 are neurons. The 302 neurons make 6393 connections to other neurons via chemical synapses and 890 via gap junctions (electrical synapses). The animal contains an additional 1410 neuromuscular junctions to drive muscle activity. The whole set of connections (the "connectome") is known and in principle it can be simulated in a computer model. There is a project with several dozens participants devoted to construct a simulation of the whole worm with focus on the nervous system[1]. However, until today only strongly simplified models simulating isolated aspects of *C. elegans* exist [8]. What are the reasons for this? The problem is not the computational cost. The full set of 302 neurons and the synapses in principle can easily be simulated with sufficient detail on modern computers. The problem preventing the construction of the nematode model in a computer is the incomplete knowledge about the synaptic connections. Neurons can be seen as the "hardware", while the synapses express the "software" of the brain. They are characterised by their "synaptic weight", which is the degree of influence an active presynaptic neuron exerts on an efferent postsynaptic neuron. Synaptic weights can take on a vast range of values, therefore it is not enough to simply determine the physical locations of synapses. The output of a specific neuron downstream of a neuronal population crucially depends on the joint afferent synaptic weights. In other words, the synapses determine the time of activity and consequentially the computation performed by this neuron. Therefore, although synapses are structures orders of magnitude smaller than neurons, they are in fact extremely important for the function of the brain. To determine the parameters of a single synapse, the neurons it connects need to be manipulated individually, preferrably in the living animal. This is still prohibitively difficult and costly to do for all synapses of any animal. Another problem turns up in the fact that synapses are by no means constant over the animals' life time. The simple fact that most behaving animals can (and will) change their behavior over time shows that. Even an organism as simplistic as *C. elegans* was shown to be capable of learning [9]. Because the synaptic weights can be thought of as the software of the brain, the source of altered behavior likely is the change of synaptic weights,

[1] As of this writing, the project webpage can be found under http://www.openworm.org/

leading to different neuronal output firing patterns and muscle activations when the animal is presented the same stimulus. Thus, even if the synaptic state of a living organism was determined at some point in time, it will be different in the future. All these problems currently prohibit the construction of a model of *C. elegans* and more complex organsisms at the cellular level.
While these crucial details seem to worsen the situation, synaptic plasticity actually opens a window to gain insight into the function of a brain. Synapses do not change their weights randomly. In fact, the picture of synapses as the "software" of the brain is at least incomplete. Experiments performed on pairwise connected neurons showed that there are "synaptic plasticity rules" in effect. They express "meta-software" that sets the rules of computations performed by the brain. The joint activity patterns of a pair of neurons shape the synapse, which in turn will shape activity patterns in the future. Therefore, a neuronal network can be thought of as a self-organizing system that is driven to some working point depending on the external stimuli and synaptic plasticity rules. An astonishing example was provided by Anna Roe and colleagues in the ferret brain [10]: Research has shown that the mammalian brain is divided into areas with distinct tasks. Visual input is preprocessed and then routed to the so-called visual cortex, which consists of several consecutive stages of processing that extract relevant features of the input. Visual cortex areas are functionally distinct from auditory cortical areas that receive inputs from the ears. Neurons of both areas usually also differ in their intrinsic properties. Roe and colleagues rewired ferret brains by routing visual input into the auditory cortex of ferrets before birth. Despite the physiological differences of neurons in both areas, the ferrets were able to see and the response properties of single neurons in the auditory cortex showed that they were sensitive to visual input similar to neurons in the visual cortex of unaltered animals. If we understand how these response properties come about from synaptic plasticity, we will likely have an opportunity to understand the computations performed by the visual area on the cellular level without the need to completely map the synaptic connections and their weights.
Historically, our understanding of synaptic plasticity was driven by the interplay of theoretical considerations and experimental research. One of the most influential hypotheses on brain function was posited by Donald Hebb in his 1949 book "The organization of behavior" [11, 12]:

> When an axon of cell A is near enough to excite a cell B and repeatedly or persistently takes part in firing it, some growth process or metabolic change takes place in one or both cells such that A's efficiency, as one of the cells firing B, is increased.

The key to understand this hypothesis is to know that Donald Hebb assumed that the concerted firing of neurons in "cell assemblies" is the neuronal correlate of a thought or memory item. His "Hebbian plasticity" is the way memories are formed, by linking neurons into assemblies corresponding to a mental item. If due to some stimulus a set of neurons is excited repeatedly at the same time, then the synapses that interconnect these neurons will get stronger (potentiate). This makes it more

likely that they will fire together in the future, even if only a subset of the cell assembly gets excited by an incomplete stimulus. For example, if we observe a bird singing a characteristic song, we will later be able to identify the type of bird if we only hear its song. Around 20 years after Hebbs original proposal, Bliss and Lomo found Hebbian plasticity in the mammalian brain [13]. In their experiment, they identified two neurons connected by a synapse and measured the average response in the postsynaptic neuron to a spike in the presynaptic neuron. Next, they excited the presynaptic neuron to fire at a high rate for an extended time, and afterwards measured the average response of the postsynaptic neuron again. They found that this response was boosted, which is equivalent to an increase (or potentiation) in synaptic weight. This was an excellent validation of Hebbian plasticity. However, from theoretical considerations it is clear that Hebbs hypothesis is incomplete. If synapses can only potentiate and potentiation occurs in response to elevated firing rates this leads to runaway activity. Therefore, it is necessary that synapses undergo weakening (also called depression). A specific proposal for bidirectional plasticity was given by Bienenstock, Cooper and Munro in 1982 with the theoretically motivated BCM rule [14]. In this rule, for a plastic neuron a sliding threshold equivalent to the average postsynaptic firing rate is introduced. If the neuron is active at a rate below the threshold, its synapses will depress, if it is active above, they will potentiate; in each case the weight change is also proportional to the presynaptic firing rate. Similar to Hebbs hypothesis, the BCM hypothesis is dual. It posits a concrete target for synaptic plasticity, namely the formation of selectivity only for specific inputs, and also a plasticity mechanism to achieve this end. Later, bidirectional plasticity in the vein of the BCM rule was found in experiments by Dudek and Bear [15].

In the mid 90's new experimental techniques became available to control the activity of neurons on a millisecond scale. This prompted the discovery of timing-based plasticity rules [12, 16], which have been hypothesized before [17, 18]. Concretely, it was found that firing rates are not the most important determinant for synapses to change, but the precise relative timing of spikes in pre- and postsynaptic neurons. Henry Markram and colleagues induced pairs of spikes in connected excitatory neurons of the mammalian cortex. They found that if a presynaptic spike preceded a postsynaptic spike by a few milliseconds, the synapse potentiates. If the order was reversed, i.e. the presynaptic spike followed the postsynaptic spike by a few milliseconds, the synapse depresses [16]. In contrast to previous experiments, the average firing rate was the same in both cases. This was a spectacular finding at the time and since then has been replicated by many groups in many different neuronal systems on many species, like mammalian hippocampal neurons [19], inhibitory neurons [20], living tadpoles [21], locusts [22], or human cortex [23]. An important side effect of these results was that the notion of temporal coding became more popular. The sensitivity of synaptic plasticity to the precise time of spikes was named "Spike Timing Dependent Plasticity" (STDP) by Song and colleagues [24]. STDP is often subsumed in the so-called "STDP curve"; see figure 2.2 in chapter 2 for two examples. Song and colleagues also provided a simple computational model to

capture the experimental findings up to this point. To differentiate the model from the biological phenomenon, I will call the model "spike pair STDP" or spSTDP in short.
spSTDP was later tested in experiments using complex spike patterns, and it was found that the predictions of this model very often were wrong. Particularily illuminating tests of spSTDP have been conducted by Froemke and Dan [25] and Wang and colleagues [26]. They used spike triplets consisting of either a pre-, then a post-, then again a presynaptic spike with equal time difference, or with reversed location of the spikes. spSTDP predicts the same synaptic change for both different triplets. However, both experiments showed that different triplets led to different weight changes. Despite the fact that it is a poor description of experimental results, spSTDP is used very widely in modelling and network simulations. The reason is its simplicity. Artificial neuronal networks with spSTDP can be analyzed analytically and simulated on computers with low computational cost. The underlying assumption is that the model is a sufficiently good approximation to the behavior to real synapses. However, the known shortcomings of spSTDP have led to the development of many alternative models. Similar to spSTDP, some models are kept as simple as possible while capturing more phenomena. The reason is to retain analytical accessibility and low computational cost in network implementations. In some sense, these models are higher order approximations to biological synaptic plasticity. A prime example for this kind of model is the Triplet model of Pfister and Gerstner [27], which introduces higher-order interactions between spikes by using spike pairs and triplets as the basic motif the synapse is sensitive to. Other models start from biophysical considerations. They include knowledge about physical synapses like the kinetics of receptors and intracellular molecules determining synaptic strength. Examples are the calcium-based models of Shouval and colleagues [28] and Graupner and Brunel [29]. If probed with spike pairs, many of these models reproduce the characteristic STDP curve found in early experiments. The motivation for these models usually is to find out more about the underlying processes governing synaptic plasticity. If a biophysical model describes observations well, the assumptions going into the model are likely correct. The common drawback is that they usually are quite complex, which makes analysis difficult and implementation in network simulations costly.
The connection between synaptic plasticity and learning is at this time still a hypothesis. It has not been shown convincingly yet in living animals that altered synaptic weigths are the cause of altered behavior, due to experimental difficulties to prove this. What was found instead is a link between large-scale brain oscillations and learning performance. It is possible to measure neuronal electrical activity on top of the scull via electroencephalography (EEG, [30]) or intracranially via Local Field Potential measurements (LFP, [31]). Often, the recorded time series of activities reveal oscillatory activity of the neuronal populations. A very curious observation is that the presence of oscillations in the so-called theta range (4 to 10 hertz) is a good predictor of learning success. In conditioning experiments with animals the oscillatory state of the brain can be monitored via EEG or LFP. It was shown that

there is a correlation between the presence of theta oscillations and the speed of learning, i.e. a brain in theta state learns faster [32, 33]. A similar observation was also made in humans, where high theta power during learning of items predicted correct retrieval of items afterwards [34]. These results lead to the question, if there is a general principle at work that connects large-scale oscillations to synaptic plasticity?

Publication I entitled "Theta-specific susceptibility in a model of adaptive synaptic plasticity" (section 2.5) included in this thesis sets out to provide an answer. In this publication, a new phenomenological model for Spike Timing Dependent Plasticity is developed. It is formulated as a set of differential equations describing a dynamical system, hence it is called the Contribution Dynamics model (CD model) of STDP. The model parameters are fit to four different experimental data sets, and the fit error is superior to the one of the Triplet model [27] and a calcium model devised by Uramoto and Torikai [35]. Additionally, an investigation of the response properties of synaptic plasticity rules (spSTDP, the CD model, and others) to periodic neuronal activity is performed. It is shown that spSTDP and the CD model with physiological parameters are inherently sensitive to oscillatory activity in the theta range. This provides an explanation for the improved memory performance in the presence of large scale theta oscillations in mammalian brains.

Despite the best efforts of experimental biology, our knowledge about synaptic plasticity is still quite incomplete. There are processes on a vast range of time scales, including short term synaptic plasticity which changes synaptic transmission within milliseconds seconds and relaxes back in seconds [36], or homeostatic processes like synaptic scaling that keep the neuronal network at a sensible working point [37]. For many of these processes it is hard to gather data suitable for quantitative modelling, which makes it hard to investigate the role and purpose of these plasticity processes, since many details are not known. Therefore, in theoretical studies often an alternative approach is taken. Rather than starting from known plasticity rules, the modeller assumes a desired objective the model system should fulfil. This objective usually is formulated as an input-output relation of a neuronal network. The joint synaptic weights needed for the task are not known *a priori*. Instead, they have to be learned. Appropriate synaptic plasticity rules can be derived from the objective based on the comparison of target and actual network activity. Technically, this comparison involves an instance or entity which has full knowledge of both and which is seperate from the network. This entity is referred to as the *supervisor*, which is why the respective learning rules are called "supervised learning rules". While they are derived from first principles, sometimes it can be shown that they are compatible with experimentally established plasticity rules like STDP (see e.g. [38]). Also, because often supervised learning rules can be shown to be optimal in some sense, like having maximal capacity, they are useful to explore the capabilities of neuronal systems [39]. However, until today there is no hint of supervisory signals similar to those necessary in many of the existing models and supervised learning rules.

In publication II entitled "Perfect Associative Learning with Spike-Timing-Dependent

Plasticity" (chapter 3) and chapter 4 a solution for the biological implementation of supervised learning rules is presented. The main idea is the combination of Anti-Hebbian STDP rules with spike after-hyperpolarization (SAHP). The neuronal membrane potential after a spike typically is slightly below the resting potential, which results in a unresponsive neuronal state for a limited time. In the learning schemes developed, a teacher induces spikes at desired times causing SAHP, which allows the neuron to sum up input without undesired spurious spiking. This allows the comparison of the total input with a target by its synapses through synaptic plasticity rules that are sensitive to subthreshold voltages. In publication II it is shown how perceptrons and tempotrons, basic neuronal models of memory, can be trained using Anti-Hebbian STDP sensitive to subthreshold events. In the case of the perceptron, the plasticity rule with SAHP can be mapped exactly to the Perceptron Learning Rule, which has favorable properties. In chapter 4, a plasticity rule that is only dependent on the membrane potential is developed. It is used to imprint precisely timed spikes into a neuronal network. Also, the plasticity rule is compatible with inhibitory STDP, and it therefore provides a biologically plausible mechanism for this learning task. A quantitative analysis shows that the memory capacity with this rule is roughly half of the attainable maximum, which is a good result given that the maximal capacity is achieved by highly technical and artificial learning rules.

Organization of the thesis

The body of work presented in this thesis consists of two peer-reviewed articles, referred to as publication I and II, and a manuscript. The content of this manuscript represents a major conceptual step forward over the content of publication II[2]. To prepare the reader for publication I, the next chapter (chapter 2) gives an introduction to the basic biology involved. It provides qualitative information on the typical neuron, synapses and synaptic plasticity. Additionally, common quantitative models of neurons are introduced. They are necessary to understand all publications and the manuscript. Publication I performs a broad comparative analysis of models for synaptic plasticity, therefore the models used are presented in chapter 2. The end of chapter 2 is the publication I with the title "Theta-specific susceptibility in a model of adaptive synaptic plasticity". Publication II and the manuscript require an introduction to supervised learning algorithms, which is provided in chapter 3. Since in the manuscript in chapter 4 a quantitative analysis of the properties of a range of different learning rules is performed, they are presented in chapter 3 as well. Publication II with the title "Perfect Associative Learning with Spike Timing Dependent Plasticity" follows at the end of chapter 3. Chapter 4 contains the (yet) unpublished manuscript with the title "Learning of Precise Spike Times with Homeostatic Membrane Potential Dependent Plasticity". The last chapter ummarises the presented results and provides the discussion and outlook on future work.

[2]As of this writing, this manuscript is under review

Chapter 2

Biological background and basic models

In this chapter I give an overview of the biological background necessary to understand the content of publications I and II and chapter 4. Alternating with the biological description I present common basic models for neurons. The description of the biology is purely qualitative, while the models provide a quantitative way of describing the behavior of neurons and synapses. After that, I present a range of contemporary models for synaptic plasticity. They are used for a comparison of fit quality to data and response properties to periodic neuronal activity in publication I. Additionally, the reader gets an overview over the current state of modelling of synaptic plasticity and the problems faced today.

The phenomenology of neurons and synapses is extremely diverse. It is not even known how to categorize the different neuron types in a mammalian brain, but it is likely that there are several hundreds distinct types of neurons, with at least as many different types of synapses. Out of necessity any general description of biological neurons has to restrict itself to a prototypical neuron. In this thesis the prototypical neurons is an excitatory pyramidal neuron, the most common type of neuron in the mammalian cortex.

The biological description of a neuron follows the book from Mark Bear and colleagues [1]. The mathematical modelling of neurons follows the books by Dayan and Abbott [40] and Gerstner and Kistler [41]. The Leaky Integrate-and-Fire neuron model is a standard dynamical model for the behavior of neurons and is widely used. In contrast, models for synaptic plasticity are more diverse, since the details of synaptic plasticity are more disputed than those of neuronal activity. Therefore, except the model for spike pair STDP the models of synaptic plasticity presented can not be considered to be standard models. Additional information on them can be read up in the referenced articles.

2.1 The neuron

2.1.1 Biological description of neurons

Neurons are cells found predominantly in brain tissue of animals. They make up about 10% of the functionally important cells in the brain. The other 90 % are glia cells, which are assumed to be important for maintenance of the brain, but less so for immediate computations. Neurons are set apart from most other cells by their morphology. They feature long appendices that reach lengths up to hundred to thousand times the diameter of the cell body and that grow far into the surrounding tissue. These neuronal appendices (called neurites) are anatomically and functionally divided into two distinct types, the axons and the dendrites. Dendrites have earned their name because of their resemblance to trees; they branch out extensively. Axons are more smooth with few branches. A typical neuron has one axon and several dendrites. Whenever an axon and a dendrite from two different neurons come close, they may form a "synapse", a specialised structure identifiable under the microscope, which is used to transmit information from one neuron to the next[1]. The axon is the sender, and the dendrite the receiver of a neuron; the respective parts of the physically divided synapse are called pre- and postsynapse. Alternatively they are named after their physical appearance as bouton for the presynaptic structure and spine for the postsynaptic one. Each neuron makes up to ten thousand connections to other neurons. This high degree of connectivity enables the brain to perform its computations. Figure 2.1 shows the morphology of typical neurons and synapses of the mammalian cortex.
The basis for the electrical function of a single neuron is its membrane. It separates the intra- and extracellular fluids. The functionally important difference between the two are the concentrations of calcium, potassium and sodium ions inside and outside the cell. Concentrations of calcium and sodium are higher outside, and the potassium concentration is higher inside the cell. These differences of concentrations result from the action of the so-called ion pumps. They are large proteines embedded in the neuronal membrane which use metabolic energy to remove calcium and sodium ions from the intracellular fluid and ingest potassium ions into the neuron. The gradient in ion species concentrations results in a gradient of charge, which is equivalent to a voltage across the membrane. In equilibrium the voltage or membrane potential is typically around -70 mV. The equlibrium state can be perturbed by the action of ion channels, proteines similar to ion pumps. They also reside in the membrane; a functional difference is that ion channels are selective to a specific ion species. Also, they open and close depending on a specific trigger. A subclass of channels opens when particular molecules called neurotransmitters bind to their ligands outside the cell, which is why they are called "receptors". They are mostly located at postsynapses facing the bouton; see section 2.2 for more information on the synapse. Others open and close depending on the current voltage across the membrane. In general, the opening of channels leads to an electric current across

[1] There are also "autapses", synapses of a neuron onto itself.

the membrane due to the flow of ions. In the living brain a neuron constantly receives synaptic input through activated receptors perturbing its membrane potential. From its source in the dendritic tree the charge quickly flows into the rest of the neuron, in particular towards the soma where the incoming charges from the dendrites are summed up. The direction of the perturbance depends on the type of ion channel involved. Because sodium is more concentrated on the outside, the opening of sodium selective channels leads to a flow of positive charges into the neuron. The membrane potential changes towards less negative values, which is called depolarisation. Upon opening, channels selective for potassium have the opposite effect and move the membrane potential towards more negative values (hyperpolarization). The terminology changes if the ion channels in question are receptors. In this case, receptors permeable for sodium are also called excitating, those permeable for potassium are called inhibiting receptors. These terms reflect the effect the receptors have on the activity of the neuron, i.e. they either excite or inhibit the neuron. Calcium channels are also depolarising, but because the concentration of calcium is comparatively low, their effect on the voltage is negligible. Instead, an elevated calcium concentration inside the cell triggers processes which can change neuronal and synaptic properties on a longer time scale.
Voltage dependent ion channels are always closed when the neuron is in or close to equilibrium, and small perturbations do not activate them. Small pertubation of the membrane potential, caused by externally triggered receptors or by manipulation by an experimentator, will relax back to the equlibrium state on the time scale of tens of milliseconds. However, if the neuronal soma is depolarized sufficiently (typically to around -50 mV), a fast feed-back process is initated at the axon hillock, the origin of the axon at the soma. First, voltage dependent sodium channels open and close in quick succession, which leads to a rapid and strong influx of sodium. Within less than a millisecond, the neuron is depolarized close to 0 mV. Slightly lagging behind the sodium channels potassium channels open, which leads to a hyperpolarization of the neuron. After around one millisecond, the channels are closed again and the neuron is at its "reset potential", which is usually below the equilibrium potential. From there it relaxes back to resting state. This process is called action potential (AP) or "spike". Because of their quickness APs are localized, which means that at a given time the region of strong depolarization is restricted to only a part of the neuron. However, APs travel through the neuron from the axon hillock down the axon, and also from the soma down the dendrites. The latter AP has a different function than the one going down the axon; therefore, it is referred to as backpropagating action potential (bAP).
Recording the time course of the voltage during APs reveals that they are very stereotypic with little change over different occurances[2]. Furthermore, when an AP going down an axon reaches a presynapse, the strong depolarization invades the presynaptic bouton. This leads to the release of neurotransmitters into the extracellular space, which then can open postsynaptic receptors leading to a perturbation of the postsynaptic membrane potential. This perturbation is called the "postsy-

[2]This fact is used to identify specific neurons in extracellular recordings.

naptic potential" (PSP), or depending on the type of the synapse "excitatory PSP" (EPSP) or "inhibitory PSP" (IPSP). In the living brain, neurons add up synaptic inputs until the firing threshold is crossed, at which time they generate their own signal (spike) that is transmitted to other neurons.

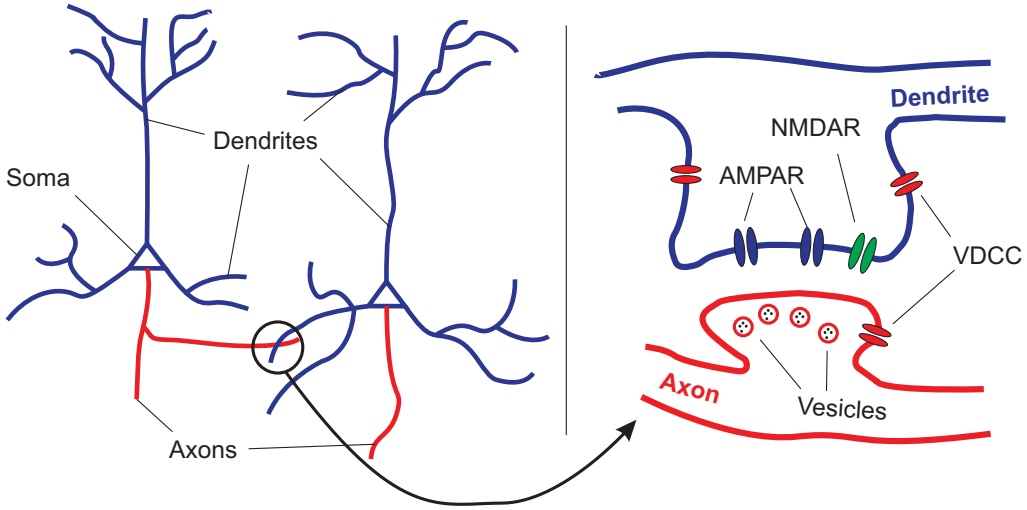

Figure 2.1: Schematic drawing of typical pyramidal neurons and a single synapse of the mammalian cortex. The left picture shows two neighboring neurons. The axon and a dendrite come close enough to form a synapse, shown in detail on the right. The axonal structure is called the bouton, the dendritic structure is called the spine. If a spike arrives in the bouton, the vesicles can fuse with the cell membrane and release the stored neurotransmitters into the synaptic cleft, where they activate AMPA and NMDA receptors. Both structures also contain voltage dependent calcium channels (VDCCs). See sections 2.1.1 and 2.2 for more details.

2.1.2 Point neuron models

Neurons are modelled on a vast range of detail, from the maximally reduced threshold units with only one parameter to point neuron models capturing the essence of membrane potential dynamics to models that recreate neuronal morphology and the function of single ion channels and pumps. Choosing the neuron model always includes a trade-off. Complex models potentially capture the biological neuron better, while simple models have better analytical tractability and allow large-scale simulations at a moderate computational cost. However, all models incorporate the defining dynamical property of a neuron: its ability to spike. Spiking is a strongly nonlinear process. As long as the voltage is below the firing threshold, summation of inputs is mostly linear. Crossing the threshold leads to the action potential which resets the current neuronal state.
Most often the spatial structure of neurons is explicitly omitted from modelling, which allows to describe the state of a neuron using only one variable, namely its

somatic membrane potential or any surrogate value. Therefore, this kind of model is called "point neuron". In the following I will describe the neuron models used in the publications I and II and chapter 4. More in-depth explanations of the models can be found in [40–42].

Rate neurons

The term "rate neuron" encompasses many different models, since there are many ways the implementation can be tweaked. However, the common trait is that a rate neuron receives input from its presynaptic neurons and converts it to an output. Input and output are mathematically described as real numbers. The most general way to write down the activation of a rate neuron is

$$y_i = g(h_i) = g\left(\sum_j w_{ij}x_j + h_i^{ext}\right) \ . \tag{2.1}$$

$w_{ij} \in \mathbb{R}$ is the synaptic weight from presynaptic neuron j to postsynaptic neuron i, x_j is the activity (or output) of presynaptic neuron j, h_i^{ext} is the external (non-synaptic) input to neuron i, and $g(s)$ is the activation function that converts the total input into the neurons' output. Common choices are the logistic function for real-valued bounded output, the rectifying bracket $[s]_+ = s$ if $s > 0$ and 0 otherwise, or the Heaviside function $\Theta(s) = 1$ if $s \geq 0$ and 0 otherwise. A rate neuron with the Heaviside function represents the simplest possible neuron model and the strongest abstraction which still captures the nonlinear nature of neuronal activity.
Explicit dependence on time can be included or excluded in rate neuron models. Biological neurons are time dependent, but sometimes neuronal network states can be considered as constant for some limited duration. Therefore, networks models are often used explicitely without time dependence of the neurons. Instead, the activity propagates through several layers of the network. On the other hand, it is possible to use time dependent rate neurons. In this case, the state of a neuron is a function of time dependent synaptic and external input, and depeding on the network structure its output might be fed back into the network.

The leaky integrate-and-fire neuron

The leaky integrate-and-fire neuron (LIF) is the simplest dynamical model for the neuronal membrane potential. Its origin is the insight that the behavior of a neuron is well approximated by an electrical capacitor in an electric circuit and it therefore can be described by a simple differential equation for the voltage $V(t)$ across the membrane:

$$\tau_m \dot{V} = (V_{eq} - V) + R_m(I_{syn} + I_{ext}) \ . \tag{2.2}$$

R_m is the membrane resistance and τ_m is the so-called membrane time constant, which is the product of the membranes' capacitence and resistance, $\tau_m = C_m \cdot R_m$. For simplicity of notation, in the following I assume $R_m = 1$[3]. The first term on the

[3]The resistance can always be absorbed in the synaptic weights.

right hand side is the leak current across the membrane, coming from the fact that the membrane is not a perfect insulator. In the absence of any other currents the membrane potential will settle into the equilibrium potential V_{eq}. For simplicity, in this thesis I set $V_{eq} = 0$. Setting V_{eq} to realistic values is a simple transformation that does not change the behavior of the neuron, as long as the respective thresholds (see below) are transformed as well. The input currents are separated into synaptic currents I_{syn} and external currents I_{ext}. Synaptic currents are induced by the activity of presynaptic neurons. External currents are the analogue for manipulations performed by an experimentator in a biological experiment and in network simulations allow to induce spikes in the neuron at desired times. For the spiking mechanism a threshold potential V_{thr} is introduced. Whenever the voltage reaches the threshold, a spike is registered and relayed to all postsynaptic neurons. Also, the membrane potential undergoes an instantaneous reset to V_{reset}. Commonly, $V_{reset} < V_{eq}$, i.e. the reset brings the neuron to a hyperpolarized state.
There are several possible choices for the shape of synaptic currents. The opening of receptors is a very fast process, and the closing can be modelled to be equally fast. Therefore the synaptic current is the sum of weighted delta pulses at the times of presynaptic spikes:

$$I_{syn}(t) = \tau_m \sum_i \sum_k w_i \delta(t - t_k^i - \tau_a - \tau_d) \ , \tag{2.3}$$

where w_i is the synaptic strength of presynaptic neuron i, and t_k^i is the time of the kth spike in neuron i. For completeness, I here include the delays of transmission, τ_a for the delay resulting from the transmission of the AP through the axon of the presynaptic neuron until it reaches the bouton and τ_d for the time the charge needs to travel through the dendrite to the soma. For simplicitely they are dropped in the rest of this chapter, but it is important to keep in mind that the signals are not transmitted instantaneously along axons and dendrites, but take a finite amount of time to reach the postsynaptic neuron.
If synaptic currents are modelled as delta pulses, the resulting PSPs in the membrane potential are an instantaneous rise and an exponential decay with time constant τ_m. The time course of the membrane potential in response to a single presynaptic spike at time $t = 0$ with unit synaptic weight ($w = 1$) is given by

$$V_\delta(t) = \Theta(t) \exp\left(-\frac{t}{\tau_m}\right) \ . \tag{2.4}$$

We write V_δ to emphasize that this time course results from delta-shaped synaptic currents. However, it is more realistic to assume that synaptic receptors close in finite time. To model this, another differential equation is introduced for I_{syn}:

$$\tau_s \dot{I}_{syn} = -I_{syn} + \tau_s \sum_i w_i \sum_k \delta(t - t_k^i) \ . \tag{2.5}$$

The resulting isolated PSP is a difference of two exponential functions, as can be shown by computing the solution of equation (2.2) in conjunction with synaptic

currents given by equation (2.5) in response to a single presynaptic spike at time $t = 0$ with unit weight:

$$V_{finite}(t) = \frac{1}{\tau_m - \tau_s}\left(\exp\left(-\frac{t}{\tau_m}\right) - \exp\left(-\frac{t}{\tau_s}\right)\right)\Theta(t) \ . \tag{2.6}$$

We write V_{finite} to distinguish this time course from the one resulting from delta-shaped synaptic currents.
A general consequence of the formulation of the LIF neuron is that because of the linearity of the differential equation the synaptic input can be written as the sum of weighted PSP kernels. The responses of the membrane potential to a single input spike is equal to the respective kernel, which is depending on the shape of the input currents

$$\varepsilon_\delta(s) = \Theta(s)\exp\left(-\frac{s}{\tau_m}\right) \ , \tag{2.7}$$

or

$$\varepsilon_{finite}(s) = \frac{1}{\tau_m - \tau_s}\left(\exp\left(-\frac{s}{\tau_m}\right) - \exp\left(-\frac{s}{\tau_s}\right)\right)\Theta(s) \ . \tag{2.8}$$

Furthermore, the neuronal reset after a spike can also be written as a kernel, which is simply added to $V(t)$ after each spike. Lastly, for external currents the neuron acts as a low-pass filter. This allows us to rewrite the LIF neuron as

$$V(t) = \sum_i w_i \sum_k \varepsilon\left(t - t_k^i\right) + \sum_{t_{post}} R\left(t - t_{post}\right) + \int_{-\infty}^{t} \kappa(t-s) I_{ext}(s) ds \ . \tag{2.9}$$

Here, t_{post} are the times of postsynaptic spikes, $R(s)$ is the reset kernel, and $\varepsilon(s)$ is the PSP kernel, either given by equation (2.7) or (2.8) depending on the shape of synaptic currents. $\kappa(s) = \exp(-s/\tau_m)$ is the passive response kernel for the low-pass filtering of the input currents. For the simple LIF neuron, the reset kernel is defined as

$$R(s) = \Theta(s)\left(V_{reset} - V_{thr}\right)\exp\left(\frac{-s}{\tau_m}\right) \ . \tag{2.10}$$

This formulation ensures that immediately after each spike the voltage is equal to V_{reset}. The formulation of the LIF neuron as equation (2.9) is also known as the zero order Spike Response Model (SRM_0, [41]). This formulation is often used, as it makes the LIF neuron more amenable for analytical calculations.

The conductance based LIF neuron

The LIF neuron is a simple model for the dynamics of the membrane potential, where inputs add up linearly. A better approximation of the actual dynamics can be obtained by taking into account *reversal potentials*. The flow through ion channels strongly depends on concentration of ion species inside and outside, as well as the overall voltage. Every ion species has a distinct voltage where the flow is reduced to

zero even if all channels are open. This distinct voltage is called the reversal potential. For excitatory sodium channels the reversal potential is usually around 0 mV, for inhibitory potassium channels it is around -80 mV. In the conductance based model the current across the membrane depends on the conductivity of the membrane, determined by the number of open ion channels and the current membrane potential. Inhibitory and excitatory channels are modelled seperately. A spike in a presynaptic neuron leads to opening of postsynaptic receptors, which increases the conductance of the membrane for the respective ion species. The temporal evolution of each type of conductance is given by

$$g_x(t) = -\frac{g_x}{\tau_x} + \sum_j \Delta g_x^j \sum_k \delta\left(t - t_k^j\right) \ , \tag{2.11}$$

where $g_x(t)$ with $x \in \{e, i\}$ is the total conductance over the whole membrane for excitatory and inhibitory channels, respectively, τ_x is the decay time constant for unbinding of neurotransmitters from receptors, and Δg_x^j is the increase of conductivity in response to a spike in presynaptic neuron with index j. Δg_x^j is analogous to the synaptic weight in the linear LIF neuron model. t_k^j denotes the time of the k-th spike in presynaptic neuron j. According to this model, with each presynaptic spike the respective conductivity increases and it relaxes back to zero with some time constant. The evolution of the membrane potential is then given by

$$C_m \dot{V}(t) = -g_L(V(t) - V_L) - g_e(t)(V(t) - V_e) - g_i(t)(V(t) - V_i) + I_{ex}(t) \ , \tag{2.12}$$

where $C_m = \tau_{mem}/g_L$ is the membrane capacity, g_L is the constant leak conductance of the neuron with $V_L = V_{eq}$ being the "reversal potential" for leak currents, and $V_{e,i}$ are the reversal potentials for excitatory and inhibitory conductances. As in the basic LIF model, the neuron spikes when the voltage hits a threshold.
The main difference to the LIF model is that the amplitude of a PSP depends on the current membrane potential. An inhibitory input exerts greater effect if the neuron is depolarized. On the other hand, if it is already hyperpolarized close to the reversal potential of potassium (inhibition), increasing the conductivity g_i will have only a minor effect on the voltage.

Stochastic poissonian spiking

Usually, patching neurons and injecting electrical currents leads to highly predictable output spiking [43]. Despite this regularity, neuronal recordings *in vivo* show in general highly irregular spiking [41, 44]. The statistics of spike trains resemble poissonian processes, i.e. the mean of spike count and its variance are equal [40, 45]. The source of this irregularity is not clear. Although complex neuronal networks of deterministic neurons can display irregular spiking behavior [46], it is often simpler to explicitely inject noise into the neuron model by assuming spike generation itself is stochastic. In this case, the membrane potential gets converted into a time dependent firing rate $r(t)$. An example is the SRM_0 model with exponential escape noise [41]. In this model, the membrane potential is computed with equation (2.9),

but spike generation is handled differently. At each point in time the instantaneous firing rate r is given as a function of $V(t)$:

$$r(V(t)) = r_0 \exp\left(\frac{V(t) - V_{thr}}{\Delta V}\right) . \tag{2.13}$$

r_0 is the firing rate in the case that $V(t) = V_{thr}$, and ΔV is the slope parameter. If ΔV is large, the firing rate is insensitive to the voltage and spiking is very stochastic. In the limit of $\Delta V \ll 1$ spiking becomes deterministic as in the normal LIF model. A simpler way to model the underlying dynamics of the neuron is to take rate neurons, equation (2.1), and set $r(t) = g(h(t))$.
Stochastic spike generation transforms the continuous firing rate into a set of discrete events via

$$P(\text{Spike between } t \text{ and } t + \Delta t) = r(t)\Delta t . \tag{2.14}$$

The step size chosen in the simulation should be sufficiently small such that $r(t)\Delta t \ll 1$. This allows to neglect the probability of firing two spikes in one interval.

2.2 The synapse

Synapses may form where axons and dendrites get sufficiently close to each other. Here, a physical structure grows on both neurites adjacent to each other. The general shape is illustrated in figure 2.1. The axonal structure has the shape of a button and is called (presynaptic) bouton or terminal. On the dendrite the outgrowth is elongated, and forms a neck at the connection to the dendrite. Due to its shape, it is called the (postsynaptic) spine. Bouton and spine are physically seperated by the synaptic cleft, which is around 20-50 nm wide. The spinal membrane facing the bouton is called the postsynaptic density (PSD), and the presynaptic bouton membrane facing the PSD is called the active zone. The bouton in the active zone contains vesicles, little bubbles formed by endocytical cell membrane. These vesicles contain molecules called neurotransmitters. When a presynaptic spike arrives in the bouton, the depolarization and inflow of calcium through voltage-dependent calcium channels (VDCCs) causes vesicles to get pulled towards the cell membrane, where they can fuse with it. In case of successful fusion neurotransmitters stored in the vesicles are released into the synaptic cleft and they diffuse very quickly across it. At the PSD they will bind to receptors, which in turn open ion channels. This results in a local perturbation of the membrane potential, which then travels from the synapse to the soma where all synaptic inputs are summed up. Neurotransmitters unbind stochastically from receptors, get removed from the cleft and subsequently reuptaken into the presynapse.
This is the basic course of action for all chemical synapses[4]. Important to note is

[4]There are also electrical synapses which form a more direct and bidirectional connection between the membrane potentials of the connected neurons.

that these synapses are uni-directional, as no signal can travel from the postsynaptic to the presynaptic neuron[5]. Also, synapses are not all alike. The most obvious difference between synapses is the type of ion channels. Sodium channels depolarize the postsynaptic neuron, while potassium channels hyperpolarize it. The receptors for both channels react to different neurotransmitters. Also, the pre- and the postsynaptic part of the synapse fit each other. The PSD contains only receptors that are sensitive to a certain type of neurotransmitter, which is the only one stored presynaptically. The majority of depolarizing (or excitatory) synapses in the brain are glutamatergic synapses, i.e. synapses that use glutamate as the neurotransmitter. The respective receptors are AMPA receptors which open sodium channels. Also, glutamatergic synapses usually contain NMDA receptors, which are permeable for calcium. They play a major role in synaptic plasticity (see next section). The main type of hyperpolarizing (or inhibitory) synapses are GABAergic synapses. The receptors are sensitive to γ-aminobutyric acid (GABA) and are permeable for potassium. The type of synapse solely depends on the presynaptic neuron. Inhibitory neurons only form inhibitory synapses onto their postsynaptic neurons, excitatory neurons only form excitatory synapses. An important consequence is that because of this restriction synapses keep their type. An excitatory synapse can not change into an inhibitory one, and vice versa. This is also called "Dale's law"[6]. However, a neuron in the brain always receives excitatory and inhibitory input from (many) different neurons.
In addition, even synapses of the same type are not alike, since they generally differ in strength. To measure the strength of a synapse, an experimentator searches for a pair of connected neurons. Exciting the presynaptic neuron to fire a spike causes the activation of its synapses. The deflection of the membrane potential of the postsynaptic neuron can be measured as the PSP. Its average amplitude is different for different synapses. Because the amplitude determines the influence of the afferent presynaptic neurons, it is also called the synaptic strength or weight. The rise time of the PSP reflects the quick binding and unbinding of neurotransmitters to receptors, while the decay depends on the postsynaptic membrane time constant. The strength of a synapse, expressed as the amplitude of the PSP, depends on the combined activity history of pre- and postsynaptic neuron, and can change over different time scales. This process is called synaptic plasticity and is described in more detail in the next section.

[5]This is not completely true. There are processes in synaptic plasticity which involve retrograde messengers from the PSD to the active zone which depend on postsynaptic spiking activity. However, these messengers are only important for local synaptic plasticity processes.

[6]There are exceptions. During development of newborn rats, GABAergic synapses switch from excitatory to inhibitory.

2.3 Synaptic plasticity

2.3.1 Biological description of synaptic plasticity

The transmission properties of synapses are not only different between synapses of the same type (even from the same presynaptic neuron), they also vary over time for a single synapse. The change of transmission properties is referred to as "synaptic plasticity", although there are many different processes on many time scales subsumed under this term. The fastest plasticity processes are called "short-term plasticity". This type of plasticity changes the synaptic strength immediately after each presynaptic spike, but the synapse relaxes back to baseline strength after several seconds of inactivity. Synaptic transmission changes fast because the amount of stored neurotransmitters is limited and the probabibility of vesicle fusion is altered by spiking. Each spike leads to the fusion of some vesicles with the cellular membrane, which reduces the number of available vesicles for subsequent spikes. Typically, in a high-frequency burst the amplitude of PSPs decreases for later spikes, since they can activate less vesicles than the earlier ones. It takes a few seconds to refill the vesicles and bring back the synapse to inital strength. However, in some synapses resource depletion is to some extent offset by the increase of the probability of vesicle fusion. Vesicles do not release neurotransmitters deterministically. Each spike that invades the bouton has a certain probability to cause vesicle fusion for each vesicle. This probability depends on the concentration of calcium in the bouton. Calcium flows in through voltage dependent calcium channels that open up during the depolarization caused by the action potential. Residual calcium will usually be removed after around 100ms to a few seconds. But as long as the concentration is increased, so is the probability of release. The exact behavior of the synapse, i.e. whether it gets weaker (depresses) or stronger (potentiates) depends on the exact specifics of both processes. A good review of short-term plasticity is given in [36].

Another type of synaptic change is long-term plasticity, which depending on the direction of synaptic change is called long-term depression (LTD) or long-term potentiation (LTP) (weakening and strengthening, respectively). LTD and LTP can be induced within a few seconds of activity, and stay long after. However, the phenomenology of long-term plasticity is much more rich and diverse than for short-term plasticity. As a consequence, the mechansims involved are less clear. Early experiments found that presynaptic bursting can induce LTP [13] or LTD [15] depending on the presynaptic firing rate. Low rates tend to depress the synapse, high rates tend to potentiate it. With the availability of new experimental techniques, it became clear that the postsynaptic activity is equally important in synaptic change. Synapses can express strong changes in response to pairs of pre- and postsynaptic spikes even if the average firing frequency is as low as 0.1 Hz, much lower than in previous experiments [16, 19, 21]. This new line of experiments also revealed an astonishing effect. Synaptic plasticity in response to spike pairs is very sensitive to the order of spikes. In excitatory neurons it is generally found that if a postsynaptic spike follows a presynaptic spike with a timing difference of a few milliseconds, the

synapse will potentiate. If the order is reversed, i.e. the presynaptic spike is lagging by a few milliseconds, the synapse will depress. These results were remarkable at the time, first because very low-frequency activity unexpectedly can induce synaptic changes, and second because shifting one spike by just a few milliseconds changes the outcome drastically. Later, this phenomenon was dubbed "Spike-Timing-Dependent Plasticity" (STDP, [24], and see figure 2.2), and subsumed in a simple computational model with 4 parameters (see next section). However, subsequent research showed that the phenomenology is much more diverse. There are burst frequency effects [16, 47], nonlinear interactions between spikes [25, 26, 48] (see publication I for more details), and strong dependence on synapse type [20, 49]. All these observations make it hard to provide a description of "typical synaptic plasticity", since often the mechanisms and phenomenology are not completely clear. However, there are some commonalities. Synaptic depression as well as potentiation require an elevation of postsynaptic calcium concentration, an observation which has given rise to the "calcium control hypothesis" [50]. Often, moderate elevation leads to LTD, and high elevation leads to LTP. Injecting calcium buffers into the spine which bind calcium during acitivity protocols frequently abolishes synaptic plasticity [48].

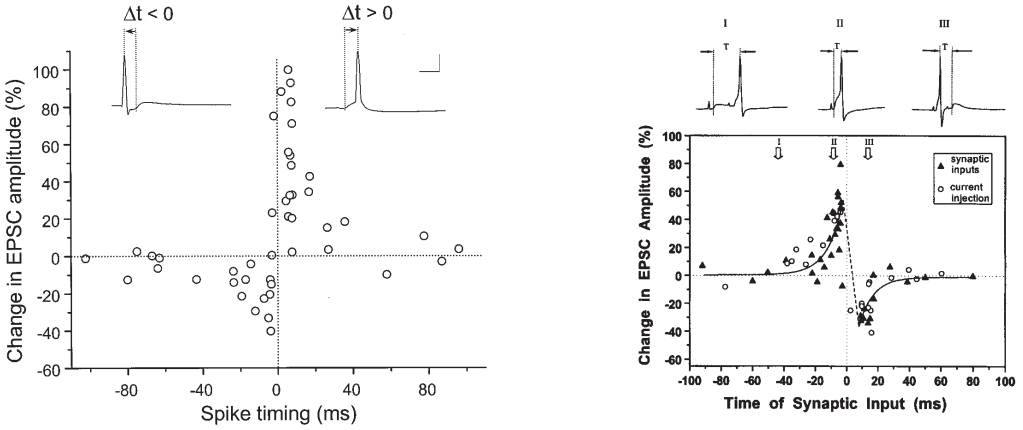

Figure 2.2: Typical STDP curves as measured in experiments. The abscissa shows the timing difference between the pre- and the postsynaptic spike. The ordinate shows the change in amplitude of the EPSP. Both figures show the sudden shift from potentiation to depression resulting from just a miniscule shift in relative timing of both spikes, as well as the exponential drop of magnitude of synaptic change with increasing timing difference. Left figure reprinted by permission from Macmillan Publishers Ltd: Nature [21], copyright 1998. Right figure reprinted by permission from the Society for Neuroscience: The Journal of Neuroscience [19], copyright 1998.

Since calcium is the most important messenger ion, the sources of calcium in the postsynaptic spine are of importance for synaptic long-term plasticity. The neuronal membrane at the postsynaptic spine usually contains voltage dependent calcium channels (VDCCs), which are opened by depolarization. However, a more important source is calcium inflow from NMDA receptors. They are quite unusual

since they do not open unconditionally if glutamate binds. At resting potential the ion channel is clogged by a magnesium ion. Depolarization of the membrane will reversibly remove the ion from the channel. But only if glutamate binds at the same time, the ion channel completely opens, allowing calcium to flow inside the cell. This positions NMDA receptors as coincidence detectors in the PSD. Only if presynaptic and postsynaptic activity coincide, the calcium level will be elevated enough that the synapse potentiates. Otherwise, it will do remain unchanged or depress; usually the calcium inflow resulting from active NMDA receptors is higher than from open VDCCs. A successful model for STDP was constructed around the peculiar dynamics of NMDA receptors [28]. However, the action of NMDARs is not the only determinant for synaptic plasticity. Nevian and Sakman [48] found that the magnitude of synaptic change correlates with peak calcium concentration, but the sign was determined by the activation of metabotropic glutamate receptors (mGluRs).
There are several candidate mechanisms for synaptic plasticity. Commonly, it is believed that calcium adjusts the activity level of a protein called CaMKII, which in turn regulates the responsiveness and amount of AMPA receptors in the membrane of the PSD [51]. More AMPA receptors lead to higher inflow of sodium during presynaptic neurotransmitter release and consequently to stronger depolarization in response to a presynaptic spike. Another way to change synaptic properties is to adjust the release probabilities of presynaptic vesicles. This usually involves nitric oxide (NO) molecules or endocannabinoids as retrograde messengers, because coincidence detection is still performed in the postsynapse [52, 53].
Lastly, there are processes less well understood which regulate synaptic weights on longer time scales. It is known that synapses regulate themselves over time scales of hours and days. If a neuron embedded in a fully formed neuronal network is artificially suppressed by constant hyperpolarization, its firing rate will be significantly reduced compared to the network average. But after a few days, it will fire on average just like before. The reason for this is that its afferent synapses will increase their strength, so that the neuron will get stronger inputs to compensate the reduced inherent excitability [54]. This phenomenon is called “synaptic scaling” and it is assumed that neurons have a target firing rate, which is compared to their current firing rate over a long time scales of hours and days. In case of mismatch processes will be initiated to remedy the situation [37].
Although this thesis is concerned mainly with “classical” LTD and LTP as induced by STDP, it is important to keep in mind the other plasticity processes.

2.3.2 Quantitative modelling of short-term synaptic plasticity

Short-term synaptic plasticity can be modelled with high precision in a very simple model. This model was originally conceived by Tsodyks and Markram, and extended in later work by Tsodyks and colleagues [55, 56]. In this section I follow the description by Morrison and colleagues [57].

In this model, a synapse has a constant amount of resources that gets redistributed between different states determined by the presynaptic activity. A "quantum of resource" can be either in a recovered, active or inactive state. The amount of resources in each state are given by x, y and z, respectively. Although resources (vesicles) are discrete, in this model they are treated as continuous, since they describe the average of an statistical ensemble. The transfer of resources between states is described by a set of differential equations:

$$\begin{aligned} \dot{x} &= \frac{z}{\tau_{rec}} - u_+ x(t-\varepsilon) \sum_{t_{pre}} \delta(t - t_{pre}) \\ \dot{y} &= -\frac{y}{\tau_I} + u_+ x(t-\varepsilon) \sum_{t_{pre}} \delta(t - t_{pre}) \\ \dot{z} &= \frac{y}{\tau_I} - \frac{z}{\tau_{rec}} \ . \end{aligned} \tag{2.15}$$

u_+ is the fraction of recovered resources used by each presynaptic spike, τ_{rec} is the time constant with which resources replenish from the inactive to the recovered state (re-uptake of neurotransmitters), and τ_I is the decay time constant of synaptic currents. This time constant is analogous to τ_{syn} in the LIF model, equation (2.5). We write $x(t-\varepsilon)$ to emphasize that in order to compute the update of x and y by a presynaptic spike, one has to use the value of x shortly *before* that spike. With this type of dynamical synapses, the synaptic current at synapse i is given by

$$I^i_{syn} = w_i \cdot y_i \ , \tag{2.16}$$

i.e. the fraction of resources in the active state scaled by the synaptic weight.
This model so far describes only depressing synapses, where the efficacy of the synapse decreases with each presynaptic spike. Synaptic short-term facilitation is caused by the increase of probability of release by residual calcium. In the model, the probability of release is given by the fraction of resource usage u_+. Therefore, to account for facilitating synapses the fraction of usage is converted to a time-dependent function. Its dynamics is given by

$$\dot{u} = \frac{u}{\tau_{fac}} + U(1 - u(t-\varepsilon)) \sum_{t_{pre}} \delta(t - t_{pre}) \ . \tag{2.17}$$

U determines the increase of u with each spike, and τ_{fac} is the time constant with which the probability of release relaxes back to baseline. To fully incooperate facilitation, in equations (2.15) u_+ needs to be set equal to $u(t+\varepsilon)$, reflecting that first the change of fraction of usage has to be computed before it can be applied correctly.
It is possible to simplify the full model for depressing synapses, equations (2.15), by separation of time scales. Usually, it is found that the time constant for recovery is much longer than the one for inactivation, $\tau_{rec} \gg \tau_I$. In this case, y decays much quicker than z, which allows to approximate the conservation of resources

$x + y + z = 1$ to $x + z = 1$. Using this, the equation for recovered resources can be written as

$$\dot{x} = \frac{1 - x}{\tau_{rec}} - u_+ x(t - \varepsilon) \sum_{t_{pre}} \delta(t - t_{pre}) \ . \tag{2.18}$$

This latter formulation is important to keep in mind, as it is used in publication I in a model of long-term synaptic plasticity.

2.3.3 Quantitative models of activity dependent long-term synaptic plasticity

The Hebbian hypothesis puts forward long-term synaptic plasticity as the neuronal correlate for the formation of memories and learning. The properties of long-term plasticity, namely that changes are induced by activity and their longevity, make this hypothesis very appealing. Because its flexibility and adaptability is one component of the power of the brain, long-term synaptic plasticity has been the focus of overwhelming attention from experimental and theoretic neuroscientists, as well from machine learners, who use biologically inspired plasticity mechanisms in neural networks to analyse data.
In experiments, synaptic strength is measured via the amplitudes of PSPs. Current experimental technology allows to monitor only a few neurons at the same time with sufficient detail to measure synaptic plasticity. Typically, experiments are performed in brain slices or cultured neurons, although there have been a few experiments performed in living animals (e.g. [58,59]). Therefore, experimental data on synaptic plasticity is usually restricted to changes in response to pairwise activity, i.e. changes of synaptic strength induced by the activity of the pre- and the postsynaptic neuron connected by the synapse of interest. This shapes the current state of modelling. Common models for plasticity take as input the activity of both neurons and compute the new synaptic state from it.
Activity dependent plasticity rules have been formulated for many purposes. Some rules were devised to explain functional properties of the brain as found in experiments. Examples are the Hebbian learning rule to train the Hopfield model which seeks to explain memory formation and recall [60, 61], and the BCM rule (Bienenstock, Cooper and Munro) [14, 62], that explains the formation of input selective neurons. Usually these rules are not well constrained by experimental data on synaptic plasticity. This is why researchers construct biophysical models, often with the goal to reproduce the STDP window from biophysical principles [28, 29]. The purpose of these models is to gain insight into the mechanisms responsible for synaptic change. Lastly, phenomenological models are constructed to give a close fit on quantitative data. The problem faced by these models is that there are only a few data sets which provide enough seperate data points to constrain quantitative models. Common models have 8 to 12 parameters, and to prevent overfitting, it is necessary to fit the model to much more data points than the number of parameters. Otherwise, they generalize badly. However, the biggest data sets available have around 10 to 18 unique data points, since recording the data is time consum-

ing and costly. Additionally, it is in general not possible to lump different data sets together, since virtually all experiments are performed under different conditions. Sometimes even the same experiment performed twice by the same group, in the same system with the same protocol can lead to different results, as exemplified by the discrepancies of the STDP window found by Bi and Poo in 1998 and Wang and colleagues in 2005 [19, 26, 27]. As a consequence, there are only a few quantitative models with the same scope as the CD model presented in publication I.
In this section, I present an overview over activity dependent plasticity rules. All of them are inspired by various experimental results and are used to explain certain aspects of data or to investigate the properties of neuronal networks which implement these rules. I picked a representative range of simple phenomenological and more sophisticated biophysical models. For brevity, I will refer to the models as spSTDP, Triplet model, Shouval model, Cai model, Graupner model and Uramoto model (in order of appearance). The parameters used for each model can be found either in publication I or in the referenced articles.

Spike pair STDP

The early experiments on STDP suggested that the basis for synaptic change is the spike pair consisting of one presynaptic and one postsynaptic spike in close proximity. In 2000, Song and colleagues proposed a simple model to account for the observations. To distinguish the model from the experimental results, here it is called spike pair STDP (spSTDP). For any given pair of one pre- and one postsynaptic spike we have to first compute the timing difference $\Delta t = t_{post} - t_{pre}$, where t_{post} is the time of the postsynaptic and t_{pre} the time of the presynaptic spike. The weight change is a function of Δt:

$$\Delta w = \begin{cases} A_+ \exp\left(-\Delta t/\tau_+\right) & \text{if } \Delta t > 0 \\ A_- \exp\left(\Delta t/\tau_-\right) & \text{else ,} \end{cases} \tag{2.19}$$

where A_+, A_-, τ_+ and τ_- are the parameters of the model. This simple model recreates the famous STDP window (Figure 2.2), which is a good description of early findings. In additive spSTDP, all weight changes computed with equation (2.19) are added up for the resulting total weight change:

$$w_{after} = w_{before} + \sum_{\Delta t} \Delta w \ .$$

Multiplicative spSTDP has also been investigated, but for the sake of simplicity here I consider only additive spSTDP. Figure 2.3 shows the weight change as a function of timing difference for a single spike pair as computed using the spSTDP model.

The Triplet model

Although spSTDP captures spike pair experiments, it fails to account for experimental results on spike triplets or more complex spike patterns (e.g. [25, 26]). A big

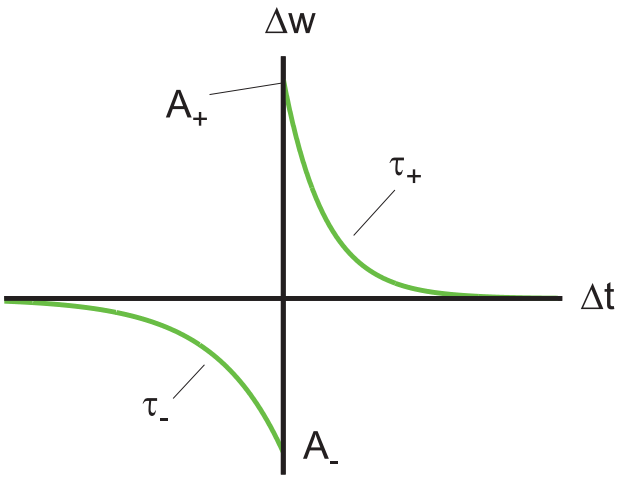

Figure 2.3: The STDP window resulting from the spike pair STDP model. The weight change as a function of the timing difference shows the exponential decay of weight change magnitude as the experimental data, figure 2.2. Additionally, it is shown how the parameters of the model shape the STDP window.

problem for spSTDP are experiments which find no synaptic change for pre-post pairs induced at low repetition frequency, but if the repetition frequency is high enough, the synapse potentiates [47, 48]; see publication I for a more detailed description of the experimental results. The only way to model no synaptic change for pre-post pairs in spSTDP is if $A_+ = 0$. But in this case, the model synapse never potentiates for any spike pattern, which clearly contradicts the observations.
Pfister and Gerstner devised their Triplet model to remedy the problems of spSTDP [27]. The Triplet model is an extension of spSTDP which involves higher-order interactions between spikes. First, they reformulate spSTDP with traces of spiking activity in both neurons:

$$\begin{aligned} \dot{r}_1(t) &= -\frac{r_1(t)}{\tau_+} \\ \dot{o}_1(t) &= -\frac{o_1(t)}{\tau_-} \ , \end{aligned} \tag{2.20}$$

and

$$\begin{aligned} &\text{if } t = t_{pre}, \text{ then } r_1(t) \to r_1(t) + 1 \\ &\text{if } t = t_{post}, \text{ then } o_1(t) \to o_1(t) + 1 \ . \end{aligned} \tag{2.21}$$

It is not specified which physiological quantities could be the neural correlate for the traces r_1 and o_1. Spikes of either side read out the trace of the opposite side:

$$w(t) \to w(t) + \begin{cases} -A_2^- \cdot o_1(t) & \text{if } t = t_{pre} \\ -A_2^+ \cdot r_1(t) & \text{if } t = t_{post} \ . \end{cases} \tag{2.22}$$

Up to this point the formulation is completely equal to spSTDP. To adjust the model to experimental data not explicable with spSTDP, another set of traces is added to the model:

$$\begin{aligned} \dot{r}_2(t) &= -\frac{r_2(t)}{\tau_x} \ , \text{ if } t = t_{pre}, \text{ then } r_2(t) \to r_2(t) + 1 \\ \dot{o}_2(t) &= -\frac{o_2(t)}{\tau_y} \ , \text{ if } t = t_{post}, \text{ then } o_2(t) \to o_2(t) + 1 \ . \end{aligned} \tag{2.23}$$

The weight change is set to

$$w(t) \to w(t) + \begin{cases} -o_1(t)\left[A_2^- + A_3^- r_2(t-\varepsilon)\right] & \text{if } t = t_{pre} \\ -r_1(t)\left[A_2^- + A_3^- o_2(t-\varepsilon)\right] & \text{if } t = t_{post}\ . \end{cases} \tag{2.24}$$

This latter equation is the full Triplet model with all-to-all interactions (A2A). It got its name from the fact that whenever a trace is updated by a spike, the existing state is not forgotten. Therefore all spikes of one synaptic side interact with all spikes of the other side. However, for some experimental data sets it turns out that limited interactions provide a better fit. A spike interacts only with the spike of the opposite directly preceding it. This is called nearest neighbor interactions (NN). The update rules for the traces get changed to

$$\begin{aligned} &\text{if } t = t_{pre}, \text{ then } r_i(t) \to 1 \\ &\text{if } t = t_{post}, \text{ then } o_i(t) \to 1\ . \end{aligned} \tag{2.25}$$

This means that each spike sets the respective traces to a constant value, and the pre-existing state of the trace is forgotten accordingly.
In their study, Pfister and Gerstner showed that the Triplet rule can be fitted well to two data sets otherwise unexplicable with spSTDP. They also showed that their model could be mapped to the BCM rule. In this case, the parameters $A_2^{+,-}$ need to be functions of time proportional to the expectation of a power of the postsynaptic firing rate.

The calcium model of Shouval and colleagues

Although spSTDP accurately captures the experimentally established STDP window, it is a purely phenomenolgical model which does not reveal insight about the mechanisms of synaptic plasticity. Shouval and colleagues [28] conceived a mechanistic model using well known characteristics of neuronal dynamics and synaptic receptors, especially of the NMDA receptor involved in regulating synaptic strength. The main idea of this model is that the change of the synapse at each point in time is mainly a function of the calcium concentration in the postsynaptic spine. This concentration in turn is governed by postsynaptic depolarisation and presynaptic release of neurotransmitters which both trigger NMDA receptors. The model assumes that the membrane potential in the spine is a linear sum of presynaptically induced EPSPs and backpropagating action potentials (bAP) that signal postsynaptic spiking:

$$\begin{aligned} V(t) &= \sum_{t_{pre}} \mathrm{EPSP}\left(t - t_{pre}\right) + \sum_{t_{post}} \mathrm{bAP}\left(t - t_{post}\right)\ \text{, with} \\ \mathrm{EPSP}(s) &= \Theta(s) A_{EPSP}\left(\exp\left(-\frac{s}{\tau_s^{EPSP}}\right) - \exp\left(-\frac{s}{\tau_f^{EPSP}}\right)\right) \\ \mathrm{bAP}(s) &= \Theta(s) A_{bAP}\left(I_s^{bAP}\exp\left(-\frac{s}{\tau_s^{bAP}}\right) + I_f^{bAP}\exp\left(-\frac{s}{\tau_f^{bAP}}\right)\right)\ . \end{aligned} \tag{2.26}$$

$t_{pre,post}$ are the times of presynaptic and postsynaptic spikes, respectively. A_{EPSP} is the amplitude of the EPSP chosen such that the maximal depolarisation by one isolated presynaptic spike is exactly 1 mV. Its actual value depends on the time constants $\tau_{s,f}^{EPSP} = 5, 50ms$ of the EPSP kernel. $A_{bAP} = 100mV$ is the amplitude of the bAP, which has time constants $\tau_{s,f}^{bAP} = 3, 25ms$. The relative amplitudes $I_{s,f}^{bAP} = 3/4, 1/4$ scale the slow and the fast component of the bAP relative to each other.
The EPSP kernel is the same as in the LIF model, i.e. it is a difference of a slow and a fast exponential decay, compare equation (2.8). The bAP is a sum of two exponentials, one fast and one slow component. This is necessary to recreate the STDP window in this model. Also, the model assumes that the rise time of a bAP is much faster than all other processes.
The Shouval model assumes that there are two different types of NMDA receptors with different decay time constants of glutamate unbinding. The fraction of open receptors of the slow and fast type is given by

$$\begin{aligned} \dot{N}_f &= -\frac{N_f}{\tau_f} + P_0 I_f \sum_{t_{pre}} (1 - \mathrm{NMDA}(t-\varepsilon))\, \delta(t - t_{pre}) \\ \dot{N}_s &= -\frac{N_s}{\tau_s} + P_0 I_s \sum_{t_{pre}} (1 - \mathrm{NMDA}(t-\varepsilon))\, \delta(t - t_{pre}) \\ \mathrm{NMDA}(t) &= N_f(t) + N_s(t) \end{aligned} \tag{2.27}$$

$I_{f,s} = 1/2, 1/2$ are the relative amplitudes of the fast and the slow component which decay back with time constants $\tau_{f,s} = 50, 200ms$. Due to the voltage-dependent magnesium block of NMDA receptors, the resulting calcium current is a function of the fraction of open receptors as well as the membrane potential:

$$\begin{aligned} I_{NMDA}(t) &= G_{NMDA}\mathrm{NMDA}(t)\,(V(t) - V_r)\,B(V(t)) \text{ , with} \\ B(V) &= (1 + 0.28\exp(-0.062V))^{-1} \text{ ,} \end{aligned} \tag{2.28}$$

with the membrane potential V given in mV, $V_r = 130mV$ and $G_{NMDA} = -0.02\mu M/(ms \cdot mV)$. The calcium concentration is a low-pass filtered version of the current with decay time constant τ_{Ca}:

$$\frac{d[Ca](t)}{dt} = I_{NMDA}(t) - \frac{[Ca](t)}{\tau_{Ca}} \text{ .} \tag{2.29}$$

The central assumption of this model is that synaptic plasticity is completely determined by the concentration of calcium in the postsynaptic spine. This is the calcium control hypothesis[7]. Low concentrations lead to LTD, high concentrations lead to LTP. Also, the learning rate η is a monotonic function of the calcium concentration:

$$\begin{aligned} \eta([\mathrm{Ca}]) &= \left(\frac{0.1sec}{[\mathrm{Ca}]^3 + 10^{-5}} + 1sec\right)^{-1} \\ \Omega([\mathrm{Ca}]) &= 0.25 + \mathrm{sig}\,([\mathrm{Ca}] - \alpha_2, \beta_2) - 0.25\,\mathrm{sig}\,([\mathrm{Ca}] - \alpha_1, \beta_1) \text{ ,} \end{aligned} \tag{2.30}$$

[7] One of the authors of this model is Leon Neil Cooper of the BCM rule.

with $\mathrm{sig}(x, \beta) = \exp(\beta x)/(1+\exp(\beta x))$. It should be noted that the calcium concentration $[Ca]$ here is measured in μM instead of mM as in equation (2.29). Finally, the weight W as a function of time is computed via

$$\dot{W}(t) = \eta([\mathrm{Ca}])\,(\Omega([\mathrm{Ca}]) - W(t)) \ . \tag{2.31}$$

Unlike spSTDP and the Triplet model, this model has bounded weights, because the driving function $\Omega([\mathrm{Ca}])$ is a bounded sigmoidal function.

The extension by Cai and colleagues

The original model by Shouval and colleagues was later modified by Cai and colleagues to include presynaptic short term plasticity and postsynaptic attenuation of bAPs [63]. The model dynamics are for most parts similar to the Shouval model described above, with some tweaks. The most important difference concerns the impact of spikes on bAPs and EPSPs, as it is modulated by the recent history of spiking of the respective synaptic side. Instead of having an EPSP be caused deterministically by any presynaptic spike, a spike invading the bouton here stochastically leads to the discharge of any of the stored vesicles. The number of vesicles is limited. Only an actual discharge leads to an EPSP. The EPSP is independent of the number of vesicles which discharge upon a spike, as the model assumes that any discharge saturates the postsynaptic receptors. Also, the synapse undergoes short-term facilitation, therefore the probability of discharge p_r develops according to

$$\dot{p}_r = -\frac{p_{dr0} - p_r}{\tau_F} + \gamma p_r \sum_{t_{pre}} \delta(t - t_{pre}) \ . \tag{2.32}$$

p_{dr0} is the baseline probability of discharge, $\tau_F = 100ms$ is the time constant with which p_r relaxes back to baseline, and γp_r is the fraction by which p_r increases after each presynaptic spike. Because this equation allows p_r to exceed unity, it is capped at $p_r \leq 1$. When a presynaptic spike arrives at time t_{pre}, each of the N vesicles in the bouton discharges with probability $p_r(t_{pre} - \varepsilon)$. Formally, we introduce a variable $x_{rel}(t_{pre})$ which is 1 if there was a neurotransmitter release (discharge) of at least one vesicle at time t_{pre}, and 0 otherwise. The resulting voltage deflections by presynaptic spiking are given by

$$\begin{aligned} V_{EPSP}(t) &= \sum_{t_{pre}} \mathrm{EPSP}(t - t_{pre}) x_{rel}(t - t_{pre}) \ , \text{with} \\ \mathrm{EPSP}(s) &= \Theta(s) A_{EPSP} \left(\exp\left(-\frac{s}{\tau_s^{EPSP}} \right) - \exp\left(-\frac{s}{\tau_f^{EPSP}} \right) \right) \ . \end{aligned} \tag{2.33}$$

In this model, backpropagating action potentials do not always yield the same efficacy, but are attenuated if there have been spikes previously. This is modelled by a resource $u_{bAP}(t)$:

$$\dot{u}_{bAP} = -\frac{1 - u_{bAP}}{\tau_{bAP}^{rec}} - c_{bAP} u_{bAP}(t - \varepsilon) \sum_{t_{post}} \delta(t - t_{post}) \ . \tag{2.34}$$

c_{bAP} is the use of resources with each postsynaptic spike, and the time constant τ_{bAP}^{rec} governs the relaxation of the resource. The available resources modulate the membrane potential deflections of a bAP:

$$\begin{aligned} V_{bAP}(t) &= \sum_{t_{post}}^{t} u_{bAP}\left((t-\varepsilon)-t_{post}\right)\mathrm{bAP}\left(t-t_{post}\right)\delta(t-t_{post}) \text{ , with} \\ \mathrm{bAP} &= \Theta(s)A_{bAP}\left(I_s^{bAP}\exp\left(-\frac{s}{\tau_s^{bAP}}\right)+I_f^{bAP}\exp\left(-\frac{s}{\tau_f^{bAP}}\right)\right) \text{ .} \end{aligned} \tag{2.35}$$

The resulting membrane potential in the postsynaptic spine is the sum of both contributions:

$$V(t) = V_{bAP}(t) + V_{EPSP}(t) \text{ .} \tag{2.36}$$

Similarly to the AMPA receptors, the NMDA receptors saturate after each presynaptic discharge. Also, the total pool of NMDA receptors is split into one subset of slow and one subset of fast receptors with different time constants for neurotransmitter unbinding. The relative sizes are given by I_f and $I_s = 1 - I_f$ for the pool of fast and slow receptors, respectively. Each discharge opens up all receptors, which leads to the following dynamical equations for the fraction of open receptors:

$$\dot{N}_{f,s} = -\frac{N_{f,s}}{\tau_{f,s}} + (I_{f,s} - N_{f,s})x_{rel}(t)\sum_{t_{pre}}\delta(t-t_{pre}) \text{ .} \tag{2.37}$$

The current of calcium through NMDA receptors depends on the fraction of open receptors and the voltage:

$$I_{NMDA} = G_{NMDA}[N_f + N_s]B(V)(V - V_r) \text{ ,} \tag{2.38}$$

where $B(V)$ is the same function as in equation (2.28), and $G_{NMDA} = -1.25mM/(s\cdot mV)$ is the conductance of the calcium receptors. The rest of the model is given by equations (2.29), (2.30) and (2.31).

The model of Graupner and Brunel

Graupner and Brunel conducted an in-depth analysis of the calcium binding behavior of CaMKII, a protein that is assumed to be an important part of the molecular cascade which changes the synaptic characteristics [51]. They identified key aspects and abstracted their findings into a relatively simple model for synaptic plasticity [29]. This model also incooperates the calcium control hypothesis put forward by the BCM theory and Shouval and colleagues. Pre- and postsynaptic spikes contribute linearly to the postsynaptic calcium concentration $c(t)$:

$$\dot{c} = -\frac{c}{\tau_{Ca}} + C_{pre}\sum_{t_{pre}}\delta(t-t_{pre}-D) + C_{post}\sum_{t_{post}}\delta(t-t_{post}) \text{ .} \tag{2.39}$$

$C_{pre,post}$ are the values the concentration increases by a pre- or postsynaptic spike, respectively. D is a delay between the time of the presynaptic spike and the time

the calcium transient becomes visible at the postsynaptic spine; this is analogous to τ_a in the LIF model. τ_{Ca} is the decay time constant of the calcium in the spine. In the Graupner model, synapses are bistable. To model this, a synaptic efficacy variable ρ is introduced evolving according to

$$\tau\dot{\rho} = -\rho(1-\rho)(\rho_\star - \rho) + \gamma_p(1-\rho)\Theta\left[c(t)-\theta_p\right] - \gamma_d\rho\Theta\left[c(t)-\theta_d\right] + \text{Noise}(t)\ . \quad (2.40)$$

τ is the time constant of the dynamics of ρ, and $\rho_\star$ is the boundary between the basins of attraction of the two stable points. In this formulation, $\rho = 0, 1$ are the two stable points. Also, in this equation there are two thresholds, θ_d and θ_p. For each of the thresholds, if the calcium concentration exceeds it, it causes a drift of ρ towards zero for $c(t) > \theta_d$ or towards one if $c(t) > \theta_p$, which magnitude γ_d and γ_p, respectively. $\rho = 0$ corresponds to the depressed synaptic state (or down state) with efficacy w_0, and $\rho = 1$ corresponds to the potentiated state (or up state) with efficacy $w_1 > w_0$. A noise term is introduced which also depends on the calcium concentration:

$$\text{Noise}(t) = \sigma\sqrt{\tau}\sqrt{\Theta\left(c(t)-\theta_d\right) + \Theta\left(c(t)-\theta_p\right)}\eta(t)\ . \quad (2.41)$$

$\eta(t)$ is a gaussian white noise process with unit variance density, and σ is the amplitude of the noise. Because of the condition given by the Heaviside function, noise is only present if there is drift of ρ anyway. Having a noise term is justified, since experimental data on synaptic plasticity shows a considerable jitter of measured weight changes for any spike pattern.
The model was fitted to different experimental data sets, for which it was necessary to introduce two more parameters related to assumptions about the initial synaptic state and the actual weights. Experiments are done on a population of synapses (i.e. several measurements per stimulation protocol), and the model introduces a parameter β that describes the fraction of synapses initially in the down state. The second parameter is the fraction of synaptic efficacies $b = w_1/w_0$. It is not necessary to specify both w_1 and w_0, because the experimental results are always reported as the fraction of PSP amplitudes after and before the inducton protocol.
In contrast to the Shouval model and Cai model, Graupner and Brunel explicitely fitted their model to experimental data from [47], [64] and [26].

The calcium model of Uramoto and Torikai

The last model presented here is the one by Uramoto and Torikai [35]. It is also a calcium based model, i.e. the synaptic change depends on the concentration of calcium in the postsynaptic spine. The model introduces two state variables: $x(t)$ is the amount[8] of open NMDA receptors, and $y(t)$ is the calcium concentration in

[8]Here the original article is inconsistent. The authors claim that x is the *fraction* of open receptors, and $x \in [0, 1]$. However, I can only reproduce their results if I keep x unbounded.

the spine. They evolve according to

$$\begin{aligned}\dot{x}(t) &= -\frac{x(t)}{\tau_x} + \sum_{t_{pre}} \delta(t - t_{pre}) \\ \dot{y}(t) &= -\frac{y(t)}{\tau_y} + \sum_{t_{post}} (f(y(t-\varepsilon))x(t) + b)\delta(t - t_{post}) \ .\end{aligned} \tag{2.42}$$

$\tau_{x,y}$ is the time constant of decay for NMDA receptors and calcium concentration, respectively. Every presynaptic spike increases x by one, and every postsynaptic spike increases y by an amount $f(y)x+b$. b represents the influx of calcium through voltage-dependent calcium channels, which is independent of presynaptic activity. The function f is a sigmoidal function of the postsynaptic calcium, which assumes that the influx of calcium through NMDA receptors reduces if calcium is already present intracellularly:

$$f(y) = a\frac{k}{k+y} \ . \tag{2.43}$$

Taken together, $f(y)x$ represents the influx through NMDA receptors depending on the number of receptors activated by neurotransmitters x and the bAP. The calcium concentration drives LTD and LTP. For both, the model posits functions of $y(t)$:

$$\begin{aligned}\text{LTD function: } M(y) &= \frac{\alpha_m y}{y + \beta_m} \\ \text{LTP function: } K(y) &= \frac{\alpha_k}{1 + \exp(-(y - \beta_k)/\gamma_k)}\end{aligned} \ , \tag{2.44}$$

which are read out by pre- or postsynaptic spikes for synaptic change:

$$\dot{w}(t) = -\sum_{t_{pre}} M(y(t+\varepsilon))\delta(t - t_{pre}) + \sum_{t_{post}} K(y(t+\varepsilon))\delta(t - t_{post}) \ . \tag{2.45}$$

In contrast to the previous models, the state variable y has to be updated first at the time of a postsynaptic spike, and only then the weight change is computed. This is signified by writing $y(t+\varepsilon)$.

2.4 Theta oscillations and memory performance

2.4.1 Measurement of large scale oscillations

Currently, single neurons in the living animal can be monitored by electrodes or glass pipettes accessing the intracellular potential. This is the most fine-grained method available at this time which provides information about the neuronal state, but only very few neurons can be accessed at the same time. Recently, methods became available which allow to record the activity of many neurons at the same time by inserting voltage sensitive dyes or transfecting neurons such that they express these dyes themselves. These methods are usually subsumed under the term

"optogenetics". Nevertheless, they are not universally applicable, since they still require physical access to the brain, which is not feasible in some situations. Also, the voltage resolution is still rather low compared to direct electrical measurement. Because of these problems, experimental neuroscience often relies on low-resolution measurement of the activity of thousands of neurons. There are two different ways to do this. A non-invasive technique is electroencephalography or "EEG" [30]. Here, electrodes are attached to the skull of a test subject (humans or animals). They measure the electric potential on the skulls surface against a reference potential. Putting many electrodes on different locations on the skull allows to monitor the activity of many regions in parallel. Another technique with similar scope is the measurement of local field potentials (LFPs) [31]. These are obtained using intracranial electrodes, which means this is an invasive technique in contrast to EEG. Its advantage is the more precise placement of electrodes, which allows to better measure the activity of the region of interest. The spatial resolution of both techniques is rather low, because they average the activity of several thousands of neurons. Temporal resolution is relatively high in the millisecond scale.
With EEG measurements it is possible to detect quite a few features of neuronal computations. For example, novel visual stimuli will elecit a detectable deviation from baseline potential after around 300 milliseconds in certain areas, commonly known as the "P300 component". An important discovery obtained with EEG is that mammalian brain activity displays pronounced oscillations. Analysis of EEG or LFP data using Fourier transform or wavelet analysis reveals that large groups of neurons engage in synchronous periodic activity, which signifies different states of the brain. For example, slow wave oscillations are tied to the sleeping state. The oscillations are put in "bands"; for example, oscillations of 40 to 100 Hz are put into the gamma band, while those around 4 to 10 Hz are put into the theta band.

2.4.2 Experimental evidence for improved learning under theta oscillations

One of the more peculiar observations is the influence of the brains' oscillatory state during memory formation on recall performance later. This can be demonstrated with a basic conditioning experiment. Blowing a puff of air into the eye of a rabbit forces it to cover its eyes momentarily with its nictitating membrane. This is called the nictitating membrane response (NMR), and this paradigm is often used in conditioning experiments [65]. The NMR is a so-called unconditioned stimulus (US), and it is paired with the presentation of a tone, which serves as the conditioned stimulus (CS). After a sufficient number of presentations, presenting the CS alone leads to the same response as if a puff of air was blown into the eye: The rabbit shuts its nictitating membrane. In 1978, Berry and Thompson conducted this experiments with rabbits which had an electrode implanted into the hippocampus [32]. They performed the experiment and afterwards analyzed the data from the brain recordings. They found a correlation between the number of learning trials until the conditioned response is aquired with the power of oscillatory activity in the theta

range, between 3 and 8 Hz. Animals which consistently were in high theta states during training needed fewer training trials until they showed a stable conditioned response. Interestingly, in another experiment only presenting the CS-US pair when hippocampal theta power is elevated also leads to faster learning compared to the control group [66]. It is therefore beneficial to initiate a training trial if theta oscillations are present even before the training trial. Similar results have been obtained in human subjects [67]. This also means that theta oscillations are not task specific, but rather represent a state with improved memory susceptibility. Lastly, theta oscillations are also beneficial even after training in the memory consolidation phase. Reiner and colleagues trained human subjects in a finger-tapping task. Afterwards, half of the subjects performed a bio-feedback task which trained them to generate theta-band activity in EEG recordings. This led to better memory consolidation than in the control group which did not generate theta activity [68].
It is a peculiar notion that the oscillatory state has impact on learning. Learning is thought to be linked to synaptic plasticity, which depends on spike timing on a scale of tens of milliseconds or even less. How can it be that theta oscillations, which happen on a time scale of hundreds of milliseconds, have such a huge impact on synaptic plasticity? Different groups have dealt with this question before. John Larson and colleagues have induced presynaptic high-frequency bursting with different intervals between the bursts in hippocampal excitatory neurons [69]. They found that bursts delivered at 5 Hz were the most effective in eliciting LTP, while higher and lower repetition frequencies led to less potentiation. This result was confirmed by Greenstein and colleagues [70]. Another discovery was that the sign of weight change depends on the phase of the theta oscillation. In anesthized rats theta oscillation was induced artificially by stimulating the mid-brain. Next, in hippocampus presynaptic neurons were stimulated to fire high-frequency spike bursts either at the peak or the trough of the theta oscillation. It was found that presynaptic stimulation at the peak leads to LTP, while stimulation at the trough in general depresses the synapse [71]. This result was later obtained also in behaving rats [72].
Despite these findings, it is still unclear how theta oscillations promote learning. In contrast, gamma oscillations (40-70 Hz) are also associated with improved learning rate, but due to the short duration of a gamma cycle, spikes occur in a short time window of around 10 ms and less to each other. This allows plasticity due to classical STDP. In a theta cycle, however, spikes are temporally much less confined and STDP seems to be a more unlikely mechanism to be useful in learning [73].

2.5 Publication I: Theta specific susceptibility in a model of adaptive synaptic plasticity

frontiers in
COMPUTATIONAL NEUROSCIENCE

ORIGINAL RESEARCH ARTICLE
published: 21 November 2013
doi: 10.3389/fncom.2013.00170

Theta-specific susceptibility in a model of adaptive synaptic plasticity

***Christian Albers*[1]*, *Joscha T. Schmiedt*[2] *and Klaus R. Pawelzik*[1]

[1] *Department of Neurophysics, Institute for Theoretical Physics, University of Bremen, Bremen, Germany*
[2] *Schmid lab, Ernst Strüngmann Institute for Neuroscience in Cooperation with Max Planck Society, Frankfurt am Main, Germany*

Edited by:
Mayank R. Mehta, University of California, Los Angeles, USA

Reviewed by:
Arvind Kumar, University of Freiburg, Germany
Tao Zhang, Nankai University, China

***Correspondence:**
Christian Albers, Institute for Theoretical Physics, University of Bremen, Hochschulring 18, Bremen, D-28359, Germany
e-mail: calbers@neuro.uni-bremen.de

Learning and memory formation are processes which are still not fully understood. It is widely believed that synaptic plasticity is the most important neural substrate for both. However, it has been observed that large-scale theta band oscillations in the mammalian brain are beneficial for learning, and it is not clear if and how this is linked to synaptic plasticity. Also, the underlying dynamics of synaptic plasticity itself have not been completely uncovered yet, especially for non-linear interactions between multiple spikes. Here, we present a new and simple dynamical model of synaptic plasticity. It incorporates novel contributions to synaptic plasticity including adaptation processes. We test its ability to reproduce non-linear effects on four different data sets of complex spike patterns, and show that the model can be tuned to reproduce the observed synaptic changes in great detail. When subjected to periodically varying firing rates, already linear pair based spike timing dependent plasticity (STDP) predicts a specific susceptibility of synaptic plasticity to pre- and postsynaptic firing rate oscillations in the theta-band. Our model retains this band-pass property, while for high firing rates in the non-linear regime it modifies the specific phase relation required for depression and potentiation. For realistic parameters, maximal synaptic potentiation occurs when the postsynaptic is trailing the presynaptic activity slightly. Anti-phase oscillations tend to depress it. Our results are well in line with experimental findings, providing a straightforward and mechanistic explanation for the importance of theta oscillations for learning.

Keywords: synaptic plasticity, STDP, learning, memory, theta oscillation

1. INTRODUCTION

Synaptic plasticity likely is the key neural substrate underlying learning and memory in the brain. Early ideas on the problem of synaptic plasticity posited that positive correlations between neuronal activities are the signal for the synapse to potentiate (see e.g., review by Markram et al., 2011); later experiments showed that the relevant signal is not just the average correlation of activity, but rather the precise temporal order of single spikes at the pre- and postsynaptic neuron (Markram et al., 1997; Bi and Poo, 1998; Zhang et al., 1998; Feldman, 2000). This phenomenon was termed Spike Timing Dependent Plasticity (STDP) and subsumed in the well-known exponential spike pair STDP window [Song et al. (2000), spSTDP in the following]. In many theoretical studies, this window serves as a look-up table to compute the weight change: Identify any pair of a pre- and a postsynaptic spike, locate the time difference between the two spikes in the STDP window and add up the respective weight changes [see Morrison et al. (2008) for a review of implementations]. While this linear approach has its appeal, it is not sufficient, because the contributions of spikes in sequences do not simply add up (Wang et al., 2005). Some experiments find that a spike can suppress the effect of later spikes of the same synaptic side (Froemke and Dan, 2002; Froemke et al., 2006). Other experiments show that contrary to expectation a single pre-post pair fails to potentiate the synapse, but a pre-post-post triplet leads to strong long term potentiation (LTP) (Sjöström et al., 2001; Nevian and Sakmann, 2006; Wittenberg and Wang, 2006). These findings highlight the need for any accurate model of STDP to include non-linearities. There are several different models available which attempt to capture the experimental results. One class of models contains phenomenologically motivated non-linear extensions of spSTDP which are tailored to explain experimental data (Froemke et al., 2006; Pfister and Gerstner, 2006; Schmiedt et al., 2010). A second class are calcium-based models, which are grounded on biophysical considerations. Most of these models invoke the calcium control hypothesis, which states that a moderate increase of the calcium concentration in the postsynaptic spine leads to long term depression (LTD), while high concentrations lead to LTP. The models then are concerned with the details of the calcium dynamics (Shouval et al., 2002; Cai et al., 2007; Graupner and Brunel, 2012; Uramoto and Torikai, 2013). A third class of models includes neuronal signals beyond spikes, most prominently the postsynaptic membrane potential (Clopath et al., 2010). There are few experimental studies which quantitatively examine the synaptic change in response to complex and versatile spike patterns (Froemke and Dan, 2002; Wang et al., 2005; Froemke et al., 2006; Nevian and Sakmann, 2006), however, none of the models covers all data sets [for the model of Uramoto and Torikai (2013), see Discussion]. An attenuated synaptic response to repeated high frequency spiking [Short term depression, (Tsodyks and

Markram, 1997; Tsodyks et al., 1998; Zucker and Regehr, 2002)] is explicitly included in several models (Froemke et al., 2006; Cai et al., 2007; Schmiedt et al., 2010), which however, do not explain the full range of experiments. In the following, we present a minimal dynamical model which includes pre- and postsynaptic adaptation as well as an activating contribution, hence we call it contribution dynamics model (CD model). Some of the elements of this model can be found in previous work (Schmiedt et al., 2010). We evaluate the validity of the model by fitting it to the four different data sets mentioned above, and compare its performance with the Triplet model of Pfister and Gerstner (2006), which is similar in scope and formulation, but lacks adaptation.

Another open question in neuroscience addresses the neural substrate for the known importance of oscillatory brain states for memory formation (Fell and Axmacher, 2011; Colgin, 2013). Many studies find that the mere presence of oscillations of increased theta power is enough to enhance the learning process, even if the oscillations are present *before* (and during) the learning trial (Seager et al., 2002; Nokia et al., 2008; Guderian et al., 2009). Other studies find that not theta power, but global theta synchronization promote good learning efficacy (Mölle et al., 2002; Burke et al., 2013). It is likely that theta synchronization is imposed on the affected brain areas by some higher area, which causes the synchronization with a phase difference of around zero, such that maxima of activity in synchronized areas occur at the same time (Fell and Axmacher, 2011). It was suggested that the reason is a specific phase dependence of synaptic plasticity in theta oscillations: If activity maxima in the pre- and postsynaptic neurons co-occur, the synapse potentiates, if the presynaptic neuron bursts during the trough of the theta oscillation, the synapse depresses (Pavlides et al., 1988; Hyman et al., 2003).

Can the combination of these findings be explained by a single mechanism? We address this question with the hypothesis that the reason lies in the filter properties of synaptic plasticity, which can be investigated with models of synaptic plasticity. To test this we assume that theta-band oscillations in large scale signals like EEG or ECoG are caused by corresponding periodic modulation of neuronal activity. For simplicity we neglect spike-spike correlations and assume stochastic spiking. We investigate the synaptic susceptibility to oscillations from the delta band to the gamma band (1–80 Hz) in spSTDP and in the CD model. For comparison, we did the same with a range of other models (Shouval et al., 2002; Pfister and Gerstner, 2006; Cai et al., 2007; Graupner and Brunel, 2012). We found that for spSTDP with physiological parameters synapses are susceptible to oscillations in the theta band (4–8 Hz). The same susceptibility is evident also in the CD model, which however, shifts the phase dependence of LTP close to zero phase difference, in accordance with experimental results. By removing single contributions from the CD model and investigating the resulting changes of the susceptibility, we find that presynaptic adaptation and a conditional activation are the necessary prerequisites for phase zero susceptibility.

2. MATERIALS AND METHODS

In the following, we use a short hand notation to denote spike patterns. "Pre" or "Post" refer to the origin of the spike, the pre- or postsynaptic neuron. A string like "pre-post" denotes first a presynaptic spike a postsynaptic spike, regardless of exact timing. "Post-pre-post-post" describes a postsynaptic spike, then a presynaptic spike, followed by two postsynaptic spikes.

2.1. MODELING SPIKE PAIR STDP WITH DIFFERENTIAL HEBBIAN LEARNING

The differential Hebbian learning rule is a rather simple algorithm for weight changes (Kosko, 1986). The synapse changes proportional to the product of the presynaptic activity and the temporal derivative of the postsynaptic activity. For spiking neurons, however, this makes little sense, and one has to introduce some kind of low pass filtering of neuronal activities to gain a signal suitable to calculate synaptic change. As usual, we use delta pulses to model neuronal spike trains:

$$x_i(t) = \sum_k \delta(t - t_i^k), \tag{1}$$

where $i \in \{\text{pre}, \text{post}\}$ denotes the location of the spiking event. Each spikes leaves an exponential trace y_i on its synaptic side, which can be described by the differential equation

$$\dot{y}_i = -\frac{y_i}{\tau_i} + x_i. \tag{2}$$

We use the dot notation to denote temporal derivatives. The weight change is given by

$$\dot{w} \propto y_{\text{pre}} \cdot \dot{y}_{\text{post}}. \tag{3}$$

This simple system of equations is equal to (balanced) spSTDP, as we show now. Consider the solution of Equation (2) to a single spike at time t_i:

$$y_i = \Theta(t - t_i) e^{-\frac{t-t_i}{\tau_i}}. \tag{4}$$

Here, $\Theta(t)$ is the Heaviside function, i.e., $\Theta(t) = 0$ for $t < 0$ and $\Theta(t) = 1$ everywhere else. The weight change is calculated via

$$\Delta w = c_w \int_{-\infty}^{+\infty} y_{\text{pre}}\, \dot{y}_{\text{post}}\, dt, \tag{5}$$

where we introduce the constant of proportionality c_w. The weight change resulting from a pair of one pre- and one postsynaptic spike is given by

$$\Delta w = c_w \begin{cases} \left(1 - \frac{1}{1 + \frac{\tau_{\text{post}}}{\tau_{\text{pre}}}}\right) \exp\left(-\frac{t_{\text{post}} - t_{\text{pre}}}{\tau_{\text{pre}}}\right) & \text{for } t_{\text{pre}} < t_{\text{post}} \\ -\frac{1}{1 + \frac{\tau_{\text{post}}}{\tau_{\text{pre}}}} \exp\left(-\frac{t_{\text{pre}} - t_{\text{post}}}{\tau_{\text{post}}}\right) & \text{for } t_{\text{pre}} > t_{\text{post}}. \end{cases} \tag{6}$$

This is the standard STDP window for balanced spSTDP, where the areas under the LTP and LTD part of the curve are of exactly equal size, and the decay time constants are given by τ_{pre} and τ_{post} for LTP and LTD, respectively. Due to the linearity of the equations, the learning rule is also completely linear, and every spike pair in a given spike pattern is treated the same by the learning rule.

The STDP window in differential Hebbian learning is determined by three parameters. To scale the LTD and LTP parts of the window relative to each other a fourth parameter is needed. We split the weight change into a depression and a potentiation part by inserting Equation (2) into (3) and introduce a scale parameter q:

$$\dot{w} = c_w y_{\text{pre}} \left(q x_{\text{post}} - \frac{y_{\text{post}}}{\tau_{\text{post}}} \right). \tag{7}$$

This manipulation changes the STDP window to:

$$\Delta w = c_w \begin{cases} \left(q - \frac{1}{1+\frac{\tau_{\text{post}}}{\tau_{\text{pre}}}} \right) \exp\left(-\frac{t_{\text{post}} - t_{\text{pre}}}{\tau_{\text{pre}}} \right) & \text{for } t_{\text{pre}} < t_{\text{post}} \\ -\frac{1}{1+\frac{\tau_{\text{post}}}{\tau_{\text{pre}}}} \exp\left(-\frac{t_{\text{pre}} - t_{\text{post}}}{\tau_{\text{post}}} \right) & \text{for } t_{\text{pre}} > t_{\text{post}}. \end{cases} \tag{8}$$

Adjusting q scales the LTP part of the STDP window as required. For example, setting $q = 1/(1 + \tau_{\text{post}}/\tau_{\text{pre}})$ cancels LTP for every possible spike pattern. There are experiments which show that for low frequencies of spike pair induction, pre-post pairs do not change the synapse, while post-pre pairs still depress the synapse (Sjöström et al., 2001; Nevian and Sakmann, 2006; Wittenberg and Wang, 2006). However, other spike patterns in these studies potentiate the synapse, which suggests that in order to generalize this description of STDP, one has to turn q into a function of time.

2.2. THE CONTRIBUTION DYNAMICS MODEL

For the CD model we use the differential Hebbian learning rule described above as basis, and extend it by several new equations. First, we introduce an adaptation variable u_i for each synaptic side. This dynamics resemble those of the presynaptic resources in models of synaptic short term depression (Tsodyks and Markram, 1997; Tsodyks et al., 1998). Its effect is the attenuation of the impact of rapid spiking on the synapse, and we model it by

$$\dot{u}_i = \frac{1 - u_i}{\tau_i^{\text{rec}}} - c_i u_i(t-0) x_i. \tag{9}$$

The update of the trace Equation (2) is now changed to

$$\dot{y}_i = -\frac{y_i}{\tau_i} + u_i(t-0) x_i, \tag{10}$$

where we write $u_i(t-0)$ to emphasize that in order to update each variable in case of a spike, one has to use the value of u_i shortly before the spike.

If the learning rule Equation (3) was left unchanged, the effect of the adaptation variables u_i would be a rescaling (shrinking) of the STDP window with consecutive spikes, and relaxation during silence. This property removes the linearity of the original STDP learning rule, as the influence of each spike on the synapse depends on the history of spiking of the respective neuron. We introduce an additional non-linearity, by allowing q (Equation 7) to vary over time:

$$\dot{q} = \frac{q_{\min} - q}{\tau_q} + c_q \Theta(y_{\text{pre}} - \vartheta_q) x_{\text{post}}, \tag{11}$$

where Θ is again the Heaviside function. q is a trace of the postsynaptic activity conditional on the presynaptic trace: Only if $y_{\text{pre}} > \vartheta_q$ at the time of a postsynaptic spike, q increases. For all other times, it relaxes back to $q_{\min}$. The actual weight change is finally given by

$$\dot{w} = c_w y_{\text{pre}} \left(q(t-0) u_{\text{post}}(t-0) x_{\text{post}} - \frac{y_{\text{post}}}{\tau_{\text{post}}} \right). \tag{12}$$

The specific formulation of q is motivated by its simplicity—linear ordinary differential equation of first order for the decay term—and several observations in the data of Nevian and Sakmann (2006). In these experiments, a pre-post pair does not change the synapse, but the pre-post-post triplet does. The translation to an STDP framework is that the LTP part of the STDP window needs to vanish when the synapse is relaxed (any previous activity took place relatively long ago), but reappear in reaction to certain activity patterns. In this example (pre-post vs. pre-post-post), the desired outcome can be achieved by Equation (11) without the Heaviside function: $\dot{q} = (q_{\min} - q)/\tau_q + c_q x_{\text{post}}$. However, in the case of a post-post-pre-post pattern (**Figure 2C** third data point from left) this would lead to a huge upscaling of the LTP part, which was not observed. This prompted us to install the threshold such that recent presynaptic activity gates the increase of q. We chose the all-or-none threshold to exclude any non-linear effects of q on the STDP window. Because of the upregulation of potentiation, we call q the activation variable.

Figure 1 gives an overview over the components of the CD model.

2.3. FITTING THE CD MODEL TO EXPERIMENTAL DATA

To evaluate the ability of the CD model to reproduce experimental findings, we matched its parameters to the following four *in vitro* data sets:

- Visual cortex of young rats, thick tufted cells in layer 5 [VC5, Sjöström et al. (2001)].
- Hippocampal neurons of rat embryos in culture [HC, Wang et al. (2005)].
- Somatosensory cortex of young rats, pyramidal cells in layer 2/3 [SC23, Nevian and Sakmann (2006)].
- Visual cortex of young rats, pyramidal cells in layer 2/3 [VC23, Froemke et al. (2006)].

In these experimental studies, the change of synaptic efficacy is given as the ratio of the isolated EPSP (which we assume to be proportional to the synaptic weight) after and before the induction protocol:

$$\begin{aligned} \text{EPSP ratio} &= \frac{\text{EPSP}_{\text{after}}}{\text{EPSP}_{\text{before}}} = \frac{w_{\text{after}}}{w_{\text{before}}} = \frac{w_{\text{before}} + \Delta w}{w_{\text{before}}} \\ &= 1 + \frac{\Delta w}{w_{\text{before}}}. \end{aligned} \tag{13}$$

We identify Δw with the weight change in the CD model. Additionally, we assume that the synaptic weight before the

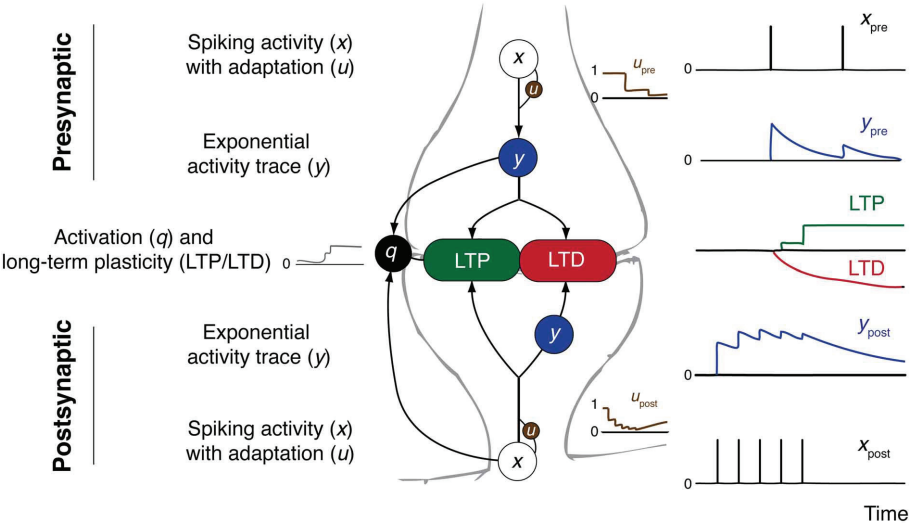

FIGURE 1 | Overview over the CD model and its constituents. Presynaptic **(top)** and postsynaptic **(bottom)** contributions to synaptic plasticity are shown. Arrows indicate direction of influence according to model equations. On the right side example spike trains and resulting traces of the variables are shown.

induction has a fixed value. The goal of the fitting process is to compare the experimental synaptic change with the model prediction Δw^{CD} and find the set of parameters $\pi = \{\tau_{\text{pre}}^{\text{rec}}, c_{\text{pre}}, \tau_{\text{post}}^{\text{rec}}, \dots\}$ which minimizes the error

$$\text{E} = \frac{1}{N}\sum_{i=1}^{N}\left(\frac{\Delta w_i^{\text{exp}} - \Delta w_i^{CD}(\pi)}{\text{SEM}_i}\right)^2, \qquad (14)$$

where N is the number of experiments in the data set, i the index of the experiment and SEM_i the published standard error of the mean for experiment i. The minimization of the error was done by a brute force search in the space of parameters. The bounds we defined for the search are given in **Table 1** (see Appendix for additional remarks on the bounds). For each data set, some parameters were set by hand to fixed values as follows: We set q_{min} according to the outcome of the pre-post spike pair experiment found in every data set. If the pre-post spike pair resulted in no change of synaptic efficacy, $q_{\text{min}} = 1/(1 + \tau_{\text{post}}/\tau_{\text{pre}})$, otherwise $q_{\text{min}} = 1$. The time constants τ_{pre} and τ_{post} turn up as the decay constants of the STDP window (see Equation 8). For the experiments in VC23 and HC these values were explicitly given, so we did not change them. For the other two cortical data sets, we used the values of the experiment in VC23. As each spike pattern contained only one presynaptic spike, no information could be obtained for presynaptic adaptation for the data from SC23. This left for fitting here $\tau_{\text{post}}^{\text{rec}}$, c_{post}, τ_q, c_q, ϑ_q and c_w. In all other data sets, $\tau_{\text{pre}}^{\text{rec}}$ and c_{pre} were additionally fitted.

Table 1 | Bounds on parameters in the CD model.

Parameter	Unit	Min	Max
$\tau_{\text{pre}}^{\text{rec}}$	s	0.001	3
c_{pre}		0	1
$\tau_{\text{post}}^{\text{rec}}$	s	0.001	3
c_{post}		0	1
τ_q	s	0.001	3
c_q		0	10
ϑ_q		0	0.2
c_w		0.001	0.1

2.4. FITTING THE TRIPLET MODEL TO EXPERIMENTAL DATA

The CD model is structurally similar to the Triplet model conceived by Pfister and Gerstner (2006). The latter is a set of linear differential equations of first order that describe traces of activity at the synapse. Each spike leaves two traces at the synapse: r_1, r_2 for the presynapse and o_1, o_2 for the postsynapse, which interact to determine the weight change. For the update of the traces, there are two possible choices. The first one is that each spike increases its respective traces by one; this is equivalent to the y_i dynamics of Equation (2). Second, at the time of a spike the respective traces always jump to unity. The equation of the traces changes to $\dot{y}_i = -y_i/\tau_i + (1 - y_i(t-0))x_i$. The first update rule is called "all to all interactions," the second "nearest neighbor interactions." The weight change in the Triplet model then consists of a standard spike pair STDP rule plus the spike triplet interaction, which is proportional the product $r_1 \cdot o_2$ ($o_1 \cdot r_2$) at the time of a postsynaptic (presynaptic) spike for LTP (LTD). The main differences between the two models are that in the CD model y_{pre} and y_{post} are subject to spike amplitude adaptation and that the triplet interactions are replaced by the (conditional postsynaptic) activation q. For comparison, we fitted the triplet model to the data sets VC23, SC23, and VC5. The Triplet model has been fitted to the HC data set, the parameters can be found in Pfister and Gerstner (2006). It has also already been fitted to the VC5 data set (same article). However, the spike induction protocol used for fitting was uniformly 60 spike pairs with $\Delta t = \pm 10$ ms delivered at different frequencies (1–40 Hz). In the study of Sjöström et al.

(2001), spike pairs for frequencies greater than 1 Hz were delivered in 15 bursts of 5 pairs with varying intra burst frequency, with bursts being 10 s apart. We re-fitted the Triplet model to VC5 to better compare the two models. In contrast to the original article, we furthermore allowed the triplet interaction parameters A_3^+ and A_3^- to become negative to account for adaptation in the data. The fitting procedure was similar to the fit of the CD model; in particular, the STDP window time constants τ_+ and τ_- were not fitted, but set to predetermined values. The bounds defined for the parameters are given in **Table 2**.

2.5. MEAN WEIGHT CHANGES IN MODELS OF STDP

The formulation of spSTDP as differential Hebbian learning allows for a simple analytical treatment of continuous firing rates rather than spike events. Under the assumption of poissonian spiking and vanishing correlations between pre- and postsynaptic spikes, one can easily compute the mean of the traces y_i:

$$\langle \dot{y}_i \rangle = \left\langle -\frac{y_i}{\tau_i} + x_i \right\rangle = -\frac{\langle y_i \rangle}{\tau_i} + r_i(t), \tag{15}$$

where $r_i(t) = \langle x_i \rangle$ is the continuous and time-dependent firing rate of neuron i. Because of the vanishing spike-spike correlations, both traces combine to give the weight change as

$$\dot{w} = \dot{w}_+ + \dot{w}_- = c_w q \langle y_{\text{pre}} \rangle r_{\text{post}} - \frac{\langle y_{\text{pre}} \rangle \langle y_{\text{post}} \rangle}{\tau_{\text{post}}}, \tag{16}$$

where $\langle y_i \rangle$ is the solution of differential Equation (15) for a given time course of the firing rates $r_i(t)$.

In the non-linear models of STDP [CD model, Triplet model, the three Calcium models (Shouval et al., 2002; Cai et al., 2007; Graupner and Brunel, 2012)], the numerous non-linearities in each model did not allow to compute and solve the mean field equations. We therefore computed the average weight change for a given stimulation protocol and model by generating many realizations of the same continuous and time dependent firing rates from inhomogeneous poisson processes (Dayan and Abbott, 2005), which we fed into each model. As in the analytical calculations for spSTDP, we assumed poissonian firing with vanishing spike-spike correlations from synaptic transmission. In this case the probability of finding a spike in a time bin of width Δt is given by

$$p(\text{spike in neuron } i \text{ in } \Delta t | t) = r_i(t) \Delta t, \tag{17}$$

where $r_i(t)$ is the firing rate of neuron i as a function of time.

Table 2 | Bounds on parameters in the Triplet model.

Parameter	Unit	Min	Max
τ_x	s	0.0001	5
τ_y	s	0.0001	5
A_2^+		0	0.1
A_3^+		−0.1	0.1
A_2^-		0	0.1
A_3^-		−0.1	0.1

2.6. STDP AND THETA OSCILLATIONS

We hypothesize that the link between theta oscillations and learning lies in certain filter properties of the synapse, which likely depend on the model of synaptic plasticity used. We investigate synaptic filter properties in a variety of different models: spSTDP, the CD model, the Triplet model, and three different calcium models, with the aim to carve out prerequisites for a synaptic filter. We used a sinusoidal oscillation to model the firing rate. For the case of spSTDP, the firing rate is given by:

$$r_i(t) = 1 + \varepsilon \cos(\omega_{\text{mod}} t - \phi_i) \,. \tag{18}$$

Here, $\varepsilon \in [0, 1]$ is a parameter that controls the amplitude of the oscillation, $\omega_{\text{mod}} = 2\pi f_{\text{mod}}$ is the modulation frequency, and ϕ_i is the phase of the oscillation. Because only relative phase is important for the weight change, we set $\phi_{\text{pre}} = 0$ and $\phi_{\text{post}} = \Delta\varphi$. We do not specify an absolute baseline firing rate for spSTDP, because it is just a scale factor and does not qualitatively change the results. The value we report is the weight change per time averaged over one period of oscillation. This is constant after transients from the onset of neuronal activity died out:

$$\Delta w = \frac{1}{T} \int_{t'}^{t'+T} y_{\text{pre}} \dot{y}_{\text{post}} dt \,. \tag{19}$$

$T = 1/f_{\text{mod}}$ is the period of the modulatory oscillation, and $t' \gg \tau_{\text{pre}}, \tau_{\text{post}}$ is chosen such that any transient behavior in the traces y_i due to switching on the activity are gone. We derive the analytical solution for Equation (19) in the appendix, and use it to generate the plots in **Figure 4**.

In the case of the non-linear models of STDP a baseline firing rate (the firing rate averaged over one period of oscillation) has to be specified. The respective firing rates of the pre- and postsynaptic neurons change to

$$\begin{aligned} r_{\text{pre}}(t) &= r_{\text{base}} \left(1 + \varepsilon \cos(\omega_{\text{mod}} t)\right) \\ r_{\text{post}}(t) &= r_{\text{base}} \left(1 + \varepsilon \cos(\omega_{\text{mod}} t) - \Delta\varphi\right) . \end{aligned} \tag{20}$$

To simplify the analysis, both neurons had the same baseline firing rate and the same modulation frequency. Similar to spSTDP, in the CD model and the Triplet model we calculated the weight change per time by averaging over an integer multiple of the oscillation period starting after enough time has passed to settle the transient:

$$\Delta w = \frac{1}{NT} \left\langle \int_{t'}^{t'+NT} \dot{w}_{\text{model}} \, dt \right\rangle, \tag{21}$$

where model $\in \{CD, \text{Triplet}\}$ refers to the model used. In all simulations, $t' = 2$ s and $NT = 98$ s; we simulated only integer values of the modulation frequencies, so NT is always a multiple of the period.

For the three calcium-based models the procedure was different. All models have inherent weight limits. As a consequence, the rate of weight change itself is a function of time which does not

settle into an equilibrium other than saturation. Therefore it is not feasible to calculate an average weight change rate as with the spike pair models. We rather let the two neurons fire with periodic firing rates for some time [2 s and 5 s in the model of Shouval et al. (2002), 10 s in the model of Cai et al. (2007), 5 s in the model of Graupner and Brunel (2012)], after which we silenced the neurons, but continued to simulate until the synapse settled into an equilibrium. With all models, we report the final weight, with $w = 1$ being the initial weight.

The fitting procedure and numerical simulations (Monte-Carlo-Simulations) were done with custom-made programs in Matlab (Mathworks Inc., Natick, MA, USA). Numerical integration of non-linear differential equations was done with Eulers method and a step size of 0.1 ms. Linear differential equations were solved analytically, and time evolution of the variables was calculated based on the spike times.

3. RESULTS

3.1. THE CD MODEL CAPTURES A WIDE RANGE OF DYNAMICAL PHENOMENA

The CD model describes the non-linear interactions between spikes on either synaptic side acting on the contributions to synaptic changes. To evaluate its ability to capture synaptic changes, we chose four studies from the literature which measure synaptic changes in response to complex spike patterns, and matched the model parameters to the experimental results. Because the experiments were conducted under different conditions (brain region, presynaptic stimulation method), the parameters had to be fitted separately for each data set. In the following we describe the experiments and how the CD model recreates them in relative detail, to illustrate the action of the different contributions.

In all experimental studies, spikes were artificially induced by application of current pulses to patched neurons, or sometimes in the case of presynaptic spikes by stimulating the tissue close to the dendritic tree of the postsynaptic neuron.

3.1.1. Area VC5 (Sjöström et al., 2001)

The experiments were a series of pre-post and post-pre pairs, with fixed timing of 10 ms between the spikes of one pair. The spike pairs were applied with 0.1 Hz (low frequency) 50 times, or organized in "5–5"-bursts (moderate to high frequency), and each burst was induced 15 times. Each burst consisted of 5 spike pairs at intervals of 100, 50, 25, and 20 ms. Two consecutive bursts were 10 s apart. Pre-post spike pairs at low frequency (0.1 Hz) do not change the synapse. We reflect this in the CD model by setting $q_{\min} = 1/(1 + \tau_{\text{post}}/\tau_{\text{pre}})$. For post-pre spike pairs of burst frequencies up to 20 Hz, the weight change remained constant (**Figure 2B**, blue bars). For pre-post pairs, however, potentiation increased with increasing burst frequencies well below 20 Hz (**Figure 2A**). In the CD model, Δw_- is proportional to the integral of the product of the pre- and postsynaptic activity traces y_{pre} and y_{post}. Consequently the time window of interaction is limited by the smaller of the two time constants of decay $\tau_{\text{pre}} = 14$ ms and $\tau_{\text{post}} = 42$ ms. Because at 20 Hz the distance between each pair is 40 ms, each spike pair remains effectively isolated, and Δw_- only depends on the number of spike pairs. For pre-post pairs, however, the outcome is determined by the state of the variable q at the time of the postsynaptic spike. The time constant τ_q is longer (50 ms), which means that as the frequency of spike pairs is increased, at the time of the next postsynaptic spike the variable q is still well above baseline level and Δw_- and Δw_+ do not cancel anymore, but Δw_+ "wins." For even higher spike pair frequencies (40 and 50 Hz), the spike pairs are so close together that the traces y_i interact. Because q has a considerable build-up under these conditions, LTP is favored regardless of spike order. This captures the experimental result that for burst frequencies of 40 and 50 Hz, post-pre pairings potentiate the synapse instead of depressing it.

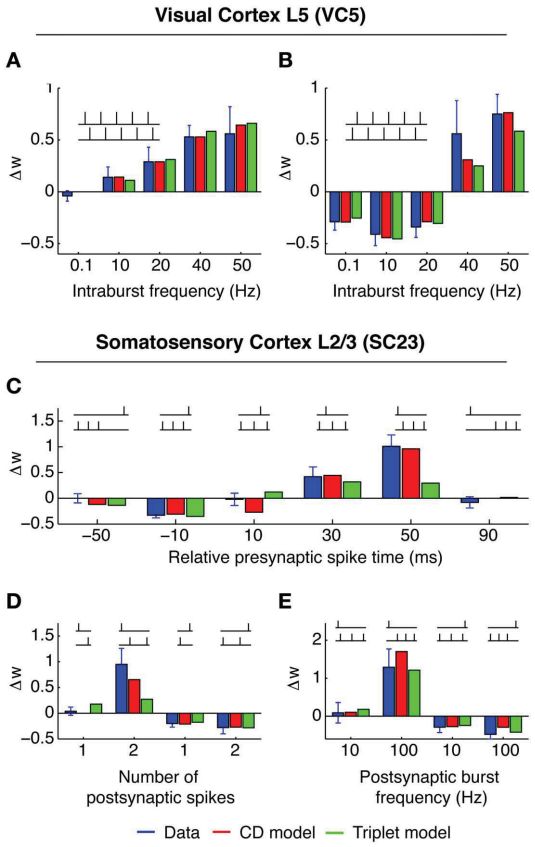

FIGURE 2 | Best fit of CD model and Triplet model to the data in VC5 (top) and SC23 (bottom). Blue bars show experimental weight change ± SEM, red bars show weight change predicted by CD model, and green bars show Triplet model for comparison. Insets show example spike patterns. **(A,B)** Experiments in VC5. **(A)** shows "5–5" bursts with pre- before postsynaptic spiking, **(B)** with order reversed. Both models capture the transition of LTD to LTP with increasing burst rate. **(C–E)** Experiments in SC23. The CD model quantitatively recreates the strong non-linearity of the transition from no change to LTP with the addition of a postsynaptic spike [**(D)**: left vs. second-to-left, and **(C)**: 50 ms].

3.1.2. Area SC23 (Nevian and Sakmann, 2006)

In this study, one presynaptic spike was paired with a train of one to three postsynaptic spikes. Each pattern was repeated 60 times at a repetition rate of 0.1 Hz. Lacking multiple presynaptic spikes the parameters of presynaptic adaptation could not be determined,

therefore we set $u_{\text{pre}} = 1$ and $c_{\text{pre}} = 0$ during the fitting procedure. The pre-post spike pair at $\Delta t = 10$ ms does not change the synaptic efficacy, consequently we set $q_{\min} = 1/(1 + \tau_{\text{post}}/\tau_{\text{pre}})$. However, LTP is reported for pre-post-post triplets of sufficient postsynaptic burst frequency (≥50 Hz, see **Figure 2**). This is an example for a "priming" of the synapse. In the CD model, the conditional modulation of LTP by q (Equation 11) achieves this. Pre-post pairs induced with low inter pair intervals (5 s and longer) do not change the synapse, but allow LTP to be expressed if a second postsynaptic spike follows the leading pair quickly.

3.1.3. Area HC (Wang et al., 2005)

The experimental setup of this study differs most from the others. The measurements were done in cultured neurons from the hippocampus of rat embryos, compared to neocortical slices of young rats in all other experiments. Also, the spike pattern repetition frequency was higher (1 Hz compared to 0.1–0.2 Hz). The main result of these experiments is the synaptic change in response to several pre-post-pre and post-pre-post spike triplets. For identical timings, spSTDP predicts the same synaptic change for both triplets, because the same post-pre and pre-post pairs occur. But in the experiment, a post-pre-post triplet leads to LTP (**Figure 3C**), while a pre-post-pre triplet does not change synaptic transmission (**Figure 3B**). This suggests that the leading postsynaptic spike "primes" the synapse for potentiation, without the need to meet the condition for q (Equation 11). In the CD model, this requires a negative threshold $\vartheta_q < 0$. Compare this to the data in SC23, where the priming is conditional on a pre-post pair, instead of a single postsynaptic spike.

3.1.4. Area VC23 (Froemke et al., 2006)

In this study, several of the features of spike integration were examined. First, "5–5" bursts were conducted similar to the experiment in VC5 (**Figure 3A**, blue bars). For post-pre spike pairs, LTD converted to LTP with burst frequencies greater than 50 Hz. Second, "$n - 1$" spike patterns were examined to characterize presynaptic adaptation (termed "suppression" in the original article). One to five presynaptic spikes in a burst at 100 Hz were paired with one postsynaptic spike either before or after the presynaptic burst. The result from this experiment can be interpreted such that only the leading presynaptic spike of the burst has a noteworthy influence on synaptic change. In the CD model, this is reflected by strong presynaptic adaptation in the fit to the data. Third and last, "$1 - n$" experiments paired one presynaptic spike with one to five postsynaptic spikes. (**Figure 3D**). An interesting result is the comparison of the post-post-post-post-pre-post pattern (**Figure 3D**, left) with the post-pre-post triplet: Both result in the same synaptic change. One possible interpretation is that the leading postsynaptic spikes had little to no influence on the synaptic change. In the CD model, this requires that the threshold ϑ_q is greater than zero, so that no modulation of Δw_+ caused by an increase of q happens in both spike patterns. If ϑ_q was smaller than zero, the postsynaptic bursting before the conclusive pre-post pair would lead to a build up of the variable q, which in turn would cause Δw_+ to be strongly upregulated and to "overwhelm" Δw_-, which was not observed.

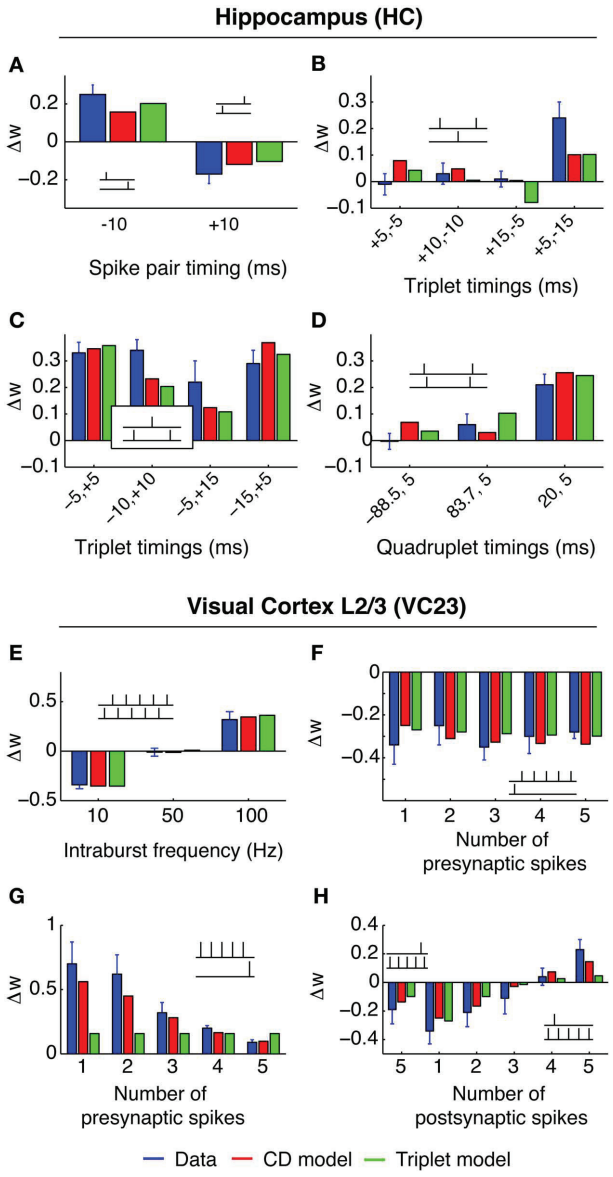

FIGURE 3 | Best fit of CD model and Triplet model to the data in HC (A–D) and VC23 (E–H). In HC, CD model and Triplet model capture the main feature of the results, where pre-post-pre triplets do not change the synapse, while post-pre-post triplets show strong LTP. The +5, −15 triplet (**B**, right) however, can not be reproduced by both models, leading to a relatively large error. In VC23, adaptation is evident in **(G)**. Adding more spikes in front of a pre-post pair decreases LTP, contrary to expectation. The Triplet model has no mechanism which can deal with that.

The parameters of the best fits to all data sets are shown in **Table 3**.

3.1.5. Testing the importance of adaptation

The parameters resulting from the fits show substantial postsynaptic adaptation only for the VC23 data set whereas postsynaptic adaptation is non-existent in VC5 or has very fast recovery reflected by short time constants in SC23 and HC. We therefore tested if postsynaptic adaptation was necessary to explain

Table 3 | Parameters of CD model of best fit for each data set.

Data set	τ_{pre} (ms)	τ_{post} (ms)	τ^{rec}_{pre}	c_{pre}	τ^{rec}_{post}	c_{post}	q_{min}	τ_q	c_q	ϑ_q	c_w	Error
VC5	14	42	94 ms	0.7	–	0	0.25	46 ms	1.93	<0	0.03	0.17
HC	17	34	3 s	0.2	10 ms	0.9	1	20 ms	3.0	<0	0.009	2.81
SC23	14	42	–	–	20 ms	1	0.25	0.5 s	8.5	0.1	0.018	0.81
VC23	14	42	0.6 s	0.7	0.3 s	0.9	1	0.3 s	6.6	0.1	0.033	0.78

Table 4 | Errors for reduced CD model.

Data set	Full model	$c_{post} = 0$	$c_{pre} = 0$	No adaptation
VC5	0.17	–	0.38	0.59
HC	2.81	2.92	3.55	3.62
SC23	0.81	1.0	–	1.0
VC23	0.78	6.1	7.3	7.8

the data by fitting it a second time with c_{post} enforced to be zero; this is effectively switching off postsynaptic adaptation. The resulting errors are given in **Table 4**. For HC, the increase in error is about 3%, for SC23 the error increases by 23%. This is not a large difference, and it follows that postsynaptic adaptation is not necessary to explain these data sets. In the VC23 data set, the error increases sevenfold. If the CD model is fitted to the data with presynaptic adaptation switched off ($c_{pre} \equiv 0$ for the fitting), the error increases for HC by 26%, for VC5 it more than doubles, and for VC23 the increase is greater than sevenfold.

3.1.6. Comparison with triplet model

The Triplet model (Pfister and Gerstner, 2006) is a model of STDP which is in scope and formulation similar to the CD model. Both extend spSTDP with several non-linearities to account for actual measurements of synaptic changes in complex spike patterns. To gain a relative measure of fitting performance of the CD model, we compare its fit to the different data sets to the ones of the Triplet model. Because in the original article the Triplet model was fitted only to VC5 and HC, we did our own fits to the remaining two data sets, and a re-fit to VC5 (see Materials and Methods). The best fits of the triplet model together with the best fits of the CD model to the different data sets are shown in **Figures 2**, **3** (green bars). The respective parameters are given in **Table 5**. For VC5 the change of the experimental protocol in the original article for this data set did not change the resulting error by much, nor the original conclusion that the error is lower with nearest neighbor interactions; the error is 0.51 for all-to-all interactions (parameters not shown). The CD model reaches a lower error (0.17 compared to 0.33), but both models follow the most prominent feature of this data set, the conversion of depression to potentiation with increasing repetition frequency. The preference of nearest neighbor interactions is also found in the fit to VC23, where the error is 25% lower for the model with nearest neighbor interactions compared to all-to-all interactions. An interesting feature of the parameters is that the amplitude of "potentiating" triplet interactions A_3^+ is negative in VC23. The reason is that the adaptation found in VC23 needs to be accounted for. The triplet model has no (explicit) adaptation, but negative values for A_3^+ mimic part of the effect.

For the data from SC23 with τ_+ and τ_- taken from VC23 the fit with all-to-all interactions led to the smallest error (1.69 compared to 1.97). The amplitude parameter A_3^+ is two orders of magnitude greater than the others. This gets outweighted by the time constant $\tau_x = 7.7$ s, which leads to an high accumulation of trace r_2 that controls the triplet depression. A second fit which allowed τ_+ and τ_- to vary (eight parameters in total) reached a lower error of 1.25, but the resulting time constants of the STDP window have the property that $\tau_+ > \tau_-$, which is the reverse of what is usually found. For the fit of the "minimal" CD model the error is 1.0, but here only four out of seven parameters were varied: τ_q, c_q, ϑ_q and the scale parameter c_w. The other three parameters are kept fixed: τ_{pre} and τ_{post} are set to the values from VC23, and q_{min} is determined by the outcome of the pre-post spike pair experiment.

3.2. SYNAPTIC THETA-SUSCEPTIBILITY IN spSTDP

Several studies found that the presence of oscillations with high theta power or large scale theta synchronization in EEG or LFP enhance learning. (Mölle et al., 2002; Seager et al., 2002; Guderian et al., 2009). A possible explanation for these findings could be an underlying filter property of the single synapse, i.e., synaptic change depends on oscillating activity of both neurons in a way specific to the oscillation frequency. To investigate this, we assume a very simple model system: Two connected neurons fire stochastically with vanishing spike-spike correlations, i.e., correlations induced when a presynaptic neuronal activity changes the probability of postsynaptic spikes. Theta oscillations found in EEG or LFP are modeled by periodic sinosoidal modulation of the baseline neuronal activity. Neurons fire spikes with an average rate that is independent of the modulatory rate. Such a modulation could be e.g., induced by periodic inhibition delivered by external sources. As a first step we investigate the filter properties of spSTDP. In **Figure 4** we display the rate of weight change as a function of modulation frequency f_{mod} and phase difference $\Delta\varphi$ for five different values of q, corresponding to differently biased STDP. For a given f_{mod} in balanced spSTDP the plot shows that synaptic change shows the greatest difference between minimum and maximum (malleability or susceptibility) in the theta range (4–10 Hz). For high or low frequencies the change decays back to zero. An analytical calculation (see Appendix) shows that the maximally effective modulation frequency lies at

$$f_{max} = \frac{1}{2\pi\sqrt{\tau_{pre}\tau_{post}}}. \quad (22)$$

Table 5 | Parameters of best fit for the triplet model.

Data set	τ_+ (ms)	τ_- (ms)	τ_x	τ_y	A_2^+	A_3^+	A_2^-	A_3^-	Error
VC5	17	34	–	38 ms	0	0.049	0.0068	0	0.33
HC	17	34	946 ms	27 ms	0.0061	0.0067	0.0016	0.0014	2.9
SC23	14	42	7.7 s	6 ms	0.006	0.211	0.0004	0.009	1.69
VC23	14	42	2.7 s	2.6 s	0.007	−0.0005	0.0104	0.01	2.78

The frequency of maximum efficiency is a function of the time constants of the STDP window. For the parameters from VC23 used in **Figure 4**, $\tau_{pre} = 14$ ms and $\tau_{post} = 42$ ms, $f_{max} = 6.56$ Hz. For the time constants from HC, $\tau_{pre} = 17$ ms, $\tau_{post} = 34$ ms, $f_{max} = 6.62$ Hz. In general, for physiological parameters the most effective frequency lies in the theta band.

This is a band-pass filter property, which discards too slow or too fast oscillations, and uses intermediate oscillation frequencies as signals for synaptic change. This is contrasted by strongly biased spSTDP (**Figures 4C,E**). Here, the region of maximal phase dependency of synaptic plasticity on relative phase (i.e., the region of high susceptibility) is not cut off anymore for low modulation frequencies. The synapse acts as a low pass filter.

3.3. SYNAPTIC SUSCEPTIBILITY IN NON-LINEAR MODELS OF SYNAPTIC PLASTICITY

We chose five different models of synaptic plasticity to compare the filter properties between them. First we examine the effects of extending spSTDP with realistic non-linearities, with the CD model and the Triplet model. Furthermore, we examine three calcium-based models. The first one is the model of Shouval et al. (2002) ("Shouval model" in the following), which introduced a formalization of the calcium control hypothesis. This hypothesis states that moderately elevated levels of calcium in the postsynaptic spine lead to synaptic depression, while high levels lead to potentiation. The goal is then to model the calcium dynamics at the synapse. For reference, we repeat the equations of the Shouval model in the appendix. The second model is an extension of the Shouval model with pre- and postsynaptic adaptation and presynaptic facilitation (Cai et al., 2007, Cai model). The adaptation is shared with the CD model. The third calcium model was developed by Graupner and Brunel (2012) ("Graupner model"). This model makes similar use of the calcium control hypothesis, however, it combines it with a bistable synapse model (Graupner and Brunel, 2007). All models start from biologically plausible first principles and derive the STDP window as a consequence. Also, each model has inherent weight limits, which force us to change the induction protocol for them (see Methods). For all models, we do the analysis with all available parameter sets.

We constrain ourselves to models which use only spikes (spike times) as relevant signals, and derive all relevant variables from them. There exist models which explicitly take subthreshold neuronal dynamics into account (see e.g., Clopath et al., 2010). Although this type of model is potentially more accurate at describing experimental results, it has to make specific assumptions about neuronal dynamics, which we want to avoid here.

For the CD model, the rate of weight change as a function of modulation frequency and phase difference is shown in **Figure 5**. Because the data in SC23 can not give information about presynaptic adaptation, we use τ_{pre}^{rec} and c_{pre} from area VC23 instead. Three of the plots show a very similar behavior. The weight change is positive almost everywhere, and the zone of maximal LTP depending on modulation frequency is tilted such that for a modulation frequency of 1 Hz highest potentiation occurs at $\Delta\varphi \approx 0$. A comparison with **Figure 4** shows that in the case of a slight bias toward LTP ($q = 1.4$) the picture looks similar. In the parameters for VC23 and HC, $q_{min} = 1$, which means that $q(t) \geq 1$ and the requirement for potentiation-biased STDP is fulfilled. In SC23, the STDP window is biased toward LTD ($q_{min} = 0.25$), however, the parameters for the activation q show that contributions to it are strong ($c_q = 8.5$) and last long ($\tau_q = 0.5$ s). Therefore the bias toward LTP results from the baseline activity. The rate of weight change in VC5 deviates strongly from this, it shows an asymmetry between maximal and minimal weight change, and is strongly biased toward LTD.

The characteristics of the susceptibility in the Triplet model are different from the CD model (**Figure 6**). In three parameter sets (HC, SC23, VC23), the weight change is depression only, and the tilt of maximal weight change (closest to zero) is inverted compared to the CD model. None of these three parameter sets shows a pronounced susceptibility specific to a certain frequency range. Increasing the baseline rate does not change the weight change qualitatively, but rather scales it up (Not shown for SC23, VC23). Comparison with spSTDP (**Figure 4**; $q = 0.7$) suggests that the respective parameters are biased toward LTD. Like in the CD model, area VC5 stands out. At 5 Hz the weight change is the same as in the CD model. For an increased baseline rate of 20 Hz, it changes from depression to strong potentiation, as comparison with **Figure 4C** shows.

In the Shouval model, the susceptibility depends little on the parameters of the induction protocol (stimulation time 2 or 5 s, baseline firing rates different from 5 Hz (not shown), **Figure 7**). The synapse potentiates for all parameters, and shows a phase dependence for slow oscillations (<3 Hz). However, the difference between maximum and minimum weight is small. The situation is similar in the Graupner model: In VC5 the phase dependence of weight change reaches into the theta band, in HC up to 20 Hz (**Figure 7**). The synapse, however, shows no band-pass properties. In contrast to the other two models, in the Cai model the synapse is susceptible to oscillations in the theta band. However, as the baseline firing rate is increased, the synapse shifts to a low pass filter.

3.4. CONTRIBUTIONS TO THETA SUSCEPTIBILITY

The CD model is the only model of synaptic plasticity tested here which retains a susceptibility specific for a certain frequency

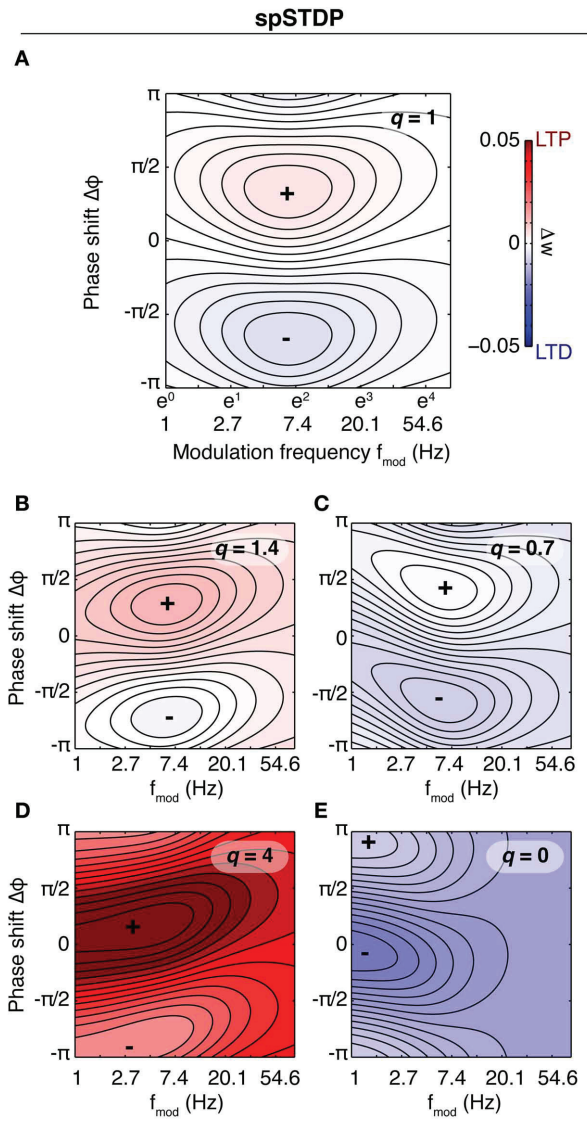

FIGURE 4 | Rate of weight change in spSTDP. These plots show the rate of weight change for simple spSTDP (Time constants taken from VC23). Contours mark lines of same weight change. Colors indicate positive (red) or negative (blue) weight change, see colorbar. Colorbar is the same for every plot. Plus and minus signs mark maximum and minimum, respectively. Weight change is a function of modulation frequency f_{mod} and phase shift $\Delta\varphi$ [see Equation (31)]. $\Delta\varphi > 0$ indicates a phase where presynaptic leads postsynaptic activity. Baseline firing rate is unspecified (see text). **(A)** Balanced spSTDP ($q = 1$). Maximal and minimal weight change occur at $f_{\mathrm{mod}} \approx 6$ Hz, while for very low and very high modulation frequencies the weight change decays to an average value (zero in this case), regardless of phase shift. We term this the band-pass property of the synapse. **(B,C)** spSTDP with a moderate bias toward LTP ($q = 1.4$) or LTD ($q = 0.7$). The bias converts the weight change to LTP or LTD almost everywhere, however, the band-pass property is mostly preserved. **(D,E)** spSTDP with a strong bias toward LTP or LTD. The rate of weight change shows a strong dependence on phase shift even for lowest oscillation frequencies instead of a decay back to an average value. Therefore, the synapse acts as a low pass filter in both cases.

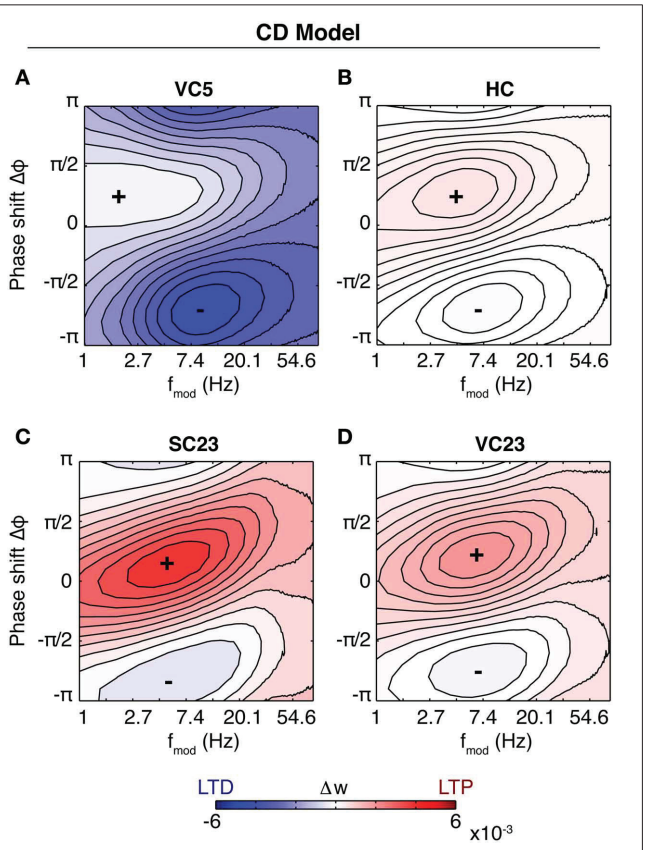

FIGURE 5 | Susceptibility of the synapse to theta oscillations in the CD model. Shown is the rate of weight change as a function of phase shift and modulation frequency (similar to **Figure 4**). Baseline firing rate is 5 Hz for each plot. Same colorbar for all plots. **(A)** Parameters of fit to VC5. The synapse depresses for all modulation frequencies and phase shifts. **(B)** Parameters of HC. The synapse is biased toward potentiation. Maximal potentiation occurs for zero or small positive phase shifts at a modulation frequency of ∼2–10 Hz. The result is similar for SC23 [**(C)**, with $\tau_{\mathrm{pre}}^{\mathrm{rec}} = 0.6$ s, $c_{\mathrm{pre}} = 0.7$ from VC23] and VC23 **(D)**, with slight variations in magnitude and size of the zone of maximal LTP. Comparison with **Figure 4** shows that spSTDP with a moderate bias toward LTP exhibits very similar characteristics.

range beyond the linear regime (low firing rates). To illustrate the behavior in the non-linear regime, we computed the rate of weight change for different baseline firing rates for the parameter set of SC23 (**Figures 8A–C**). At low firing rates, the susceptibility is very similar to that of spSTDP with a moderate bias toward depression (see **Figure 4B**). One could expect that with increasing firing rate, the bias simply gets stronger until the weight change is similar to **Figure 4C**. However, the specific susceptibility gets slightly more pronounced, and the maximum of potentiation moves toward (and for very high firing rates beyond) zero phase shift. This effect is stronger for low modulation frequencies (≈3 Hz, **Figure 8C**). Interestingly, this property resembles the experimental observation that presynaptic stimulation repeatedly delivered at the peak of a theta oscillation potentiates the synapse, while stimulation at the trough depresses it (Hyman et al., 2003).

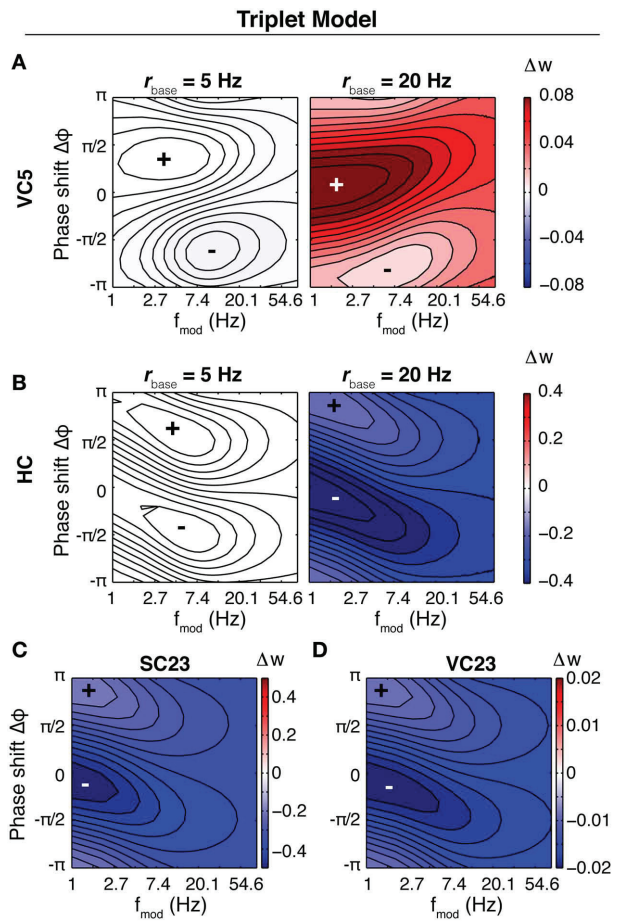

FIGURE 6 | Susceptibility of the synapse in the Triplet model. Shown is the rate of weight change of the synapse as a function of f_{mod} and $\Delta\varphi$ in the Triplet model, with each of the parameter sets and with different neuronal baseline firing rates. In contrast to **Figure 4** the colorscale is separate for each plot. **(A)** Area VC5, left: 5 Hz average firing rate, right: 20 Hz firing rate. At 5 Hz, the weight change is negative everywhere (not visible because of the order of magnitude). Changing the firing rate to 20 Hz leads to LTP everywhere. **(B)** Area HC, at 5 and 20 Hz average firing rate of the both neurons. The weight change is negative for both conditions. **(C,D)** Areas SC23 and VC23 at a baseline firing rate of 5 Hz. With both parameter sets, the weight change is purely negative.

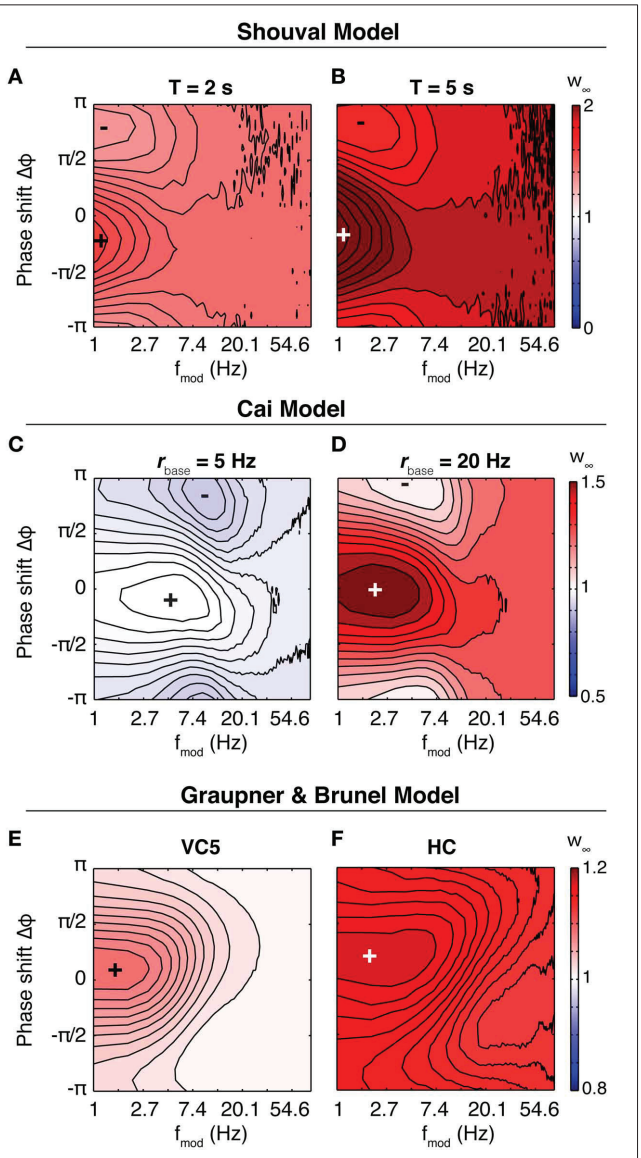

FIGURE 7 | Synaptic susceptibility in the calcium models. Top row: Final synaptic weights after 2 s **(A)** and 5 s **(B)** of stimulation in the Shouval model. Baseline firing rate is 5 Hz. The synaptic weight shows a phase dependence only for lowest modulation frequencies. The result is similar for other baseline firing rates (not shown). Middle row: Final weights in the Cai model. Baseline firing rate is 5 Hz **(C)** and 20 Hz **(D)**, duration of theta modulated firing is 10 s. At 5 Hz, the synapse shows a preference for modulation in the theta range (centered at ∼5 Hz). Neither of the two other models does something similar. Bottom row: Final synaptic weights in the model of Graupner and Brunel after 5 s of stimulation, with parameters fitted to VC5 **(E)** and HC **(F)**. Baseline firing rate is 10 Hz. Similar to above, the synapse reacts strongest to slow and slowest oscillations. Synapses in calcium models are low-pass filters.

Next, we investigate the effect of increasing oscillation amplitude on the synapse. We keep the modulation frequency fixed at 5 Hz with $\Delta\varphi = 0$, and vary the oscillation scaling parameter ε. In the case of the SC23 parameters (**Figure 9A**), the synapse potentiates for constant (unmodulated) firing for baseline rates greater than 5 Hz. Theta oscillations in the firing rates simply lead to an upscaling of this potentiation. We do the same analysis for an altered set of parameters (**Figure 9B**). We change τ_q to 50 ms instead of 500 ms. This tones down the activation and therefore potentiation, however, it affects the fitting error only slightly (increase from 0.81 to 1.1). In this case, the weight change for constant firing is negative everywhere. Introducing a periodic modulation then increases weight change, turning depression into potentiation, but only for baseline firing rates greater than 5 Hz.

To elucidate what parts of the model are responsible for this susceptibility, we did the analysis for confined versions of the CD model. The resulting weight change as a function of modulation frequency and phase difference is shown in **Figures 8D–F**, where we removed presynaptic adaptation, postsynaptic adaptation and activation q, respectively. The weight

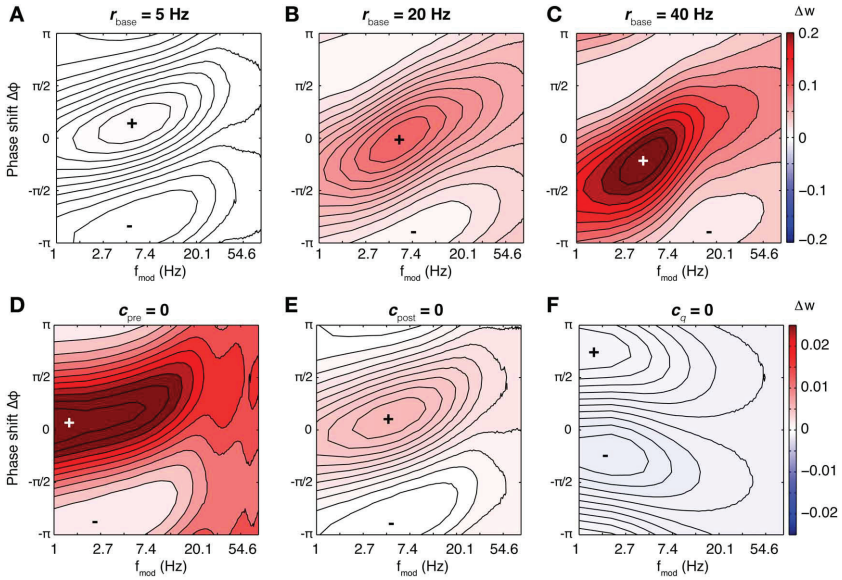

FIGURE 8 | Susceptibility in the CD model under varying conditions. For the base parameters for SC23 we repeated the simulations to compute the rate of weight change under different conditions. Top row: Weight change with increasing baseline firing rate (**A**: 5 Hz, **B**: 20 Hz, and **C**: 40 Hz). At low firing rates, the synapse behaves similar to linear spSTDP; maximal LTP occurs at $\Delta\varphi \approx \pi/6$ (compare **Figure 4**). With increasing firing rates, maximal potentiation also increases, and maximal LTP shifts toward slightly negative phase shifts (20 Hz: $\Delta\varphi \approx 0$ 40 Hz: $\Delta\varphi \approx -\pi/4$), while being centered at $f_{mod} \approx 5$ Hz. Bottom row: Influence of model constituents on susceptibility. Neurons fire at an average rate of 5 Hz. **(D)** CD model without presynaptic adaptation. The synapse is strongly sensitive to $\Delta\varphi$, however, there is no lower bound on f_{mod}. **(E)** Without postsynaptic adaptation. The susceptibility of the synapse is very similar to that of the undisturbed model (compare **A**). **(F)** Without activation q. The weight change is negative everywhere, and the synapse is not susceptible for some intermediate f_{mod}. Plots **(D,F)** change only slightly with increasing baseline firing rates. We conclude that of the model constituents, postsynaptic adaptation is not necessary to explain theta susceptibility in the non-linear regime.

change shows that presynaptic adaptation as well as activation are both important for theta susceptibility. Removing either one results in a low pass filter synapse. The link between these two variables is the threshold ϑ_q, as **Figure 9D** illustrates. Here, we show the weight change for the full model and parameters of SC23, except that $\vartheta_q < 0$. As a consequence, the synaptic susceptibility has no cutoff for low frequencies anymore. Interestingly, removing the threshold removes large part of the sensitivity to increasing oscillation amplitude (**Figure 9D**), which further underlines the importance of the interplay of presynaptic adaptation and activation for theta susceptibility.

4. DISCUSSION

We presented a new phenomenological model for dynamic synaptic plasticity, which unifies several experimental results in one framework. We analyzed the filter properties of this model, and compared them to a range of other models. We found that the CD model has unique properties which tie in with experimental findings on the connection of theta oscillations and memory formation, thus providing a mechanistic link between synaptic plasticity and the beneficial nature of theta-band oscillations for learning.

4.1. INTERPRETATION OF MODEL COMPONENTS AND PARAMETERS

Although most of the components of the CD model are only loosely guided by biophysical considerations, it is possible to relate them to specific perisynaptic processes, and to envision experiments for a more direct parameter estimation.

The spike traces y are very similar to the dynamics of bound glutamate at postsynaptic receptors and calcium dynamics in the synaptic bouton, which are essentially low-pass filtered action potentials. Due to the differential Hebbian learning rule at the core of the CD model, the decay constants of the spike traces determine the shape of the classical exponential STDP window; therefore, they can be directly estimated from varying the timing of a single pre- and postsynaptic spike pair.

The adaptive suppression u, which leads to a sublinear summation of synaptic change, has a dynamics reminiscent of presynaptic short-term depression (Tsodyks and Markram, 1997; Tsodyks et al., 1998). Its parameters can be determined by measuring the change of the synapse in response to adding leading presynaptic (postsynaptic) spikes to a pre-post (post-pre) spike pair and comparing the experimental result to the prediction of a spike pair model. Presynaptic short-term depression is a well-understood phenomenon, which has been shown to be present in many different cell types (Zucker and Regehr, 2002). Interestingly, the results of the fits of the reduced model indicate that short term depression considerably influences synaptic change and should be taken into account in quantitative models of synaptic plasticity. Some synapses show facilitation as well, and the CD model can easily be accommodated to include this also by adding one equation in a manner similar to Tsodyks et al. (1998). On the postsynaptic side, however, the mechanism behind the

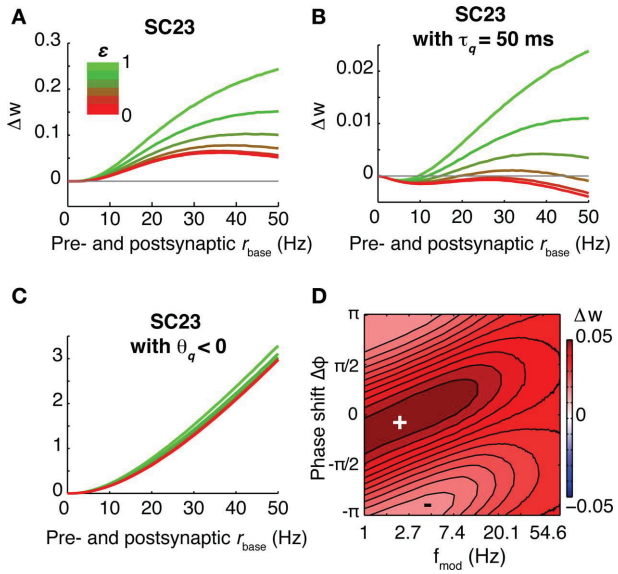

FIGURE 9 | Effect of different oscillation amplitudes, and negative threshold ϑ_q. (A–C) Show the rate of weight change as a function of common pre- and postsynaptic baseline firing rate for $\Delta\varphi = 0$, $f_{mod} = 5$ Hz and different oscillation amplitudes $\varepsilon \in [0, 1]$. **(A)** Parameters from SC23. Because of the strong contributions to q, the weight change is positive for all firing rates. Introducing the theta modulation increases weight change even more. **(B)** Parameters from SC23 with shorter time constant of activation: $\tau_q = 50$ ms instead of 500 ms. This manipulation increases the error from 0.81 to 1.1. Under this condition, imprinting theta oscillations on the neurons alters LTD to LTP. **(C)** Same as **(A)**, but with $\vartheta < 0$. Removing the threshold from the activation reduces the sensitivity to theta oscillations. **(D)** Weight change as a function of $\Delta\varphi$ and f_{mod}, with parameters as in **(C)**. The weight change is similar to spSTDP with strong bias toward LTP (**Figure 4C**). The maximal potentiation at 1 Hz modulation frequency occurs at negative phases.

adaptive process has been studied much less (Froemke et al., 2006; Gasparini, 2011); the details of the formalization will possibly have to be adapted as soon as more quantitative data becomes available.

The conditional activating variable q is a coincidence detector, which primes the synapse for supralinear potentiation. An interpretation is that q, if dependent on the presynaptic trace, reflects the calcium trace from NMDA receptors, which rely on the coincidence of glutamate binding and postsynaptic depolarization to lift the Mg^{2+} block (Clarke and Johnson, 2006). A negative threshold could mean that less calcium is needed for induction of LTP, or influx of calcium through voltage dependent calcium channels is sufficient for an elevated trace. The relaxed state value q_{min} on the other hand tunes the balance of LTP and LTD at the synapse. Under certain conditions, like in SC23, a pre-post pair leads to calcium influx which does not exceed the threshold for induction of LTP. A second postsynaptic spike added after the pair then "rides" on an elevated level of calcium, and the summed calcium contributions exceed this threshold. To estimate the parameters of activation with known postsynaptic adaptation, trailing postsynaptic spikes can be added to a pre-post-pair, with an additional post-pre-post triplet to find the sign of the threshold.

4.2. RELATION OF THE CD MODEL TO OTHER MODELS

In the last decade, a number of models for synaptic plasticity in response to spiking activity have been developed. Some of them are extensions of spSTDP, like the Triplet model, others are grounded on more biophysically plausible considerations, like the calcium models in general. The only model we know of which was fitted to the same four data sets as the CD model here is the recent calcium model by Uramoto and Torikai (2013). They used a different way to calculate the error of their fit, as they did not normalize the experimental results with the standard error of the mean (SEM). We repeated the calculation of the error with normalization by SEM, with the parameters given in the original article. The resulting errors are 0.85 for VC5, 2.4 for HC, 0.27 for SC23, and 27.39 for VC23. See **Tables 3**, **5** for comparison. The last value mostly results from the omission of the "$1 - 5 \times$ pre-post" experiments by the authors [**Figure 4D** in the original article of Froemke et al. (2006)], although the error without these experiments is still 9.2. These experiments most prominently highlight the role of presynaptic adaptation: Adding more presynaptic spikes in front of the pre-post pair reliably decreases the magnitude of synaptic potentiation. The Uramoto model has no mechanism which results in less postsynaptic calcium (less LTP) with increasing number of presynaptic spikes, a property shared with the Triplet model, Graupner model and Shouval model. Our quantitative analysis in the CD model showed that in the data sets where applicable (SC23 used only one presynaptic spike in each induction pattern), adding presynaptic adaptation considerably improves the error. However, presynaptic (and postsynaptic) adaptation can easily be implemented in all these models, for example by introducing Equation (9). Different formalizations are realized by Cai et al. (2007) and Kumar and Mehta (2011). We propose that adaptation is a mechanism that should in general be considered for the quantitative modeling of synaptic plasticity.

Among the existing phenomenological models of STDP, the Triplet model is the one most similar to our CD model. Both show similar fitting performance on visual cortex layer 5 and hippocampal data sets. Although it lacks true adaptation, two properties of the Triplet model partially mimic it: (1) with nearest neighbor interactions a spike causes the trace to attain a certain, constant value (from where it relaxes back). If the trace still is greater than zero, the impact of the subsequent spike is reduced; (2) a negative value for the triplet interaction A_3^+ works in the opposite direction of the normal spike pair interaction, leading to a sublinear summation of potentiation. In total, the CD model reaches a lower error than the Triplet model on all data sets, in SC23 and VC23 by a considerable margin. This suggests that the CD model generalizes better than the Triplet model. In addition, the components of the CD model have a more straightforward interpretation.

4.3. THETA SUSCEPTIBILITY IN DIFFERENT PLASTICITY MODELS

We investigated the filter properties of synaptic plasticity in a range of different models. For balanced spSTDP, we can give an explanation of the origin of the susceptibility to intermediate neuronal activity oscillation. spSTDP is equivalent to the formulation as differential Hebbian learning, Equations (2), (3). The traces y_i are driven by the spike trains x_i, and they "smear" out

the spike over time, which is basically the action of a low-pass filter. However, the weight change is proportional to the product of the presynaptic trace and the temporal derivative of the postsynaptic trace, $\dot{y}_{\text{post}}$. A temporal derivative accentuates (fast) changes, and its effect is similar to a high-pass filter. The result is a band-pass filter with an oscillation frequency of maximal efficiency given by Equation (22). If a moderate bias is introduced (see **Figures 4B,C**), the basic finding is distorted only slightly.

For non-linear models of synaptic plasticity that are based on spSTDP, the picture in general is similar as long as the average firing rate stays low, which keeps the dynamic equations in the linear regime. If the firing rate gets high enough that spikes in a neuron start to interact with each other, non-linear interactions will start to distort the susceptibility. For a mean firing rate of 5 Hz, the CD model stays in a near-linear regime, while in the Triplet model non-linear effects abandon susceptibility. Interestingly enough, with the right parameter choice the non-linearities in the CD model retain a band-pass behavior similar to the linear regime (**Figures 8A–C**). The susceptibility in the non-linear regime depends on the interplay of u_{pre} and q with a threshold for activation ϑ greater than zero. The action of presynaptic adaptation is to suppress y_{pre} for sustained constant firing of the presynaptic neuron. In fact, a mean field calculation shows that for parameters in VC23 in equilibrium and in the limit of high firing rates $\left\langle y_{\text{pre}}^{\infty} \right\rangle = 0.033 < \vartheta_q$. However, with oscillating neuronal firing, y_{pre} reaches a maximum early during the rise of the rate. The condition on the activation q leads to maximal increase if the postsynaptic firing rate is maximal at the same time. Therefore, q is maximal for slightly negative phases, which leads to the observed phase shift in the transition to the non-linear regime (increasing baseline firing rates).

We found that in contrast to spSTDP-based models, the synapse in the two calcium models without adaptation is simply a low pass filter, and prefers oscillations of both neurons that are in phase. This is due to the extensive low-pass filtering in the dynamical equations in these models. In both models, the contributions to the calcium concentration are low-pass filtered spike signals, which get low-pass filtered again in the calcium dynamics. As the calcium concentration depends on the sum of pre- and postsynaptic contributions, it is not surprising that maximal LTP occurs close to zero phase and slow oscillations. The Cai model is an example of a calcium model with synaptic short term dynamics. Here, the synapse shows a susceptibility to oscillatory modulation in the theta band, if the average firing rate is sufficiently low. Interestingly, our result seemingly conflicts with previous results. In the study of Kumar and Mehta (2011), it was shown that with the Shouval model the STDP window shows maximal malleability, that is the difference between maximal and minimal synaptic change, if the spike pairs are delivered with a repetition frequency of 5–15 Hz. This is very similar to our definition of susceptibility, where there exists a region of f_{mod} with pronounced and maximal difference between maximal and minimal weight change. However, in our study neuronal firing rate and oscillatory modulation (f_{mod}) are decoupled, while in the aforementioned study they are equal. Furthermore, we investigated the malleability under the condition of stochastic spiking. Here, spSTDP based models in a near linear regime show a preferred window of modulation frequency, while calcium based models prefer slow oscillations.

4.4. THETA SUSCEPTIBILITY IN SYNAPTIC PLASTICITY

Theta band (4–8 Hz) oscillations of both cortical (Landfield et al., 1972) and hippocampal (Berry and Thompson, 1978) local field potentials have been associated with memory processes early on. Later studies extended these findings across species and spatial scales, i.e., from intracellular membrane potential fluctuations in the rodent hippocampus (Harvey et al., 2009) to intracranial recordings in monkey cortex (Liebe et al., 2012) and extracranial EEG in humans (Kahana et al., 2001). Despite being observed throughout the brain, theta band oscillations appears to be generated by a network of hippocampal oscillators (Colgin, 2013), which is then transferred into cortical areas.

Although many studies have established a correlation between activity in the theta frequency band, so far no direct explanation for how theta rhythms influence memory processes has been found (Colgin, 2013). Some studies (Berry and Thompson, 1978; Seager et al., 2002; Nokia et al., 2008) report that the indicator for learning success is the increased oscillation amplitude before the onset of a trial. In other words, theta can be present without being linked to a certain task and still be beneficial. Others find that bursts delivered at theta frequency are optimal for induction of LTP (Larson et al., 1986), and LTD and LTP are inducted by bursting at different phases of a background theta oscillation: Presynaptic bursts at the peak of the oscillation potentiate the synapse, while bursts at the trough lead to synaptic depression (Pavlides et al., 1988; Hyman et al., 2003). In humans though, the situation is not as clear. Some studies find that increased theta power predicts learning success (Sederberg et al., 2003; Guderian et al., 2009; Lega et al., 2012), others emphasize theta synchronization and sometimes find decreased theta power (Mölle et al., 2002; Burke et al., 2013). One experimental study found that in successful learning single neurons show enhanced phaselocking to a background theta oscillation in the LFP, with a wide distribution of specific phase relations to this theta oscillation (Rutishauser et al., 2010). All these observations make it very likely that theta oscillations play a constructive role in the formation of memory.

The synaptic filter properties of several plasticity models reported here provide an explanation, as they endow the synapse with a susceptibility that is specific to oscillations in the theta range. This susceptibility does not rely on precise spike timing, i.e., a fixed phase relation of repeated spikes to an ongoing background theta oscillation. The distinction between the linear (similar to spSTDP) and non-linear regimes we found in the models makes two different scenarios likely of how theta susceptibility plays a role in learning. With low baseline firing rates [<10 Hz, reported in Rutishauser et al. (2010)] and a wide distribution of pairwise relative phases the synaptic changes are also expected to show a wide distribution of values. In a neuronal population firing at higher baseline rates the interplay of presynaptic adaptation and conditional activation shifts the phase requirement for strongest LTP to synchronous (phase zero) oscillation. How can a synapse capitalize on that? The scenario in **Figure 9** provides a possible answer. The synapse depresses

uniformly for neuronal constant firing. Introduction of theta band oscillations (5 Hz) shift up the weight change, but only for elevated baseline firing rates. The result is Hebbian learning ("those who fire together wire together"), as synapses between neurons which get no external excitation slightly depress. In this scenario, theta oscillations can be present before external stimulation, preparing the synapses for learning correlations of neuronal firing.

ACKNOWLEDGMENTS

We are grateful to Rob Froemke and colleagues for sharing their data from Froemke and Dan (2002) and Froemke et al. (2006) with us.

FUNDING

Christian Albers was funded by the German ministry of science and education (BMBF), grant number 01GQ0964. Joscha T. Schmiedt was funded by DFG Emmy Noether grant to Michael C. Schmid.

REFERENCES

Berry, S. D., and Thompson, R. F. (1978). Prediction of learning rate from the hippocampal electroencephalogram. *Science* 200, 1298–1300. doi: 10.1126/science.663612

Bi, G. Q., and Poo, M. M. (1998). Synaptic modifications in cultured hippocampal neurons: dependence on spike timing, synaptic strength, and postsynaptic cell type. *J. Neurosci.* 18, 10464–10472.

Burke, J. F., Zaghloul, K. A., Jacobs, J., Williams, R. B., Sperling, M. R., Sharan, A. D., et al. (2013). Synchronous and asynchronous theta and gamma activity during episodic memory formation. *J. Neurosci.* 33, 292–304. doi: 10.1523/JNEUROSCI.2057-12.2013

Cai, Y., Gavornik, J. P., Cooper, L. N., Yeung, L. C., and Shouval, H. Z. (2007). Effect of stochastic synaptic and dendritic dynamics on synaptic plasticity in visual cortex and hippocampus. *J. Neurophysiol.* 97, 375–386. doi: 10.1152/jn.00895.2006

Clarke, R. J., and Johnson, J. W. (2006). NMDA receptor NR2 subunit dependence of the slow component of magnesium unblock. *J. Neurosci.* 26, 5825–5834. doi: 10.1523/JNEUROSCI.0577-06.2006

Clopath, C., Büsing, L., Vasilaki, E., and Gerstner, W. (2010). Connectivity reflects coding: a model of voltage-based STDP with homeostasis. *Nat. Neurosci.* 13, 344–352. doi: 10.1038/nn.2479

Colgin, L. L. (2013). Mechanisms and functions of theta rhythms. *Annu. Rev. Neurosci.* 36, 295–312. doi: 10.1146/annurev-neuro-062012-170330

Dayan, P., and Abbott, L. F. (2005). *Theoretical Neuroscience: Computational and Mathematical Modeling of Neural Systems*. Cambridge, MA: MIT Press. ISBN: 978-0262541855.

Feldman, D. E. (2000). Timing-based LTP and LTD at vertical inputs to layer II/III pyramidal cells in rat barrel cortex. *Neuron* 27, 45–56. doi: 10.1016/S0896-6273(00)00008-8

Fell, J., and Axmacher, N. (2011). The role of phase synchronization in memory processes. *Nat. Rev. Neurosci.* 12, 105–118. doi: 10.1038/nrn2979

Froemke, R. C., and Dan, Y. (2002). Spike-timing-dependent synaptic modification induced by natural spike trains. *Nature* 416, 433–438. doi: 10.1038/416433a

Froemke, R. C., Tsay, I. A., Raad, M., Long, J. D., and Dan, Y. (2006). Contribution of individual spikes in burst-induced long-term synaptic modification. *J. Neurophysiol.* 95, 1620–1629. doi: 10.1152/jn.00910.2005

Gasparini, S. (2011). Distance- and activity-dependent modulation of spike back-propagation in layer V pyramidal neurons of the medial entorhinal cortex. *J. Neurophysiol.* 105, 1372–1379. doi: 10.1152/jn.00014.2010

Graupner, M., and Brunel, N. (2007). STDP in a bistable synapse model based on CaMKII and associated signaling pathways. *PLoS Comput. Biol.* 3:e221. doi: 10.1371/journal.pcbi.0030221

Graupner, M., and Brunel, N. (2012). Calcium-based plasticity model explains sensitivity of synaptic changes to spike pattern, rate, and dendritic location. *Proc. Natl. Acad. Sci. U.S.A.* 109, 3991–3996. doi: 10.1073/pnas.1109359109

Guderian, S., Schott, B. H., Richardson-Klavehn, A., and Düzel, E. (2009). Medial temporal theta state before an event predicts episodic encoding success in humans. *Proc. Natl. Acad. Sci. U.S.A.* 106, 5365–5370. doi: 10.1073/pnas.0900289106

Harvey, C. D., Collman, F., Dombeck, D. A., and Tank, D. W. (2009). Intracellular dynamics of hippocampal place cells during virtual navigation. *Nature* 461, 941–946. doi: 10.1038/nature08499

Hyman, J. M., Wyble, B. P., Goyal, V., Rossi, C. A., and Hasselmo, M. E. (2003). Stimulation in hippocampal region CA1 in behaving rats yields long-term potentiation when delivered to the peak of theta and long-term depression when delivered to the trough. *J. Neurosci.* 23, 11725–11731.

Kahana, M. J., Seelig, D., and Madsen, J. R. (2001). Theta returns. *Curr. Opin. Neurobiol.* 11, 739–744. doi: 10.1016/S0959-4388(01)00278-1

Kosko, B. (1986). Differential Hebbian learning. *AIP Conf. Proc.* 151, 277–282. doi: 10.1063/1.36225

Kumar, A., and Mehta, M. R. (2011). Frequency-dependent changes in NMDAR-dependent synaptic plasticity. *Front. Comput. Neurosci.* 5, 150–155. doi: 10.3389/fncom.2011.00038

Landfield, P. W., McGaugh, J. L., and Tusa, R. J. (1972). Theta rhythm: a temporal correlate of memory storage processes in the rat. *Science* 175, 87–89. doi: 10.1126/science.175.4017.87

Larson, J., Wong, D., and Lynch, G. (1986). Patterned stimulation at the theta frequency is optimal for the induction of hippocampal long-term potentiation. *Brain Res.* 368, 347–350. doi: 10.1016/0006-8993(86)90579-2

Lega, B. C., Jacobs, J., and Kahana, M. (2012). Human hippocampal theta oscillations and the formation of episodic memories. *Hippocampus* 22, 748–761. doi: 10.1002/hipo.20937

Liebe, S., Hoerzer, G. M., Logothetis, N. K., and Rainer, G. (2012). Theta coupling between V4 and prefrontal cortex predicts visual short-term memory performance. *Nat. Neurosci.* 15, 456–462, S1–S2. doi: 10.1038/nn.3038

Markram, H., Gerstner, W., and Sjöström, P. J. (2011). A history of spike-timing-dependent plasticity. *Front. Syn. Neurosci.* 3, 1–24. doi: 10.3389/fnsyn.2011.00004

Markram, H., Lubke, J., Frotscher, M., and Sakmann, B. (1997). Regulation of synaptic efficacy by coincidence of postsynaptic APs and EPSPs. *Science* 275, 213–215. doi: 10.1126/science.275.5297.213

Mölle, M., Marshal, L., Fehm, H. L., and Born, J. (2002). EEG theta synchronization conjoined with alpha desynchronization indicate intentional encoding. *Eur. J. Neurosci.* 15, 923–928. doi: 10.1046/j.1460-9568.2002.01921.x

Morrison, A., Diesmann, M., and Gerstner, W. (2008). Phenomenological models of synaptic plasticity based on spike timing. *Biol. Cybern.* 98, 459–478. doi: 10.1007/s00422-008-0233-1

Nevian, T., and Sakmann, B. (2006). Spine Ca2+ signaling in spike-timing-dependent plasticity. *J. Neurosci.* 26, 11001–11013. doi: 10.1523/JNEUROSCI.1749-06.2006

Nokia, M. S., Penttonen, M., Korhonen, T., and Wikgren, J. (2008). Hippocampal theta (3–8 Hz) activity during classical eyeblink conditioning in rabbits. *Neurobiol. Learn. Mem.* 90, 62–70. doi: 10.1016/j.nlm.2008.01.005

Pavlides, C., Greenstein, Y. J., Grudman, M., and Winson, J. (1988). Long-term potentiation in the dentate gyrus is induced preferentially on the positive phase of theta-rhythm. *Brain Res.* 439, 383–387. doi: 10.1016/0006-8993(88)91499-0

Pfister, J. P., and Gerstner, W. (2006). Triplets of spikes in a model of spike timing-dependent plasticity. *J. Neurosci.* 26, 9673–9682. doi: 10.1523/JNEUROSCI.1425-06.2006

Rutishauser, U., Ross, I. B., Mamelak, A. N., and Schuman, E. M. (2010). Human memory strength is predicted by theta-frequency phase-locking of single neurons. *Nature* 464, 903–907. doi: 10.1038/nature08860

Schmiedt, J.-T., Albers, C., and Pawelzik, K. (2010). "Spike timing-dependent plasticity as dynamic filter," in *Advances in Neural Information Processing Systems 23* (Columbia: MIT Press), 2110–2118. doi: 10.3389/conf.fncom.2010.51.00084

Seager, M. A., Johnson, L. D., Chabot, E. S., Asaka, Y., and Berry, S. D. (2002). Oscillatory brain states and learning: impact of hippocampal theta-contingent training. *Proc. Natl. Acad. Sci. U.S.A.* 99, 1616–1620. doi: 10.1073/pnas.032662099

Sederberg, P. B., Kahana, M., Howard, M. W., Donner, E. J., and Madsen, J. R. (2003). Theta and gamma oscillations during encoding predict subsequent recall. *J. Neurosci.* 23, 10809–10814.

Shouval, H. Z., Bear, M. F., and Cooper, L. N. (2002). A unified model of NMDA receptor-dependent bidirectional synaptic plasticity. *Proc.*

Natl. Acad. Sci. U.S.A. 99, 10831–10836. doi: 10.1073/pnas.152343099

Sjöström, P. J., Turrigiano, G. G., and Nelson, S. B. (2001). Rate, timing, and cooperativity jointly determine cortical synaptic plasticity. *Neuron* 32, 1149–1164. doi: 10.1016/S0896-6273(01)00542-6

Song, S., Miller, K. D., and Abbott, L. F. (2000). Competitive Hebbian learning through spike-timing-dependent synaptic plasticity. *Nat. Neurosci.* 3, 919–926. doi: 10.1038/78829

Tsodyks, M., and Markram, H. (1997). The neural code between neocortical pyramidal neurons depends on neurotransmitter release probability. *Proc. Natl. Acad. Sci. U.S.A.* 94, 719–723. doi: 10.1073/pnas.94.2.719

Tsodyks, M., Pawelzik, K., and Markram, H. (1998). Neural networks with dynamic synapses. *Neural Comput.* 10, 821–835. doi: 10.1162/089976698300017502

Uramoto, T., and Torikai, H. (2013). A calcium-based simple model of multiple spike interactions in spike-timing-dependent plasticity. *Neural Comput.* 25, 1853–1869. doi: 10.1162/NECO_a_00462

Wang, H. X., Gerkin, R. C., Nauen, D. W., and Bi, G. Q. (2005). Coactivation and timing-dependent integration of synaptic potentiation and depression. *Nat. Neurosci.* 8, 187–193. doi: 10.1038/nn1387

Wittenberg, G. M., and Wang, S. S.-H. (2006). Malleability of spike-timing-dependent plasticity at the CA3-CA1 synapse. *J. Neurosci.* 26, 6610–6617. doi: 10.1523/JNEUROSCI.5388-05.2006

Zhang, L. I., Tao, H. W., Holt, C. E., Harris, W. A., and Poo, M.-M. (1998). A critical window for cooperation and competition among developing retinotectal synapses. *Nature* 395, 37–44. doi: 10.1038/25665

Zucker, R. S., and Regehr, W. G. (2002). Short-term synaptic plasticity. *Annu. Rev. Physiol.* 64, 355–405. doi: 10.1146/annurev.physiol.64.092501.114547

Conflict of Interest Statement: The authors declare that the research was conducted in the absence of any commercial or financial relationships that could be construed as a potential conflict of interest.

Received: 28 June 2013; accepted: 04 November 2013; published online: 21 November 2013.

*Citation: Albers C, Schmiedt JT and Pawelzik KR (2013) Theta-specific susceptibility in a model of adaptive synaptic plasticity. Front. Comput. Neurosci. **7**:170. doi: 10.3389/fncom.2013.00170*

This article was submitted to the journal Frontiers in Computational Neuroscience.

APPENDIX

THE MODEL OF Shouval et al. (2002)

We decided to include a full description of the model from Shouval et al. (2002) here. We found the description given in the original article not sufficiently clear.

In this model, spikes from either the pre- or postsynaptic neuron influence the postsynaptic membrane potential with an EPSP (pre) or a back propagating action potential (bAP; post), which add linearly:

$$\begin{aligned} V(t) &= \int_{-\infty}^{t} \mathrm{EPSP}\left(t-t'\right) x_{\mathrm{pre}}\left(t'\right) dt' \\ &\quad + \int_{-\infty}^{t} \mathrm{bAP}\left(t-t'\right) c_{\mathrm{post}}\left(t'\right) dt' \qquad (23) \\ \mathrm{EPSP}(s) &= \Theta(s) A_{\mathrm{EPSP}}\left(e^{-s/\tau_s^{\mathrm{EPSP}}} - e^{-s/\tau_f^{\mathrm{EPSP}}}\right) \\ \mathrm{bAP}(s) &= \Theta(s) A_{bAP}\left(I_f^{\mathrm{bAP}} e^{-s/\tau_f^{\mathrm{bAP}}} + e^{-s/\tau_s^{\mathrm{bAP}}}\right), \end{aligned}$$

with $A_{\mathrm{bAP}} = 100\,\mathrm{mV}$, $\tau_{f,s}^{\mathrm{bAP}} = 3, 25\,\mathrm{ms}$, $I_{f,s}^{\mathrm{bAP}} = 0.75, 0.25$, and $\tau_{f,s}^{\mathrm{EPSP}} = 5, 50\,\mathrm{ms}$. A_{EPSP} depends on the time constants such that the maximum of the EPSP is exactly 1 mV. The model assumes that the only source of calcium into the postsynapse are the NMDA receptors. Each presynaptic spike opens a fraction of $P_0 = 0.5$ of all receptors still in the closed state, and in inter spike intervals the open receptors decay exponentially back to the closed state, however, with two components with different time constants. This translates to the following equations, where $\mathrm{NMDA}(t)$ is the fraction of open receptors at time t:

$$\begin{aligned} \dot{N}_f &= -\frac{N_f}{\tau_f} + P_0 I_f (1 - \mathrm{NMDA}\,(t-0)) x_{\mathrm{pre}} \\ \dot{N}_s &= -\frac{N_s}{\tau_s} + P_0 I_s (1 - \mathrm{NMDA}\,(t-0)) x_{\mathrm{pre}} \qquad (24) \\ \mathrm{NMDA}(t) &= N_f(t) + N_s(t)\,. \end{aligned}$$

$I_{f,s} = 0.5, 0.5$ set the relative amplitudes of the fast and the slow component, which decay back with time constants $\tau_{f,s} = 50, 200\,\mathrm{ms}$. Due to the voltage-dependent magnesium block of NMDA receptors, the resulting calcium current is a function of both the fraction of open receptors as well as the membrane potential:

$$\begin{aligned} I_{\mathrm{NMDA}}(t) &= G_{\mathrm{NMDA}} \cdot \mathrm{NMDA}(t)(V(t) - V_r) B(V)\,, \text{ with} \\ B(V) &= \left(1 + 0.28\exp(-0.062V)\right)^{-1}, \end{aligned} \qquad (25)$$

with V in mV, $V_r = 130\,\mathrm{mV}$ and $G_{\mathrm{NMDA}} = -0.02\frac{\mu M}{\mathrm{ms}\cdot\mathrm{mV}}$. The calcium concentration is a low pass filtered version of the current, with decay time constant τ_{Ca}:

$$\frac{d[Ca](t)}{dt} = I_{\mathrm{NMDA}}(t) - \frac{[Ca](t)}{\tau_{Ca}}\,. \qquad (26)$$

The central assumption in this model is now that synaptic change is completely ruled by the concentration of calcium in the postsynaptic spine. Low concentrations lead to LTD, high concentrations lead to LTP. Also, the learning rate is a monotonic function of calcium concentration:

$$\begin{aligned} \eta([Ca]) &= \left(\frac{0.1\,s}{[Ca]^3 + 10^{-5}} + 1s\right)^{-1} \\ \Omega([Ca]) &= 0.25 + \mathrm{sig}([Ca] - \alpha_2, \beta_2) \qquad (27) \\ &\quad - 0.25\mathrm{sig}([Ca] - \alpha_1, \beta_1) \\ \mathrm{sig}(x, \beta) &= \exp(\beta x)/(1 + \exp(\beta x)), \end{aligned}$$

where $[Ca]$ is measured in μM [in Equation 26 it is measured in mM]. The resulting weight change is finally:

$$\dot{W} = \eta([Ca])\left(\Omega([Ca]) - W(t)\right) \qquad (28)$$

STDP AND MEAN WEIGHT CHANGE WITH OSCILLATING FIRING RATES

In the mean field case, we investigated the rate of weight change in spSTDP with periodically oscillating firing rates. The rate as a function of time is given by Equation (18) We solved Equation (15) with these $r_i(t)$. After sufficient time ($t \gg \tau_i$), the transient is gone, and the solution for the traces is

$$y_i = \tau_i \left[1 + \frac{\varepsilon\cos\left(\omega t - \phi_i + \arctan(-\omega\tau_i)\right)}{\sqrt{1 + \omega^2\tau_i^2}}\right], \qquad (29)$$

where we replaced $\omega = 2\pi f_{\mathrm{mod}}$ for convenience. We now assume stable conditions, and calculate the rate of weight change:

$$\Delta w = \frac{1}{T}\int_0^T \left(q y_{\mathrm{pre}} r_{\mathrm{post}} - \frac{y_{\mathrm{pre}} y_{\mathrm{post}}}{\tau_{\mathrm{post}}}\right) dt\,. \qquad (30)$$

We replace $A_i = \varepsilon/\sqrt{1 + \omega^2\tau_i^2}$ and $\psi_i = \arctan(-\omega\tau_i)$ and get the solution:

$$\begin{aligned} \Delta w &= \Delta w_+ + \Delta w_- \\ &= \tau_{\mathrm{pre}}(q-1) + \frac{A_{\mathrm{pre}}}{2}\left(\varepsilon\cos(\psi_{\mathrm{pre}} + \Delta\varphi) - A_{\mathrm{post}}\cos\left(\psi_{\mathrm{pre}}\right.\right. \\ &\quad \left.\left. + \Delta\varphi - \psi_{\mathrm{post}}\right)\right). \qquad (31) \end{aligned}$$

DERIVATION OF $f_{\max}$

To gain insight into the reasons for theta susceptibility, we investigate spSTDP in the balanced case ($q = 1$). We are interested in the oscillation frequency at which the difference between potentiation and depression depending on phase difference becomes maximal. Instead of computing the derivative of Equation (31) with respect to ω, we explicitly use the functional form of y_{pre} and $\dot{y}_{\mathrm{post}}$ (see Equation 29):

$$\begin{aligned} y_{\mathrm{pre}} &= \tau_{\mathrm{pre}}\left[1 + A_{\mathrm{pre}}\cos\left(\omega t + \psi_{\mathrm{pre}}\right)\right] \\ \dot{y}_{\mathrm{post}} &= \omega\tau_{\mathrm{post}} A_{\mathrm{post}}\cos\left(\omega t + \psi_{\mathrm{post}} - \Delta\varphi - \pi/2\right). \end{aligned} \qquad (32)$$

y_{pre} is bounded between $1+\varepsilon$ and $1-\varepsilon$, and because of $0<\varepsilon<1$ it is strictly positive. The weight change is the integral of the product of both functions, therefore y_{pre} acts as a weighting function for $\dot{y}_{\text{post}}$. As a consequence, potentiation is maximal if the maxima of both functions coincide, i.e., the phases have to be identical. This is true for $\Delta\varphi = \psi_{\text{post}} - \psi_{\text{pre}} - \pi/2$ (Shifted by π for depression). At this phase shift, the rate of weight change becomes

$$\Delta w = \frac{1}{T}\int_0^T y_{\text{pre}}\,\dot{y}_{\text{post}}dt = \frac{1}{2}\frac{\varepsilon^2\tau_{\text{pre}}\tau_{\text{post}}}{\sqrt{1+\omega^2\tau_{\text{pre}}^2}\sqrt{1+\omega^2\tau_{\text{post}}^2}}. \quad (33)$$

We calculate the derivative with respect to ω:

$$\frac{2}{\varepsilon^2\tau_{\text{pre}}\tau_{\text{post}}}\frac{d\Delta w}{d\omega} = \frac{1}{\sqrt{1+\omega^2\tau_{\text{pre}}^2}\sqrt{1+\omega^2\tau_{\text{post}}^2}}\cdot \left(1-\frac{\tau_{\text{pre}}^2\omega^2}{1+\tau_{\text{pre}}^2\omega^2}-\frac{\tau_{\text{post}}^2\omega^2}{1+\tau_{\text{post}}^2\omega^2}\right) \quad (34)$$

To find the maximum $\omega_{\max}$, we set $d\Delta w/d\omega = 0$ and solve for ω:

$$f_{\max} = \frac{\omega_{\max}}{2\pi} = \frac{1}{2\pi\sqrt{\tau_{\text{pre}}\tau_{\text{post}}}}. \quad (35)$$

LIMITS OF PARAMETER VALUES IN THE FITTING PROCESS

The fitting process of the CD model and the Triplet model to the data was a brute force search in parameter space. For that, we defined a volume of space wherein the search was conducted. The bounds for that space are given in **Table 1** for the CD model and **Table 2** for the Triplet model. The range of possible values for ϑ_q is given by [0, 0.2], with one additional value <0, whose magnitude does not matter. Except in two cases the parameters always sat well within this space. In the case of the data in HC (Wang et al., 2005), the presynaptic adaptation time constant $\tau_{\text{pre}}^{\text{rec}}$ should be long, and the optimum lies at even longer times than given in **Table 3**. However, the influence of this parameter on the error is very small, and changes in $\tau_{\text{pre}}^{\text{rec}}$ do not change the other parameters much. Therefore we decided to set it to 3 s. In the Triplet model, in the fit to the data in SC23, the parameters τ_x and A_3^+ lie outside the bounds. When the first fit showed that those parameters hit the bounds, we decided to redefine the parameter space for this data set, in order to find a good minimum.

Chapter 3

Supervised learning

Up to this point, the plasticity processes considered all have been purely activity dependent. They are either based on experiments which measure synaptic change as a function of the neuronal activity (as in spSTDP, Triplet model, the CD model), or they are based on biophysical considerations and display STDP as an epiphenomen (Shouval model, Graupner model, Uramoto model). However, it is often hard to link these models to specific learning processes in neuronal networks, especially if the plasticity model is convoluted.
A different way to explore learning and the underlying plasticity is the concept of "supervised learning". Here, the objective of a learning system is clearly defined, and we can derive learning algorithms that specify the plasticity rules. The objective in supervised learning in neuronal networks is always formulated as desired input-output relations, i.e. the network is presented some input and it has to generate precisely defined output activity. The problem is that input-output relations of a network are defined by the synaptic weights, but it is rarely possible to assign synaptic weights in advance such that the output of the network exactly matches the desired target output. Instead, after the network layout (like neuron type(s), number of neurons and network structure) is chosen, the synapses are initialised randomly. With this initialization it performs some random task. In supervised learning the actual output, as defined by the current set of synaptic weights, is compared to the desired output. Then, the respective learning algorithm uses the difference to compute changes of synapses such that in future presentations of the input the actual output is closer to the desired output.
In the following, I present a number of different supervised learning rules. This is done for two reasons. First, it is more instructive to explain aspects of supervised learning with concrete examples. Second, in publication II I show the equivalence of an Anti-Hebbian STDP rule to the Perceptron Learning Rule, and in chapter 4 the memory capacity of several different learning algorithms is compared to the one of Membrane Potential Dependent Plasticity (MPDP). Introducing the reader to these rules therefore also prepares for publication II and the manuscript in chapter 4.

3.1 Supervised learning rules for classifiers

A certain way to think about neuronal networks is to view them as "classifiers". A network receives input and (nonlinearly) converts it into some output. However, often inputs can be put into categories. For example, pictures can be categorized based on their content, like wether they show animals or not. This mimicks how we perceive the world: We see objects and assign labels. Our reaction to those objects is then based on the respective label. In the context of neuronal networks, this idea is usually abstracted. Inputs are neuronal firing patterns, which are caused by some stimulus. This is a reflection of basic biology; an example is the retina, where light sensitive neurons convert the image into spiking activity.
Neuronal classifiers do not intrinsically know the correct labels. Instead, they have to be *trained*. The input labels are prepared by an outside supervisor, who during training observes the learning network. Based on errors in the label output, the supervisor computes changes of synaptic weights, which incrementally bring the network to correct classification. In the following, I present the perceptron and the tempotron, two basic examples of neuronal classifiers.

3.1.1 The perceptron

Although the perceptron is not defined for spiking neuronal networks, it is an instructive example for an application of a supervised learning rule and an important model of associative memory. It has been proposed by Rosenblatt in 1958, making it one of the oldest computational neuronal network models [42, 74].

Original formulation of the Perceptron Learning Rule

The task of the perceptron is to associate a set of given input patterns with specific output states. The learning system is a single layer feed forward neuronal network with N (presynaptic) input neurons and a single (postsynaptic) output neuron[1]. The neurons are binary rate-based units with states 0 or 1, inactive or active, respectively[2]. To explore the capabilities of the perceptron, the set of P input patterns is usually randomly generated. In each pattern $\mu \in \{1, \dots, P\}$, each input neuron with index $i \in \{1, \dots, N\}$ is in state $x_i^\mu \in \{0, 1\}$. Each input pattern is assigned a desired output state (or label) $y_d^\mu \in \{0, 1\}$.
Perceptrons can be trained efficiently with the Perceptron Learning Rule (PLR). Network training with the PLR is incremental. In one so-called *learning block* each of the P patterns is presented one after the other. "Presented" here means that the state of each input neuron is set externally to the respective state in the input

[1] From here on, the terminology mostly changes to input/output instead of presynaptic/postsynaptic neuron.

[2] There are many variants of perceptrons, for example with continuous valued input states.

pattern. The output neuron computes its respective state according to

$$\begin{aligned} h^\mu &= \sum_i w_i x_i^\mu \\ y^\mu &= \Theta(h^\mu - \theta) \ . \end{aligned} \tag{3.1}$$

w_i is the synaptic weight of neuron i, θ is the activity threshold of the neuron, and h^μ is the weighted sum of the input in response to pattern μ. After each presentation, a supervisor compares actual and desired output. If they are the same, i.e. $y_d^\mu = y^\mu$, no further action is required. If they are different, the weights are adjusted according to

$$\Delta w_i^\mu = \begin{cases} -\eta x_i^\mu & \text{if } y_d^\mu = 0 \\ \eta x_i^\mu & \text{if } y_d^\mu = 1 \ . \end{cases} \tag{3.2}$$

$\eta \ll 1$ is the learning rate. Usually the network is trained in batch mode where all weight changes are only applied after the learning block. If during a learning block no weights needed to be changed, then the network has learned all desired associations and training terminates. If there was at least one $\Delta w_i^\mu \neq 0$, training continues with the next learning block.
It was shown that the PLR has several desirable properties. With this rule, a network reaches the maximal memory capacity for associations between randomly generated input patterns (with $P(x_i^\mu = 1) = P(y_d^\mu = 1) = 1/2$) and output states. It was shown that the network can on average store at most $P = 2N$ random associations in its weights [42]. Furthermore, the training terminates in a finite number of steps if the associations are learnable at all. These traits make the PLR a valuable model of associative learning even after more than 50 years since its invention.
A common (geometric) interpretation of the perceptron is that of a linear classifier in an N-dimensional space. Input patterns are generated and assigned a label given by y_d^μ. The weight vector $\vec{w}$ after training is a normal vector on an $N-1$-dimensional hyperplane in the space of inputs that seperates the patterns of different labels. This interpretation helps understanding how the PLR can be adjusted to include error tolerance. Figure 3.1 illustrates this interpretation in the 2-dimensional case.

The PLR with a margin against input noise

The PLR can be extended to include a safety margin, which ensures that the output neuron will return the correct association even if the input pattern is corrupted by noise, i.e. some of the input neurons have randomly altered their state. According to the geometric interpretation of the perceptron, the computation of h^μ is equal to a scalar product between the weight vector and the input vector in the N-dimensional space of the inputs:

$$h^\mu = \sum_i w_i x_i^\mu = \vec{w} \cdot \vec{x}^\mu \ . \tag{3.3}$$

Input patterns lie on one of the two sides of the separating hyperplane. For every pattern on one side, the scalar product with the weights is positive, and negative

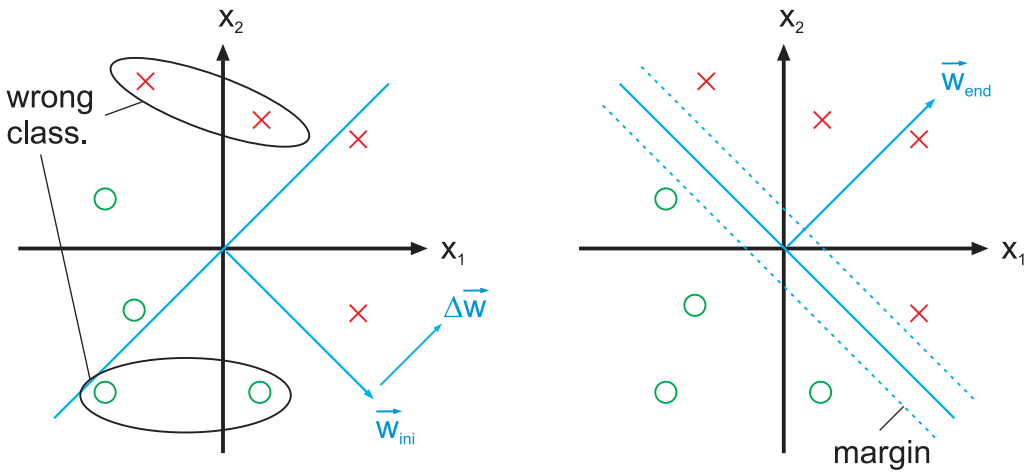

Figure 3.1: Illustration of the geometric interpretation of the perceptron. For illustration purposes the inputs x_1 and x_2 are not binary, but continuous valued. Red crosses indicate input pattern with desired output $y^\mu = 1$, green circles indicate desired output $y_d^\mu = 0$. Blue arrow shows the weight vector, the blue line perpendicular is the seperating hyperplane. Left figure shows the output before training. All patterns to the right of the seperating line generate the output $y^\mu = 1$, which is false for the green circles. The weight changes computed with the PLR rotate the weight vector in the correct direction. Right figure shows the state after learning with the PLR and the margin against noise. The weight vector has been rotated until all pattern lie on the correct side of the hyperplane. Because of the additional condition of a minimal distance of the input from the threshold the vector was rotated more than necessary for correct classification of the input. As a result, the input states can be slightly noisy and still lead to the correct output.

for those on the other side. The output of the postsynaptic neuron is determined by the sign of the weighted input and the firing threshold θ. The PLR rotates the weight vector until all patterns with one label are on one side, and those with the opposite label are on the other side. However, it stops when the last pattern is *just* on the correct side of the hyperplane. Naturally, the classification of this pattern is prone to errors. Randomly flipping input neurons is equal to random jitter of the input vector in the input space. If any input vector lies close to the separating hyperplane, it may move across it, and thus become falsely classified. This problem can be countered by over-learning until each input pattern lies at least some minimal distance, called the "margin", away from the hyperplane. Figure 3.1 illustrates the concept of the margin.
The margin is set to $N\kappa$, where κ is a parameter, and the factor N ensures the correct scaling with the number of input neurons. The PLR needs to be changed to accomodate for the margin:

$$\Delta w_i^\mu = \eta\Theta\left[N\kappa - (2y_d^\mu - 1)(h^\mu - \theta)\right](2y_d^\mu - 1)x_i^\mu \ . \tag{3.4}$$

The expression $(2y_d^\mu - 1)$ transforms the desired output states from $\{0, 1\}$ to $\{-1, +1\}$. This is necessary to have synaptic depression in the case of a pattern with $y_d^\mu = 0$; otherwise in this case weight changes would be always zero. The argument of the Heaviside function ensures that weight changes are only applied in the correct condition, i.e. the weighted input is on the wrong side of the margin. For $\kappa = 0$, this is equal to the PLR given above, equation (3.2). In the rest of this thesis, equation (3.4) is referred to as the Perceptron Learning Rule, as it is the more general formulation.

Derivation of the PLR from an objective

It is instructive to derive the PLR with the margin from an objective or error function. The objective is to make the postsynaptic neuron generate the correct output when presented with an input pattern. However, the formulation is important. The error function is zero when the weighted input h^μ has the correct sign and its magnitude is larger than the threshold against noise θ. A good choice is

$$E^\mu[\vec{w}] = \left[N\kappa - (h^\mu - \theta)(2y_d^\mu - 1)\right]_+ \ . \tag{3.5}$$

Here, $[x]_+$ is the rectifying bracket, defined as $[x]_+ = x$ if $x > 0$ and $[x]_+ = 0$ else. As previously, the output states y_d^μ have to be transformed to be in $\{-1, +1\}$, otherwise for silent output the error function would always be positive. The PLR is obtained by computing the negative derivative of equation (3.5) with respect to weight w_i:

$$-\frac{\partial E^\mu}{dw_i} = \Delta w_i^\mu = \Theta\left[N\kappa - (h^\mu - \theta)\,(2y_d^\mu - 1)\right](2y_d^\mu - 1)\,x_i^\mu \ , \tag{3.6}$$

which is equal to equation (3.4). Therefore, the PLR performs a gradient descent on the error function equation (3.5).

3.1.2 The tempotron

The perceptron is a linear classifier in an N-dimensional euclidean space and time is not defined in the perceptron setting. Translated to real neurons, a perceptron is a neuron sensitive to input firing rates which are constant for an extended period. However, this discards the ability of neurons to code for stimuli in a time-dependent manner. In an extreme case of temporal coding, all input neurons always fire with the same firing rate, but the temporal structure is specific to the respective stimulus. The tempotron is a network model that extends the idea of the perceptron classification to make use of spatio-temporal input patterns. It is a one-layered feed-forward network using spiking neurons [75]. The task is similar to the perceptron task: The output neuron should fire one or more spikes in response to a subset of the set of input patterns. Otherwise, it should remain silent. In other words, the tempotron performs a classification task on the input patterns using the temporal structure of the input.
Formally, the tempotron is defined as follows. The postsynaptic neuron is a LIF

neuron, equation (2.9). The presynaptic input neurons represent different stimuli through distinct spatio-temporal input patterns. In each input pattern, each presynaptic neuron spikes exactly once at time t_i^μ, where $i\{\in 1,\dots,N\}$ is the index of the input neuron and $\mu \in \{1,\dots,P\}$ is the index of the pattern. The times are drawn i.i.d. from the interval $[0,T]$, where T is the duration of the input. Because of the way the input patterns are generated, the firing rate in each pattern and each neuron is always the same. However, a presynaptic spike has an impact on the postsynaptic membrane potential only for the duration of its PSP. Therefore, at each point in time the "configuration" of inputs is different, and an appropriate learning rule allows the output neuron to identify characteristic sub-patterns. For each of the P input pattern a desired output is generated. We introduce a binary variable $y^\mu \in \{0,1\}$ that holds the desired responses or labels (to spike or not to spike). Usually, labels are generated such that $y^\mu = 1$ for one half of the patterns μ and zero for the other half. The network is initialized randomly, therefore before training the output is also random. During training, an input pattern is presented to the postsynaptic neuron, while spike generation is switched off. This means that the membrane potential is simply the sum of weighted PSPs at the respective spike times. After the presentation, the point in time t_{max} where the membrane potential reached its maximum is determined. Depending on y_μ and $V(t_{max})$ there are four different relevant cases: If $y^\mu = 1$ and $V(t_{max}) > V_{thr}$, or $y^\mu = 0$ and $V(t_{max}) < V_{thr}$, the actual response matches the desired one. Otherwise, weights need to be adjusted according to

$$\Delta w_i^\mu = \eta(2y^\mu - 1)\lambda_i(t_{max}) \ . \tag{3.7}$$

For simplicity we here introduce the "PSP sum", which is used several times throughout this chapter:

$$\lambda_i(t) = \sum_k \varepsilon(t - t_i^k) \ . \tag{3.8}$$

For generality, we here assume that presynaptic patterns can consist of more than only one spike, therefore t_i^k is the k-th spike of neuron i. $\varepsilon(s)$ is the PSP kernel given by equation (2.8). To put this in words, if the neuron should spike but the voltage stayed below the firing threshold for the entire duration of the input pattern, weights of neurons that fired before t_{max} have to be increased relative to their contribution to $V(t_{max})$. If the neuron should not spike but the voltage crossed the firing threshold, weights contributing to the absolute maximum have to be depressed. From these different cases it follows that the learning rule stops changing weights if for each of the P pattern the actual output matches the desired one.
Important analytical results were later obtained by Ran Rubin and colleagues [76]. They examined the memory capacity of a tempotron, i.e. the question of how many associations $\{\{t_i^\mu\}, y^\mu\}$ can be stored in the synaptic weights of an output neuron. They computed the cricital load $\alpha_c = N \cdot P_{max}$ were the probability of correct recall is still unity. They found that $\alpha_c \approx 3$, depending on the length of the input patterns and the parameters of the PSP kernel τ_s and τ_m.

3.2 The δ-rule

The δ-rule (also called e.g. Widrow-Hoff rule, adaline rule, and others [42]) is a very basic example of a supervised learning rule. To prepare for the δ-rule, in the following I first present the Rescorla-Wagner model of classical conditioning. It shares its formulation with the δ rule and provides a link between experimentally established animal behavior and abstract computational supervised learning algorithms. After that, I introduce the δ-rule. Its significance for this thesis is that it builds a bridge from results in behavioral experiments (captured in the Rescorla-Wagner model) to the abstract computational learning rules in artificial neuronal networks. The ReSuMe learning rule is directly derived from the δ-rule, and several recently developed supervised learning algorithms for spiking neuronal networks include a term that is very similar to the δ-rule.

The Rescorla-Wagner model

Classical conditioning is a training method to transfer the reaction to a so-called "unconditioned stimulus" (US) to a "conditioned stimulus" (CS) [65]. The most famous example is the Pavlovian dog, who through contingency learning is trained to salivate not only to the presentation of food (the US), but also when it hears a bell ringing (the CS). Another example is the classical eyeblink conditioning, where a tone or light signal is presented at the same time a puff of air is blown into the eye of an animal (commonly rabbits or rats) [77].
In the Rescorla-Wagner model, the magnitude of the response to the US is represented by λ. V is the magnitude of the response if the animal is presented the CS alone. Initially, it is zero. During training, both US and CS are presented simultaneously, and this presentation transfers the response to the CS. The change of the conditioned response is given by

$$V \to V + \Delta V = V + \beta(\lambda - V) \ . \tag{3.9}$$

β is the learning rate. This model correctly captures the fact that initially in each conditioning trial there is a relatively large change in behavior. Later in training, if the response to the CS is close to the one of the US, learning takes place in small steps, which is due to the proportionality to the difference of both responses.

Formulation of the δ-rule

The δ-rule is used to train neuronal networks. Similar to the perceptron, a number of input-output association should be imprinted in the weights of a (one-layered) feed-forward neuronal network. The inputs are real valued neuronal states ξ_i^μ, with i the index of the presynaptic neuron and μ the index of the pattern. Each input pattern has a target output, ζ^μ. The real-valued output is computed using

$$\mathcal{O}^\mu = g\left(\sum_i w_i \xi_i^\mu\right) \ . \tag{3.10}$$

$g(h)$ is the activation function of the postsynaptic neuron, which in the case of the δ-rule is often chosen to be linear, $g(h) = h$. Before training, the actual output will differ from the desired response. Therefore, the synaptic weights have to be changed to transform the actual output towards the desired one. The synaptic change is given by

$$w_i \to w_i + \Delta w_i = w_i + \eta \xi_i^\mu \left(\zeta^\mu - \mathcal{O}^\mu\right) \ . \tag{3.11}$$

Again, η is the learning rate. The formulation of the weight changes is the same as the change of conditioned response in the Rescorla-Wagner model, except that there is no explicit term for "presynaptic activity" in the latter model. However, implicitely, the change in the conditioned response results from the co presentation of the US with the CS, which can be considered as analogue to presynaptic activity in the δ-rule.
Similar to the PLR, the δ-rule can be derived as a gradient descent from a quadratic error function. It is given by

$$E(w) = \sum_\mu \left(\zeta^\mu - \mathcal{O}^\mu\right)^2 \ . \tag{3.12}$$

Computing the negative derivative with respect to weight w_i using (3.10) and $g(h) = h$ will lead to equation (3.11).

3.3 Learning algorithms in networks of stochastic spiking networks

In the recent years several supervised learning algorithms have been developed to train spiking neuronal networks to generate time dependent activity patterns. One example was recently proposed by Urbanczik and Senn [78]. Here I reproduce this model, since it presents an elaborate way to introduce a teacher into the learning system. Also, the principal learning rule is very similar to the rules of Xie and Seung [79], Pfister and colleagues [80] and Brea and colleagues [38]. I relate the rule of Urbanczik and Senn to the other ones at the end of this section.
In the model of Urbanczik and Senn, the postsynaptic neuron is divided into two separate but connected compartments: the soma and the dendritic tree. Soma and dendritic tree receive seperate synaptic input. The somatic membrane potential $U(t)$ is modelled as a conductance based LIF neuron, given by

$$\dot{U} = -g_L U + g_D(V_w - U) + I_U^{som} \ . \tag{3.13}$$

g_L is the leak conductance, g_D is the uni-directional coupling conductance of the dendritic compartement to the soma, V_w is the membrane potential in the dendritic compartement, and I_U^{som} is the input current from the synapses projecting directly onto the soma. This latter term is given by

$$I_U^{som} = g_E(E_E - U) + g_I(E_I - U) \ , \tag{3.14}$$

where $g_{E,I}$ are the time dependent total conductances of excitatory and inhibitory synapses, and $E_{E,I}$ are the respective reversal potentials. Spiking is stochastic and the instantaneous firing rate is a function of the somatic voltage, $r(U(t))$. The dendritic membrane potential is modelled as a simple LIF neuron without spiking and without feedback from the soma. Therefore, the dendritic voltage is a simple sum of the weighted PSPs:

$$V_w = \sum_i w_i \sum_k \varepsilon\left(t - t_i^k\right) \ , \tag{3.15}$$

where as usual t_i^k denotes the time of the k-th input spike of presynaptic neuron i with synaptic weight w_i. To derive the learning rule, two seperate cases of interest for the evolution of the somatic voltage are investigated. In the first case, the somatic synapses stay silent, so that the input to the somatic compartement is completely determined by the dendritic voltage. The somatic potential is a low-pass filtered version of the dendritic potential and if $g_D \gg g_L$, it can be approximated by

$$V_w^\star(t) \approx \frac{g_D}{g_D + g_L} V_w(t) \ . \tag{3.16}$$

The respective firing rate of the soma is $r(V_w^\star)$. In the second case, the dendrite receives no input, therefore $V_w(t) \equiv 0$. The time course of the somatic synaptic conductances defines the so-called matching potential, effectively a time-dependent reversal potential defined by g_E and g_I:

$$U_M(t) = \frac{g_E(t)E_E + g_I(t)E_I}{g_E(t) + g_I(t)} \ . \tag{3.17}$$

The given task is to associate a dendritic input pattern with a "teacher" input pattern of the somatic synapses. The latter input defines a matching potential, and the dendritic inputs have to generate a "prediction" of the somatic potential such that after training $V_w^\star(t) = U_M(t)$. It would be easiest to base the learning rule on the difference of $V_w^\star$ and U_M, however they are not readily available at synapses. Instead, what is compared are the firing rate estimations, $r(U(t)) - r(V_w^\star)$. The actual somatic membrane potential $U(t)$ can be used because it is situated between U_M and $V_w^\star$. Shifting $V_w^\star$ towards U_M therefore also shifts U towards the target. The estimation of the current firing rate is done by the actual spiking, since any postsynaptic spike train $S(t) = \sum_{out} \delta(t - t_{out})$ is a stochastic realization of the underlying firing rate. This additionally means that learning has to be averaged over several teaching trials. Altogether, the difference analogous to the δ-rule is $S(t) - r(V_w^\star(t))$[3], with which we can define a plasticity induction variable:

$$\mathrm{PI}_i(t) = \left(S(t) - r(V_w^\star(t))\right) h\left(V_w^\star(t)\right) \lambda_i(t) \ . \tag{3.18}$$

$\lambda_i(t)$ is again the PSP sum defined in equation (3.8)[4]. $h(x)$ is a positive weighting function that effectively determines "sensitive" regions of the plasticity rule. Here,

[3] Reference [78] gives the full derivation. See also [80].

[4] Technically, the PSP sum is the derivative of V_w with respect to weight w_i.

$h(x) = d/dx \ln r(x) = r'(x)/r(x)$. The weight change is finally computed by low-pass filtering $\mathrm{PI}_i(t)$:

$$\begin{aligned} \tau_s \dot{\Delta}_i &= \mathrm{PI}_i(t) - \Delta_i \\ \dot{w}_i &= \eta \Delta_i \ . \end{aligned} \tag{3.19}$$

The rules devised by Xie and Seung [79] and Brea and colleagues [38] work on a different setting. The neurons are modelled as single compartement LIF neurons, either in a feed-forward network or recurrent network. Pfister and colleagues derive the learning rule, equation (3.18), from the probability of emitting a desired spike train $S(t)$ given the time course of the membrane potential $V(t)$ as a function of input spikes weighted by synaptic weights and spike-induced voltage resets. The rule proposed by Brea and colleagues differs slightly in the function $h(r)$. In the model of Xie and Seung, the spike train is self-generated, i.e. it is a function of synaptic inputs. In each training trial, the weight changes are collected in an eligibility trace, and afterwards the spiking activity is compared to a target. From the similarity a reward is computed, and the effective weight change is the product of eligibility trace and reward[5]. In the work of Brea and colleagues, the postsynaptic neuron is clamped to spike at desired times to produce a teacher signal for the learning rule.

3.4 Spike time learning in deterministic networks

In the following, I present learning algorithms designed to train a network to produce spikes at precisely defined times. The basic setting is identical for all learning rules. It is a single-layer feed-forward network of spiking neurons with a LIF output neuron. In contrast to the previous section, the output neuron is fully deterministic. The goal is to learn a number of input-output associations. Inputs are defined as spatio-temporal spike patterns, while the the output is defined as precisely timed spikes of the output neuron. In comparison, in tempotron training the timing of output spikes is not important. Because of this difference, the trained network is sometimes called a "chronotron" [81]. Training always takes place over several learning blocks until the actual output matches the target.

3.4.1 The Remote Supervised Method (ReSuMe)

The δ-rule is defined for neuronal networks of rate-based neurons and has no time dependency: Updates are assigned after presentation of a (static) pattern. The rules devised for stochastic neurons are basically equivalent to a time-dependent δ-rule, but because of the strong non-linearity of spike generation, they are not suited for deterministic neurons. However, the δ-rule can be made amenable for these, as shown by Ponulak and Kasinski [82] in their Remote Supervised Method algorithm (ReSuMe). The formerly static weight change equation (3.11) is replaced

[5] Urbanczik and Senn highlight that the same can be done using their model

by a temporal derivative of the weight, which also necessitates to treat the activities as functions of time:

$$\dot{w}_i = \xi_i^\mu(t)\left(\zeta^\mu(t) - \mathcal{O}^\mu(t)\right) \ . \tag{3.20}$$

The learning rate is set to $\eta = 1$ (see below). The total weight change is the integral of $\dot{w}_i$. Spikes are modelled as sums of δ-functions:

$$S_x(t) = \sum_{t_x} \delta(t - t_x) \ . \tag{3.21}$$

Here, $x \in \{i, d, o\}$ denotes the location and the type of spike. For example, t_i denotes input spike times, t_d denotes desired or target spike times for the postsynaptic neuron, and t_o are the times of spikes the postsynaptic neuron generates in response to the synaptic input. However, it is not possible to replace the activities in equation (3.20) directly with the spike trains $S_x(t)$, since the δ-functions has zero width in time and therefore the weight change term would always be zero. Instead, the effect of spikes gets spread out in time, by convolving the input spikes with a temporal kernel. The input activity is replaced by

$$\xi_i(t) = \left[c + \int_0^\infty \phi(s) S_i(t-s) ds \right] \ . \tag{3.22}$$

$\phi(s)$ is a kernel which converts the discrete spiking events into a function in time with finite width. c is a constant whose significance is explained below. This transformation of the presynaptic activity allows to use the postsynaptic spike trains to compute weight changes:

$$\dot{w}_i = (S_d(t) - S_o(t)) \left[c + \int_0^\infty \phi(s) S_i(t-s) ds \right] \ . \tag{3.23}$$

Now the role of c can be clarified. The first term on the right hand side of equation (3.23) is the difference of the target spike train and the actual spike train. If we assume for the moment that the kernel $\phi(s)$ is zero, then for each desired spike each weight will increase by c, while for each actual spike it would decrease by c. The weight changes become balanced if the number of actual spikes matches the number of desired spikes. Therefore, c is a constant which assures that the postsynaptic output neuron displays the desired activity level.

Specificity of the weight changes to the input can be achieved with a suitable choice of the kernel ϕ. It has to make sure that after a learning trial the probability that the output neuron generates the desired spikes increases. For this it is necessary that the kernel is causal, i.e. that it only changes synaptic weight w_i if the presynaptic neuron fired a spike before either a desired or actual output spike. The reason is that presynaptic spikes can only causally influence the postsynaptic neuron. Furthermore, the kernel should be restricted, because the influence of a presynaptic spike is restricted by the duration of the PSP. In practice, a good choice for the

kernel is an exponential decay, $\phi(s) = A\Theta(s)\exp(-s/\tau)$. A is the amplitude of the kernel, which also sets the learning rate. τ is the decay time constant of the exponential function, and it sets the range of temporal interactions of pre- and postsynaptic spikes. It should be in the order of the membrane time constant such that both plasticity interactions and PSP decay on a similar time scale.
ReSuMe can be understood on a heuristic level. Similar to the CD model (see publication I), presynaptic spikes leave a decaying trace at the synapse. At the time of a desired spike t_d a signal is send to all synapses, and they potentiate proportional to the current value of the trace. This way, target spikes are always reinforced. The opposite is true for actual spikes. Each time the postsynaptic neuron spikes by itself, a signal is send to synapses to depress proportional to the current trace. Therefore, actual spikes are treated as spurious. However, ReSuMe has a stop condition: Weight changes cancel as soon as the actual spike train is identical to the target spike train, $S_o(t) \equiv S_d(t)$.

3.4.2 E-Learning

While ReSuMe is a simple and easy to understand learning algorithm, its performance was found to be lacking [81]. The number of spike associations that can be imprinted in a feed-forward neuronal network with ReSuMe is quite low. A learning algorithm with better performance is E-Learning[6], which was conceived by Răzvan Florian in 2012 [81]. E-Learning is a gradient descent rule on the Victor-Purpura (VP) distance between spike trains [83]. To explain the E-Learning algorithm, I first describe the VP distance and the algorithm to compute it.
Suppose we are given two different spike trains defined by their spike times $S_o = t_o^1, t_o^2, \ldots, t_o^m$ and $S_d = t_d^1, t_d^2, \ldots, t_d^n$. In the context of E-Learning, S_o is the set of actual output spike times, and S_d is the set of desired spike times to be learned. The general goal is to compute a measure of the similarity $K(S_o, S_d)$ between the two. In the VP distance, the similarity is computed by transforming one spike train into the other. Transformation is performed by either deleting, inserting, or shifting spikes of one spike train until it is equivalent to the other. Each operation is assigned a cost, and the VP distance is the minimal cost necessary for the complete transformation. Deletion and insertion of a spike each have a cost of 1, while shifting a spike has a cost of $\Delta t/\tau_q$, where τ_q is a parameter of the VP distance, and Δt is the distance in time of the starting and end point of the shifted spike. If a spike has to be shifted a distance $\Delta t > 2\tau_q$, then the cost of this operation is greater than 2, and it is cheaper to just delete the spike and re-insert it at the desired time. In figure 3.2 the basic process is illustrated.
A simple and fast algorithm can be used to compute the minimal cost of transforming spike trains. $G_{i,j}$ is the cost to transform the partial spike train of the first i spikes of S_o into the partial spike train of the first j spikes of S_d. This cost is computed as

$$G_{i,j} = \min\left\{G_{i-1,j} + 1, G_{i,j-1} + 1, G_{i-1,j-1} + q|t_o^i - t_d^j|\right\} \ . \tag{3.24}$$

[6]Florian gives no explanation for the name.

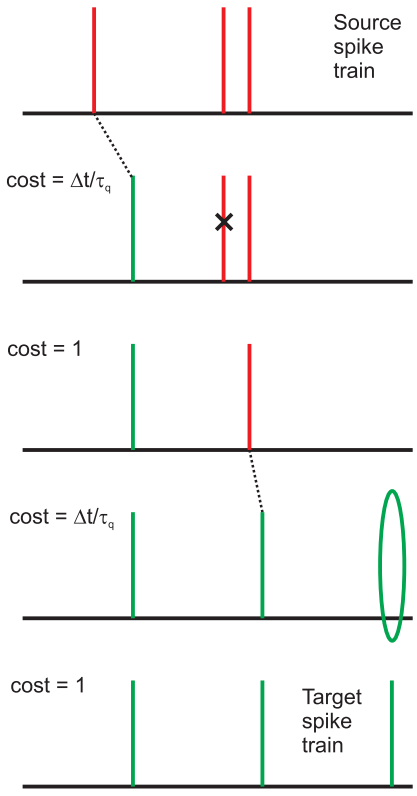

Figure 3.2: Illustration of the transformation of source spike train into the target spike train. Spikes can be shifted, deleted or added, with a specific cost for each transformation step. In this example the left spike gets shifted, then the second spike is deleted, the third spike is shifted, and a new spike is inserted. The cost for each transformation step is given in the graphic. The VP-algorithm (see text) can be used to compute the minimal transformation cost.

Therefore, by successively adding spikes to partial spike trains and testing which addition minimizes the cost, the total minimal cost of transformation can be computed. Starting from $G_{m,n}$, it is possible to reconstruct the actual transformations of the minimal distance.
During training with E-Learning, the input pattern is presented and the output S_o is recorded. Afterwards, the VP distance of both patterns is computed and all spikes in sets S_o and S_d are sorted into three distinct sets:

- Output spikes which got deleted from S_o by the VP algorithm are put into the set $D = \{t^{del}\}$.
- Desired spikes which got inserted into S_o are put into the set $J = \{t^{ins}\}$.
- The last set contains the spike pairs from S_o and S_d which got shifted, $S = \{t^{act}, t^{des}\}$.

The spikes in D and J are "unpaired". S contains paired spikes, which means that each t^{act} in S has a spike t^{des} in S which is closer in time than $2/q$. With these sets of spikes, the full E-Learning rule is then:

$$\Delta w_i = \gamma \left[\sum_{t^{ins}} \lambda_i(t^{ins}) - \sum_{t^{del}} \lambda_i(t^{del}) + \frac{\gamma_r}{\tau_q^2} \sum_{(t^{act},t^{des})} (t^{act} - t^{des}) \lambda_i(t^{act}) \right] . \qquad (3.25)$$

The first two terms are similar to ReSuMe, except E-Learning uses the PSP kernel. t_{ins} are unpaired desired spikes which need reinforcement, comparable to the set

S_d in ReSuMe. Similarly, t^{del} are actual spurious output spikes which should be extinguished. The difference is the treatment of paired spikes in E-Learning. The weight changes scale with the timing difference. This leads to a much smoother convergence of learning and subsequently to an increase of the memory capacity by a factor of 5 over ReSuMe [81]; and see chapter 4 for similar quantitative results.

3.4.3 FP-Learning

Another heuristic learning algorithm was proposed by Memmesheimer and colleagues with FP-Learning [39] (short for Finite Precision-Learning). They identified a central problem of learning rules like ReSuMe: Spurious spikes distort the membrane potential for a short period of time behind them, which usually leads to false (spurious) weight changes. This hinders convergence and therefore reduces capacity. To prevent this problem, the FP-Learning algorithm continuously monitors the output of the learning neuron and stops the learning trial if any error is encountered. For every desired output spike, it checks if there is exactly one actual output spike within some window of tolerance around the desired spike. If not, the algorithm stops the learning trial immediately. Synaptic potentiation is applied to make it more probable that the output neuron generates the spike in future learning trials. Also, if the algorithm encounters a spurious spike, the algorithm stops the learning trial and depresses weights contribution to the unwanted spike. In both cases, after changing weights the algorithm starts a new learning trial from the beginning.
FP-Learning is formally defined as follows. The network and task are similar as in ReSuMe and E-Learning, i.e. a set of desired spike times S_d has to be imprinted in the weights of a single layered feed-forward network. The single output neuron is a LIF neuron, equation (2.9). A difference to the other learning algorithms is that the output spikes do not need to be exactly at the times t_d. Instead, a window of tolerance of width 2ϵ is introduced, where ϵ is a parameter of the learning algorithm. The desired output spike can be anywhere in the interval $[t_d - \epsilon, t_d + \epsilon]$, and there has to be exactly one output spike within each interval, and no spikes at any other time. In a learning trial, the output neuron receives input and the membrane potential $V(t)$ and output spikes are computed. Each time the output neuron spikes, the algorithm checks the following:

1. If the output spike is the first spike in any window of tolerance around any desired spike time t_d, then everything is in order and the learning trial continues without further interference.

2. If the output spike lies outside any window of tolerance, or if it is the second spike within such a window, it is treated as a spurious spike. The time of this spike is called t_{err}. The learning trial is interrupted and synaptic weights are changed according to
$$\Delta w_i = -\eta \lambda_i(t_{err}) \ . \tag{3.26}$$
After changing the weights, a new learning trial from the beginning is initated.

λ_i is the PSP sum at synapse i, equation (3.8). Additionally, the algorithm performs a second type of check at each time $t_d + \epsilon$. If there is exactly one spike within the respective window of tolerance, the desired output was generated and the learning trial continues without further interference. If there was no spike within this window, then this is an error needing correction. Weights are changed by

$$\Delta w_i = +\eta \lambda_i (t_d + \epsilon) \ . \tag{3.27}$$

Also, the training trial ends immediately and a new trial from the beginning is initiated. Learning has converged if all learning trials (of a learning block) have been have finished uninterrupted.
The window of tolerance ϵ around each t_d gives FP-Learning its name, since it is central to the algorithm. After the first spike has been learned successfully, the algorithm will try to learn the next spike. However, weight changes applied to learn the latter spike will usually nudge the first spike out of its position. Without tolerance in the output spike times, any nudging, no matter how small, will cause the algorithm to nudge it back, which then impacts the second spike, and so on. Therefore, the output is given some leeway to allow the algorithm to converge.
Memmesheimer and colleagues compared the memory capacity attainable with FP-Learning to the one of another algorithm with optimal memory capacity (the HTP learning algorithm [39]), and found that FP-Learning achieves maximal capacity in the spike time learning task.

3.5 Publication II: Perfect Associative Learning with Spike-Timing-Dependent Plasticity

Perfect Associative Learning with Spike-Timing-Dependent Plasticity

Christian Albers
Institute of Theoretical Physics
University of Bremen
28359 Bremen, Germany
calbers@neuro.uni-bremen.de

Maren Westkott
Institute of Theoretical Physics
University of Bremen
28359 Bremen, Germany
maren@neuro.uni-bremen.de

Klaus Pawelzik
Institute of Theoretical Physics
University of Bremen
28359 Bremen, Germany
pawelzik@neuro.uni-bremen.de

Abstract

Recent extensions of the Perceptron as the Tempotron and the Chronotron suggest that this theoretical concept is highly relevant for understanding networks of spiking neurons in the brain. It is not known, however, how the computational power of the Perceptron might be accomplished by the plasticity mechanisms of real synapses. Here we prove that spike-timing-dependent plasticity having an anti-Hebbian form for excitatory synapses as well as a spike-timing-dependent plasticity of Hebbian shape for inhibitory synapses are sufficient for realizing the original Perceptron Learning Rule if these respective plasticity mechanisms act in concert with the hyperpolarisation of the post-synaptic neurons. We also show that with these simple yet biologically realistic dynamics Tempotrons and Chronotrons are learned. The proposed mechanism enables incremental associative learning from a continuous stream of patterns and might therefore underly the acquisition of long term memories in cortex. Our results underline that learning processes in realistic networks of spiking neurons depend crucially on the interactions of synaptic plasticity mechanisms with the dynamics of participating neurons.

1 Introduction

Perceptrons are paradigmatic building blocks of neural networks [1]. The original Perceptron Learning Rule (PLR) is a supervised learning rule that employs a threshold to control weight changes, which also serves as a margin to enhance robustness [2, 3]. If the learning set is separable, the PLR algorithm is guaranteed to converge in a finite number of steps [1], which justifies the term 'perfect learning'.

Associative learning can be considered a special case of supervised learning where the activity of the output neuron is used as a teacher signal such that after learning missing activities are filled in. For this reason the PLR is very useful for building associative memories in recurrent networks where it can serve to learn arbitrary patterns in a 'quasi-unsupervised' way. Here it turned out to be far more efficient than the simple Hebb rule, leading to a superior memory capacity and non-symmetric weights [4]. Note also that over-learning from repetitions of training examples is not possible with the PLR because weight changes vanish as soon as the accumulated inputs are sufficient, a property

which in contrast to the naïve Hebb rule makes it suitable also for incremental learning of associative memories from sequential presentation of patterns.

On the other hand, it is not known if and how real synaptic mechanisms might realize the success-dependent self-regulation of the PLR in networks of spiking neurons in the brain. For example in the Tempotron [5], a generalization of the perceptron to spatio-temporal patterns, learning was conceived even somewhat less biological than the PLR, since here it not only depends on the potential classification success, but also on a process that is not local in time, namely the localization of the absolute maximum of the (virtual) postsynaptic membrane potential of the post-synaptic neuron. The simplified tempotron learning rule, while biologically more plausible, still relies on a reward signal which tells each neuron specifically that it should have spiked or not. Taken together, while highly desirable, the feature of self regulation in the PLR still poses a challenge for biologically realistic synaptic mechanisms.

The classical form of spike-timing-dependent plasticity (STDP) for excitatory synapses (here denoted CSTDP) states that the causal temporal order of first pre-synaptic activity and then postsynaptic activity leads to long-term potentiation of the synapse (LTP) while the reverse order leads to long-term depression (LTD)[6, 7, 8]. More recently, however, it became clear that STDP can exhibit different dependencies on the temporal order of spikes. In particular, it was found that the reversed temporal order (first post- then presynaptic spiking) could lead to LTP (and vice versa; RSTDP), depending on the location on the dendrite [9, 10]. For inhibitory synapses some experiments were performed which indicate that here STDP exists as well and has the form of CSTDP [11]. Note that CSTDP of inhibitory synapses in its effect on the postsynaptic neuron is equivalent to RSTDP of excitatory synapses. Additionally it has been shown that CSTDP does not always rely on spikes, but that strong subthreshold depolarization can replace the postsynaptic spike for LTD while keeping the usual timing dependence [12]. We therefore assume that there exists a second threshold for the induction of timing dependent LTD. For simplicity and without loss of generality, we restrict the study to RSTDP for synapses that in contradiction to Dale's law can change their sign.

It is very likely that plasticity rules and dynamical properties of neurons co-evolved to take advantage of each other. Combining them could reveal new and desirable effects. A modeling example for a beneficial effect of such an interplay was investigated in [13], where CSTDP interacted with spike-frequency adaptation of the postsynaptic neuron to perform a gradient descent on a square error. Several other studies investigate the effect of STDP on network function, however mostly with a focus on stability issues (e.g. [14, 15, 16]). In contrast, we here focus on the constructive role of STDP for associative learning. First we prove that RSTDP of excitatory synapses (or CSTDP on inhibitory synapses) when acting in concert with neuronal after-hyperpolarisation and depolarization-dependent LTD is sufficient for realizing the classical Perceptron learning rule, and then show that this plasticity dynamics realizes a learning rule suited for the Tempotron and the Chronotron [17].

2 Ingredients

2.1 Neuron model and network structure

We assume a feed-forward network of N presynaptic neurons and one postsynaptic integrate-and-fire neuron with a membrane potential U governed by

$$\tau_U \dot{U} = -U + I_{syn} + I_{ext}, \tag{1}$$

where I_{syn} denotes the input from the presynaptic neurons, and I_{ext} is an input which can be used to drive the postsynaptic neuron to spike at certain times. When the neuron reaches a threshold potential U_{thr}, it is reset to a reset potential $U_{reset} < 0$, from where it decays back to the resting potential $U_\infty = 0$ with time constant τ_U. Spikes and other signals (depolarization) take finite times to travel down the axon (τ_a) and the dendrite (τ_d). Synaptic transmission takes the form of delta pulses, which reach the soma of the postsynaptic neuron after time $\tau_a + \tau_d$, and are modulated by the synaptic weight w. We denote the presynaptic spike train as x with spike times t_{pre}:

$$x(t) = \sum_{t_{pre}} \delta(t - t_{pre}). \tag{2}$$

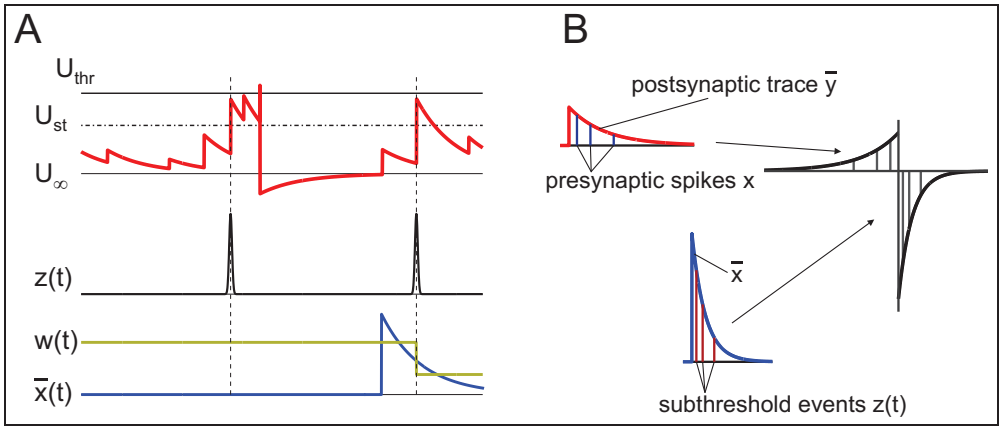

Figure 1: **Illustration of STDP mechanism**. **A**: Upper trace (red) is the membrane potential of the postsynaptic neuron. Shown are the firing threshold U_{thr} and the threshold for LTD U_{st}. Middle trace (black) is the variable $z(t)$, the train of LTD threshold crossing events. Please note that the first spike in $z(t)$ occurs at a different time than the neuronal spike. Bottom traces show $w(t)$ (yellow) and $\bar{x}$ (blue) of a selected synapse. The second event in z reads out the trace of the presynaptic spike $\bar{x}$, leading to LTD. **B**: Learning rule (4) is equivalent to RSTDP. A postsynaptic spike leads to an instantaneous jump in the trace $\bar{y}$ (top left, red line), which decays exponentially. Subsequent presynaptic spikes (dark blue bars and corresponding thin gray bars in the STDP window) "read" out the state of the trace for the respective $\Delta t = t_{pre} - t_{post}$. Similarly, $z(t)$ reads out the presynaptic trace $\bar{x}$ (lower left, blue line). Sampling for all possible times results in the STDP window (right).

A postsynaptic neuron receives the input $I_{syn}(t) = \sum_i w_i x_i(t - \tau_a - \tau_d)$. The postsynaptic spike train is similarly denoted by $y(t) = \sum_{t_{post}} \delta(t - t_{post})$.

2.2 The plasticity rule

The plasticity rule we employ mimics reverse STDP: A postsynaptic spike which arrives at the synapse shortly before a presynaptic spike leads to synaptic potentiation. For synaptic depression the relevant signal is not the spike, but the point in time where $U(t)$ crosses an additional threshold U_{st} from below, with $U_\infty < U_{st} < U_{thr}$ ("subthreshold threshold"). These events are modelled as δ-pulses in the function $z(t) = \sum_k \delta(t - t_k)$, where t_k are the times of the aforementioned threshold crossing events (see Fig. 1 A for an illustration of the principle). The temporal characteristic of (reverse) STDP is preserved: If a presynaptic spike occurs shortly before the membrane potential crosses this threshold, the synapse depresses. Timing dependent LTD without postsynaptic spiking has been observed, although with classical timing requirements [12].

We formalize this by letting pre- and postsynaptic spikes each drive a synaptic trace:

$$\begin{aligned} \tau_{pre}\dot{\bar{x}} &= -\bar{x} + x(t - \tau_a) \\ \tau_{post}\dot{\bar{y}} &= -\bar{y} + y(t - \tau_d). \end{aligned} \tag{3}$$

The learning rule is a read–out of the traces by different spiking events:

$$\dot{w} \propto \bar{y}x(t - \tau_a) - \gamma\bar{x}z(t - \tau_d), \tag{4}$$

where γ is a factor which scales depression and potentiation relative to each other. Fig. 1 B shows how this plasticity rule creates RSTDP.

3 Equivalence to Perceptron Learning Rule

The Perceptron Learning Rule (PLR) for positive binary inputs and outputs is given by

$$\Delta w_i^\mu \propto x_0^{i,\mu}(2y_0^\mu - 1)\Theta\left[\kappa - (2y_0^\mu - 1)(h^\mu - \vartheta)\right], \tag{5}$$

where $x_0^{i,\mu} \in \{0,1\}$ denotes the activity of presynaptic neuron i in pattern $\mu \in \{1,\dots,P\}$, $y_0^\mu \in \{0,1\}$ signals the desired response to pattern μ, $\kappa > 0$ is a margin which ensures a certain robustness against noise after convergence, $h^\mu = \sum_i w_i x_0^{i,\mu}$ is the input to a postsynaptic neuron, ϑ denotes the firing threshold, and $\Theta(x)$ denotes the Heaviside step function. If the P patterns are linearly separable, the perceptron will converge to a correct solution of the weights in a finite number of steps. For random patterns this is generally the case for $P < 2N$. A finite margin κ reduces the capacity.

Interestingly, for the case of temporally well separated synchronous spike patterns the combination of RSTDP-like synaptic plasticity dynamics with depolarization-dependent LTD and neuronal hyperpolarization leads to a plasticity rule which can be mapped to the Perceptron Learning Rule. To cut down unnecessary notation in the derivation, we drop the indices i and μ except where necessary and consider only times $0 \le t \le \tau_a + 2\tau_d$.

We consider a single postsynaptic neuron with N presynaptic neurons, with the condition $\tau_d < \tau_a$. During learning, presynaptic spike patterns consisting of synchronous spikes at time $t = 0$ are induced, concurrent with a possibly occuring postsynaptic spike which signals the class the presynaptic pattern belongs to. This is equivalent to the setting of a single layered perceptron with binary neurons. With x_0 and y_0 used as above we can write the pre- and postsynaptic activity as $x(t) = x_0\delta(t)$ and $y(t) = y_0\delta(t)$. The membrane potential of the postsynaptic neuron depends on y_0:

$$\begin{aligned} U(t) &= y_0 U_{reset} \exp(-t/\tau_U) \\ U(\tau_a+\tau_d) &= y_0 U_{reset} \exp(-(\tau_a+\tau_d)/\tau_U) = y_0 U_{ad}. \end{aligned} \tag{6}$$

Similarly, the synaptic current is

$$\begin{aligned} I_{syn}(t) &= \sum_i w_i x_0^i \delta(t-\tau_a-\tau_d) \\ I_{syn}(\tau_a+\tau_d) &= \sum_i w_i x_0^i = I_{ad}. \end{aligned} \tag{7}$$

The activity traces at the synapses are

$$\begin{aligned} \bar{x}(t) &= x_0 \Theta(t-\tau_a) \frac{\exp(-(t-\tau_a)/\tau_{pre})}{\tau_{pre}} \\ \bar{y}(t) &= y_0 \Theta(t-\tau_d) \frac{\exp(-(t-\tau_d)/\tau_{post})}{\tau_{post}}. \end{aligned} \tag{8}$$

The variable of threshold crossing $z(t)$ depends on the history of the postsynaptic neurons, which again can be written with the aid of y_0 as:

$$z(t) = \Theta(I_{ad} + y_0 U_{ad} - U_{st})\delta(t-\tau_a-\tau_d). \tag{9}$$

Here, Θ reflects the condition for induction of LTD. Only when the postsynaptic input at time $t = \tau_a + \tau_d$ is greater than the residual hyperpolarization ($U_{ad} < 0$!) plus the threshold U_{st}, a potential LTD event gets enregistered. These are the ingredients for the plasticity rule (4):

$$\begin{aligned} \Delta w \propto& \int \left[\bar{y} x(t-\tau_a) - \gamma \bar{x} z(t-\tau_d)\right] dt \\ =& x_0 y_0 \frac{\exp(-(\tau_a+\tau_d)/\tau_{post})}{\tau_{post}} - \gamma x_0 \frac{\exp(-2\tau_d/\tau_{pre})}{\tau_{pre}} \Theta(I_{ad} + y_0 U_{ad} - U_{st}). \end{aligned} \tag{10}$$

We shorten this expression by choosing γ such that the exponential factors of both terms are equal, which we can drop subsequently:

$$\Delta w \propto x_0 \left(y_0 - \Theta(I_{ad} + y_0 U_{ad} - U_{st})\right). \tag{11}$$

We expand the equation by adding and substracting $y_0\Theta(I_{ad} + y_0 U_{ad} - U_{st})$:

$$\begin{aligned} \Delta w \propto& x_0 \left[y_0(1 - \Theta(I_{ad} + y_0 U_{ad} - U_{st})) - (1-y_0)\Theta(I_{ad} + y_0 U_{ad} - U_{st})\right] \\ =& x_0 \left[y_0 \Theta(-I_{ad} - U_{ad} + U_{st}) - (1-y_0)\Theta(I_{ad} - U_{st})\right]. \end{aligned} \tag{12}$$

We used $1 - \Theta(x) = \Theta(-x)$ in the last transformation, and dropped y_0 from the argument of the Heaviside functions, as the two terms are seperated into the two cases $y_0 = 0$ and $y_0 = 1$. We do a similar transformation to construct an expression G that turns either into the argument of the left or right Heaviside function depending on y_0. That expression is

$$G = I_{ad} - U_{st} + y_0(-2I_{ad} - U_{ad} + 2U_{st}), \tag{13}$$

with which we replace the arguments:

$$\Delta w \propto x_0 y_0 \Theta(G) - x_0(1 - y_0)\Theta(G) = x_0(2y_0 - 1)\Theta(G). \tag{14}$$

The last task is to show that G and the argument of the Heaviside function in equation (5) are equivalent. For this we choose $I_{ad} = h$, $U_{ad} = -2\kappa$ and $U_{st} = \vartheta - \kappa$ and keep in mind, that $\vartheta = U_{thr}$ is the firing threshold. If we put this into G we get

$$\begin{aligned} G =& I_{ad} - U_{st} + y_0(-2I_{ad} - U_{ad} + 2U_{st}) \\ =& h - \vartheta + \kappa + 2y_0 h + 2y_0\kappa + 2y_0\vartheta - 2y_0\kappa \\ =& \kappa - (2y_0 - 1)(h - \vartheta), \end{aligned} \tag{15}$$

which is the same as the argument of the Heaviside function in equation (5). Therefore, we have shown the equivalence of both learning rules.

4 Associative learning of spatio-temporal spike patterns

4.1 Tempotron learning with RSTDP

The condition of exact spike synchrony used for the above equivalence proof can be relaxed to include the association of spatio-temporal spike patterns with a desired postsynaptic activity. In the following we take the perspective of the postsynaptic neuron which during learning is externally activated (or not) to signal the respective class by spiking at time $t = 0$ (or not). During learning in each trial presynaptic spatio-temporal spike patterns are presented in the time span $0 < t < T$, and plasticity is ruled by (4). For these conditions the resulting synaptic weights realize a Tempotron with substantial memory capacity.

A Tempotron is an integrate-and-fire neuron with input weights adjusted to perform arbitrary classifications of (sparse) spike patterns [5, 18]. To implement a Tempotron, we make two changes to the model. First, we separate the time scales of membrane potential and hyperpolarization by introducing a variable ν:

$$\tau_\nu \dot{\nu} = -\nu \; . \tag{16}$$

Immediately after a postsynaptic spike, ν is reset to $\nu_{spike} < 0$. The reason is that the length of hyperpolarization determines the time window where significant learning can take place. To improve comparability with the Tempotron as presented originally in [5], we set $T = 0.5s$ and $\tau_\nu = \tau_{post} = 0.2s$, so that the postsynaptic neuron can learn to spike almost anywhere over the time window, and we introduce postsynaptic potentials (PSP) with a finite rise time:

$$\tau_s \dot{I}_{syn} = -I_{syn} + \sum_i w_i x_i(t - \tau_a), \tag{17}$$

where w_i denotes the synaptic weight of presynaptic neuron i. With $\tau_s = 3ms$ and $\tau_U = 15ms$ the PSPs match the ones used in the original Tempotron study. This second change has little impact on the capacity or otherwise. With these changes, the membrane potential is governed by

$$\tau_U \dot{U} = \nu + I_{syn}(t - \tau_d) - U. \tag{18}$$

A postsynaptic spike resets U to $\nu_{spike} = U_{reset} < 0$. U_{reset} is the initial hyperpolarization which is induced after a spike, which relaxes back to zero with the time constant $\tau_\nu \gg \tau_U$. Presynaptic spikes add up linearly, and for simplicity we assume that both the axonal and the dendritic delay are negligibly small: $\tau_a = \tau_d = 0$.

It is a natural choice to set $\tau_U = \tau_{pre}$ and $\tau_\nu = \tau_{post}$. τ_U sets the time scale for the summation of EPSP contributing to spurious spikes, τ_ν sets the time window where the desired spikes can lie. They therefore should coincide with LTD and LTP, respectivly.

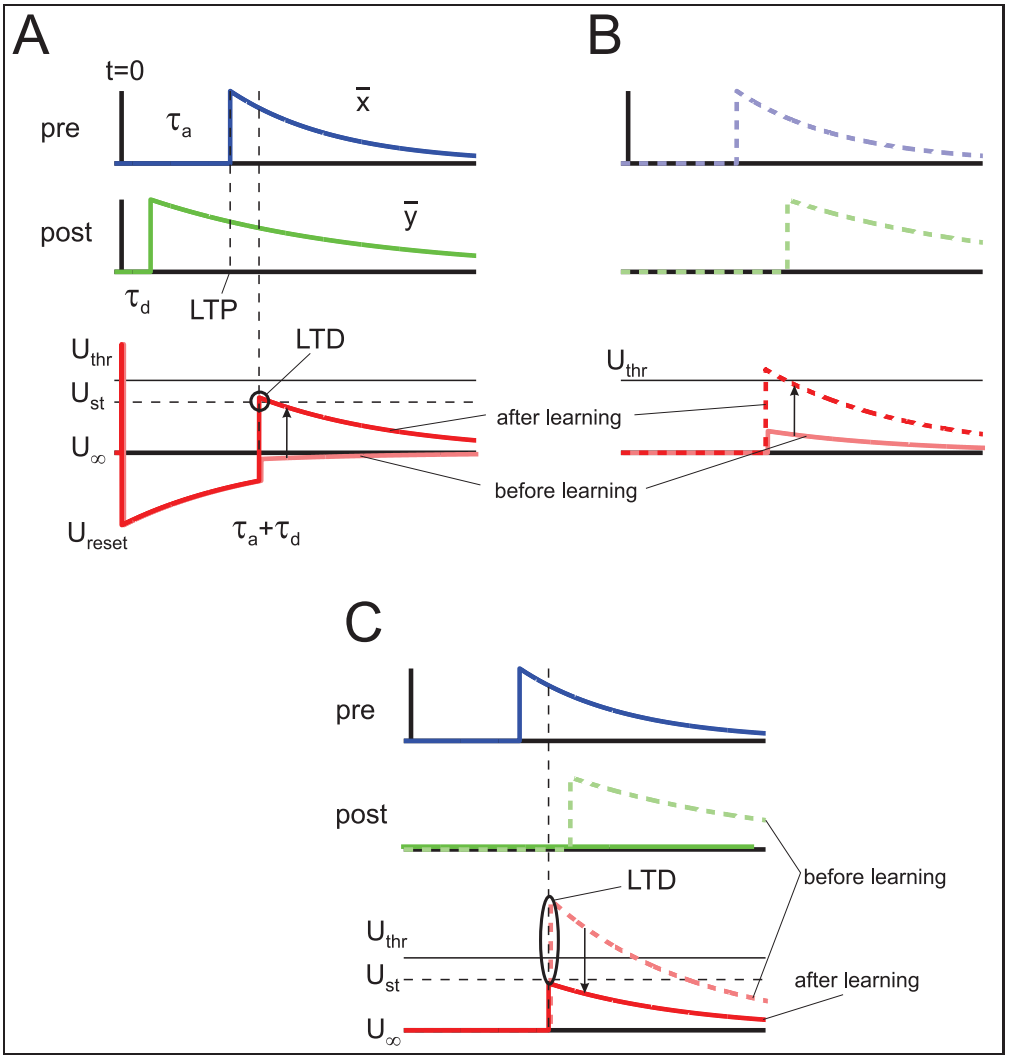

Figure 2: Illustration of Perceptron learning with RSTDP with subthreshold LTD and postsynaptic hyperpolarization. Shown are the traces $\bar{x}$, $\bar{y}$ and U. Pre- and postsynaptic spikes are displayed as black bars at $t = 0$. **A:** Learning in the case of $y_0 = 1$, i.e. a postsynaptic spike as the desired output. Initially the weights are too low and the synaptic current (summed PSPs) is smaller than U_{st}. Weight change is LTP only until during pattern presentation the membrane potential hits U_{st}. At this point LTP and LTD cancel exactly, and learning stops. **B:** Pattern completion for $y_0 = 1$. Shown are the same traces as in A at the absence of an inital postsynaptic spike. The membrane potential after learning is drawn as a dashed line to highlight the amplitude. Without the initial hyperpolarization, the synaptic current after learning is large enough to cross the spiking threshold, the postsynaptic neuron fires the desired spike. Learning until U_{st} is reached ensures a minimum height of synaptic currents and therefore robustness against noise. **C:** Pattern presentation and completion for $y_0 = 0$. Initially, the synaptic current during pattern presentation causes a spike and consequently LTD. Learning stops when the membrane potential stays below U_{st}. Again, this ensures a certain robustness against noise, analogous to the margin in the PLR.

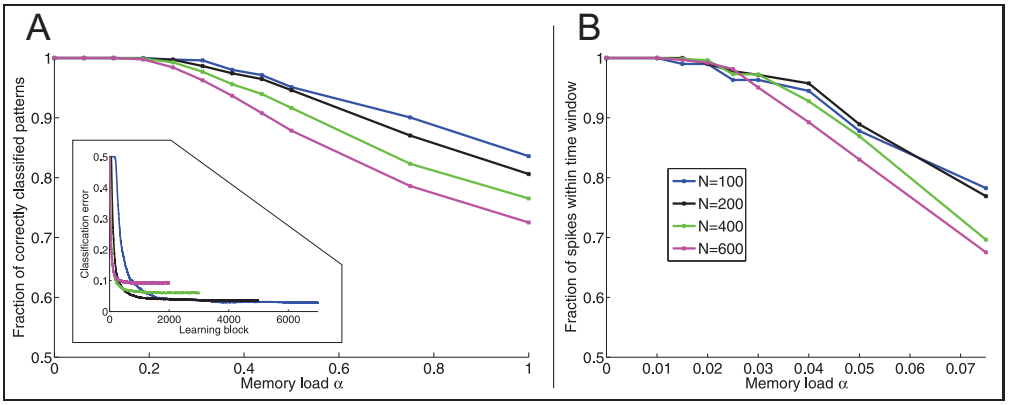

Figure 3: Performance of Tempotron and Chronotron after convergence. **A:** Classification performance of the Tempotron. Shown is the fraction of pattern which elicit the desired postsynaptic activity upon presentation. Perfect recall for all N is achieved up to $\alpha = 0.18$. Beyond that mark, some of the patterns become incorrectly classified. The inset shows the learning curves for $\alpha = 7/16$. The final fraction of correctly classified pattern is the average fraction of the last 500 blocks of each run. **B:** Performance of the Chronotron. Shown is the fraction of pattern which during recall succeed in producing the correct postsynaptic spike time in a window of length 30 ms after the teacher spike. See supplemental material for a detailed description. Please note that the scale of the load axis is different in A and B.

Table 1: Parameters for Tempotron learning

τ_U, τ_{pre}	τ_ν, τ_{post}	τ_s	U_{thr}	U_{st}	ν_{spike}	η	γ
15 ms	200 ms	3 ms	20 mV	19 mV	-20 mV	10^{-5}	2

4.1.1 Learning performance

We test the performance of networks of N input neurons at classifying spatio-temporal spike patterns by generating $P = \alpha N$ patterns, which we repeatedly present to the network. In each pattern, each presynaptic neuron spikes exactly once at a fixed time in each presentation, with spike times uniformly distributed over the trial. Learning is organized in learning blocks. In each block all P patterns are presented in randomized order. Synaptic weights are initialized as zero, and are updated after each pattern presentation. After each block, we test if the postsynaptic output matches the desired activity for each pattern. If during training a postsynaptic spike at $t = 0$ was induced, the output can lie anytime in the testing trial for a positive outcome. To test scaling of the capacity, we generate networks of 100 to 600 neurons and present the patterns until the classification error reaches a plateau. Examples of learning curves (Classification error over time) are shown in Fig. 3. For each combination of α and N, we run 40 simulations. The final classification error is the mean over the last 500 blocks, averaged over all runs. The parameters we use in the simulations are shown in Tab. 1. Fig. 3 shows the final classification performance as a function of the memory load α, for all network sizes we use. Up to a load of 0.18, the networks learns to perfectly classify each pattern. Higher loads leave a residual error which increases with load. The drop in performance is steeper for larger networks. In comparison, the simplified Tempotron learning rule proposed in [5] achieves perfect classification up to $\alpha \approx 1.5$, i.e. one order of magnitude higher.

4.2 Chronotron learning with RSTDP

In the Chronotron [17] input spike patterns become associated with desired spike trains. There are different learning rules which can achieve this mapping, including E–learning, I–learning, ReSuMe and PBSNLR [17, 19, 20]. The plasticity mechanism presented here has the tendency to generate postsynaptic spikes as close in time as possible to the teacher spike during recall. The presented learning principle is therefore a candidate for Chronotron learning. The average distance of these

spikes depends on the time constants of hyperpolarization and the learning window, especially τ_{post}. The modifications of the model necessary to implement Chronotron learning are described in the supplement. The resulting capacity, i.e. the ability to generate the desired spike times within a short window in time, is shown in Fig. 3 B. Up to a load of $\alpha = 0.01$, the recall is perfect within the limits of the learning window $\tau_{lw} = 30ms$. Inspection of the spike times reveals that the average distance of output spikes to the respective teacher spike is much shorter than the learning window ($\approx 2ms$ for $\alpha = 0.01$, see supplemental Fig. 1).

5 Discussion

We present a new and biologically highly plausible approach to learning in neuronal networks. RSTDP with subthreshold LTD in concert with hyperpolarisation is shown to be mathematically equivalent to the Perceptron learning rule for activity patterns consisting of synchronous spikes, thereby inheriting the highly desirable properties of the PLR (convergence in finite time, stop condition if performance is sufficient and robustness against noise). This provides a biologically plausible mechanism to build associative memories with a capacity close to the theoretical maximum. Equivalence of STDP with the PRL was shown before in [21], but this equivalence only holds on average. We would like to stress that we here present a novel approach that ensures exact mathematical eqivalence to the PRL.

The mechanism proposed here is complementary to a previous approach [13] which uses CSTDP in combination with spike frequency adaptation to perform gradient descent learning on a squared error. However, that approach relies on an explicit teacher signal, and is not applicable to auto-associative memories in recurrent networks. Most importantly, the approach presented here inherits the important feature of selfregulation and fast convergence from the original Perceptron which is absent in [13].

For sparse spatio-temporal spike patterns extensive simulations show that the same mechanism is able to learn Tempotrons and Chronotrons with substantial memory capacity. In the case of the Tempotron, the capacity achieved with this mechanism is lower than with a comparably plausible learning rule. However, in the case of the Chronotron the capacity comes close to the one obtained with a commonly employed, supervised spike time learning rule. Moreover, these rules are biologically quite unrealistic. A prototypical example for such a supervised learning rule is the Temptron rule proposed by Gütig and Sompolinski [5]. Essentially, after a pattern presentation the complete time course of the membrane potential during the presentation is examined, and if classification was erroneous, the synaptic weights which contributed most to the absolute maximum of the potential are changed. In other words, the neurons would have to able to retrospectivly disentangle contributions to their membrane potential at a certain time in the past. As we showed here, RSTDP with subthreshold LTD together with postsynaptic hyperpolarization for the first time provides a realistic mechanism for Tempotron and Chronotron learning.

Spike after-hyperpolarization is often neglected in theoretical studies or assumed to only play a role in network stabilization by providing relative refractoriness. Depolarization dependent STDP receives little attention in modeling studies (but see [22]), possibly because there are only few studies which show that such a mechanism exists [12, 23]. The novelty of the learning mechanism presented here lies in the constructive roles both play in concert. After-hyperpolarization allows synaptic potentiation for presynaptic inputs immediately after the teacher spike without causing additional non-teacher spikes, which would be detrimental for learning. During recall, the absence of the hyperpolarization ensures the then desired threshold crossing of the membrane potential (see Fig. 2 B). Subthreshold LTD guarantees convergence of learning. It counteracts synaptic potentiation when the membrane potential becomes sufficiently high after the teacher spike. The combination of both provides the learning margin, which makes the resulting network robust against noise in the input. Taken together, our results show that the interplay of neuronal dynamics and synaptic plasticity rules can give rise to powerful learning dynamics.

Acknowledgments

This work was in part funded by the German ministry for Science and Education (BMBF), grant number 01GQ0964.

References

[1] Hertz, J., Krogh, A. & Palmer, R.G.(1991) *Introduction to the Theory of Neural Computation.*, Addison-Wesley.

[2] Rosenblatt, F. (1957) The Perceptron–a perceiving and recognizing automaton. *Report* 85-460-1.

[3] Minsky M. L. & Papert S. A. (1969) *Perceptrons* Cambridge, MA: MIT Press.

[4] Diederich, S. & Opper, M. (1987) Learning of correlated patterns in spin-glass networks by local learning rules*Physical Review Letters* **58**(9):949-952.

[5] Gütig R. & Sompolinsky H. (2006) The Tempotron: a neuron that learns spike timing-based decisions.*Nature Neuroscience* **9**(3):420-8.

[6] Dan, Y. &Poo, M.(2004) Spike Timing-Dependent Plasticity of Neural Circuits *Neuron* **44**:2330.

[7] Dan, Y. &Poo, M.(2006) Spike timing-dependent plasticity: from synapse to perception. *Physiological Reviews* **86**(3):1033-48.

[8] Caporale, N. & Dan, Y. (2008) Spike TimingDependent Plasticity: A Hebbian Learning Rule *Annual Review of Neuroscience* **31**:2546.

[9] Froemke, R. C., Poo, M.-M., Dan, Y. (2005) Spike-timing-dependent synaptic plasticity depends on dendritic location. *Nature* **434**:221-225.

[10] Sjöström, P. J., Häusser, M. (2006) A Cooperative Switch Determines the Sign of Synaptic Plasticity in Distal Dendrites of Neocortical Pyramidal Neurons. *Neuron* **51**:227-238.

[11] Haas, J.S., Nowotny,T. & Abarbanel,H.D.I.(2006) Spike-Timing-Dependent Plasticity of Inhibitory Synapses in the Entorhinal Cortex *Journal of Neurophysiology* **96**(6):3305-3313.

[12] Sjöström, P.J., Turrigiano, G.G. and Nelson, S.B. (2004) Endocannabinoid-Dependent Neocortical Layer-5 LTD in the Absence of Postsynaptic Spiking. *J Neurophysiol* **92**:3338-3343

[13] D'Souza, P.,Liu, S.-C. & Hahnloser, R. H. R. (2010) Perceptron learning rule derived from spike-frequency adaptation and spike-time-dependent plasticity *PNAS* **107**(10):47224727.

[14] Song, S., Miller, K. D., Abbott, L. F. (2000) Competitive Hebbian learning through spike-timing-dependent synaptic plasticity. *Nature Neuroscience* **3**:919-926.

[15] Izhikevich, E. M., Desai, N. S. (2003) Relating STDP to BCM. *Neural Computation* **15**:1511-1523

[16] Vogels, T. P., Sprekeler, H., Zenke1, F., Clopath, C. & Gerstner, W. (2011) Inhibitory Plasticity Balances Excitation and Inhibition in Sensory Pathways and Memory Networks *Science* **334**(6062):1569-1573.

[17] Florian, R.V. (2012) The Chronotron: A Neuron That Learns to Fire Temporally Precise Spike Patterns *PLoS ONE* **7**(8): e40233

[18] Rubin, R., Monasson, R. & Sompolinsky, H. (2010) Theory of Spike Timing-Based Neural Classifiers *Physical Review Letters* **105**(21): 218102.

[19] Ponulak, F., Kasinski, A. (2010) Supervised Learning in Spiking Neural Networks with ReSuMe: Sequence Leanring, Classification, and Spike Shifting *Neural Computation* **22**:467-510

[20] Xu, Y., Zeng, X., Zhong, S. (2013) A New Supervised Learning Algorithm for Spiking Neurons *Neural Computation* **25**: 1475-1511

[21] Legenstein, R., Naeger, C., Maas, W. (2005) What Can a Neuron Learn with Spike-Timing-Dependent Plasticity? *Neural Computation* **17**:2337-2382

[22] Clopath, C., Büsing, L., Vasilaki, E., Gerstner, W. (2010) Connectivity reflects coding: a model of voltage-based STDP with homeostasis *Nature Neuroscience* **13**:344-355

[23] Fino, E., Deniau, J-M., Venance, L. (2009) Brief Subthreshold Events Can Act as Hebbian Signals for Long-Term Plasticity *PLoS ONE* **4**(8): e6557

Supplementary material for: Perfect Associative Learning with Spike-Timing-Dependent Plasticity

Christian Albers
Institute of Theoretical Physics
University of Bremen
28359 Bremen, Germany
calbers@neuro.uni-bremen.de

Maren Westkott
Institute of Theoretical Physics
University of Bremen
28359 Bremen, Germany
maren@neuro.uni-bremen.de

Klaus Pawelzik
Institute of Theoretical Physics
University of Bremen
28359 Bremen, Germany
pawelzik@neuro.uni-bremen.de

1 Chronotron learning with RSTDP, subthreshold LTD and Hyperpolarization

1.1 Introduction

Here, we present model and scenario used to generate the capacity curves for the Chronotron. The model for the Tempotron learning (equations (16) to (18) in the main article) is slightly modified. The main reason is that during presentation, synaptic depression which precedes every postsynaptic teacher spike will be induced at every iteration. This would prevent convergence and destroys desired system states with perfect recall. This is not a concern in the Tempotron learning, because the teacher spike always occurs before any presynaptic activity. Therefore, the major change to the model for the Chronotron is to add synaptic scaling acting only on the negative weights.

1.2 Model description

Spike trains are sums of δ-pulses:

$$x(t) = \sum_{t_{pre}} \delta(t - t_{pre}) \ , \quad y(t) = \sum_{t_{post}} \delta(t - t_{post}) \ . \tag{1}$$

The synaptic current is

$$I_{syn}(t) = \sum_i w_i x_i(t) \ . \tag{2}$$

As in the Tempotron, we neglect axonal and dendritic delays. The membrane potential is governed by equation (1) of the main article, which means that we discarded the variable ν from the Tempotron model. The external current is used to deliver the teacher spikes and consists of a suprathreshold delta pulse at the desired times. The plasticity rule (equations (3) and (4)) remains in place. Pattern presentation and association protocol is similar to the Tempotron case. There are N presynaptic and one postsynaptic neurons. We generate $P = \alpha N$ different random patterns. In each pattern $\mu \in P$, each presynaptic neuron spikes exactly once at a fixed time uniformly drawn from the interval $[0, T]$. Each presynaptic activity pattern is assigned one postsynaptic spike time t^{μ}_{teach}, at which during the pattern presentation (associative learning) a teacher spike is induced by a suprathreshold external current. The teacher spike time is drawn from a slightly smaller interval (see below). Learning is

Table 1: Parameters for Chronotron learning

τ_U, τ_{pre}	τ_{post}	U_{thr}	U_{st}	U_{reset}	η	γ	β
10 ms	10 ms	20 mV	19.5 mV	-20 mV	$10^{-6}/N$	1	0.05

organized in learning blocks. During each block, each pattern is presented once, with the order of presentation randomized for every block. The weights are updated after each pattern presentation. Due to the considerations presented above, we introduce an additional weight decay term, which acts only on the (currently) inhibitory synapses. We denote the set of negative weights by $W^I(t)$. After each learning block, the negative weights are slightly reduced proportionally to their respective magnitude:

$$\Delta w_i = \begin{cases} \beta w_i & \text{for } w_i \in W^I(t) \\ 0 & \text{else .} \end{cases} \tag{3}$$

This simple form of synaptic scaling has the disadvantage that the decay depends on the number of patterns. However, we found that the results are very insensitive to the parameter β, which justifies this choice.

After each learning block and after the synaptic scaling, we present each presynaptic pattern without the teacher input and with plasticity turned off. The pattern is counted as correctly completed if a postsynaptic spike occurs in the time window $[t^\mu_{teacher}, t^\mu_{teacher} + \tau_{lw}]$, where τ_{lw} is a parameter which controls the length of the learning window. Because the postsynaptic spike can occur over a finite time window, we reduced the time interval the teacher spike times are drawn from to $[0, T - \tau_{lw}]$ to make sure correct association can be achieved by every pattern.

We choose the length of the presentation interval $T = 200ms$ and $\tau_U = 10ms$ to match the respective parameters in the original Chronotron study [1]. The length of the learning window is $\tau_{lw} = 30ms$ is associated to the time constants of the STDP window. From the perspective of the learning task the Tempotron is really just a special case of the Chronotron with a very long learning window ($t^\mu_{teach} \equiv 0$, $\tau_{lw} = T$). To allow plasticity over the whole window, we seperated the time scale of hyperpolarization from the membrane time scale, and set $\tau_{post} = \tau_{nu} \approx T$. For the Chronotron, the postsynaptic spike has to occur as soon as possible after the time of the teacher spike, which requires a short time constant of LTP, τ_{post}. Compared to the Tempotron, this parameter choice sacrifices capacity for precision. The learning window we use is relatively long compared to the millisecond (or even submillisecond) precision which is achieved with the alternative learning rules (E-Learning, [1], ReSuMe [2], PBSNLR [3]). However, in our case the mean time difference of the actual output spike to the teacher spike is much shorter than the learning window, between 2 ms and 14 ms. Higher loads α lead to larger time mismatches (See Fig. 1). It was shown by Florian [1] that ReSuMe and his own unoptimized I-Learning rule both reach a capacity of around 0.02, to which our own plasticity rule is very close. With this load, the average distance of desired to actual spike is small ($\approx 2ms$). We have to mention that the highly optimized E-learning rule has a much higher memory capacity (0.2), however at the expense of biological plausibility.

References

[1] Florian, R.V. (2012) The Chronotron: A Neuron That Learns to Fire Temporally Precise Spike Patterns *PLoS ONE* **7**(8): e40233

[2] Ponulak, F., Kasinski, A. (2010) Supervised Learning in Spiking Neural Networks with ReSuMe: Sequence Leanring, Classification, and Spike Shifting *Neural Computation* **22**:467-510

[3] Xu, Y., Zeng, X., Zhong, S. (2013) A New Supervised Learning Algorithm for Spiking Neurons *Neural Computation* **25**: 1475-1511

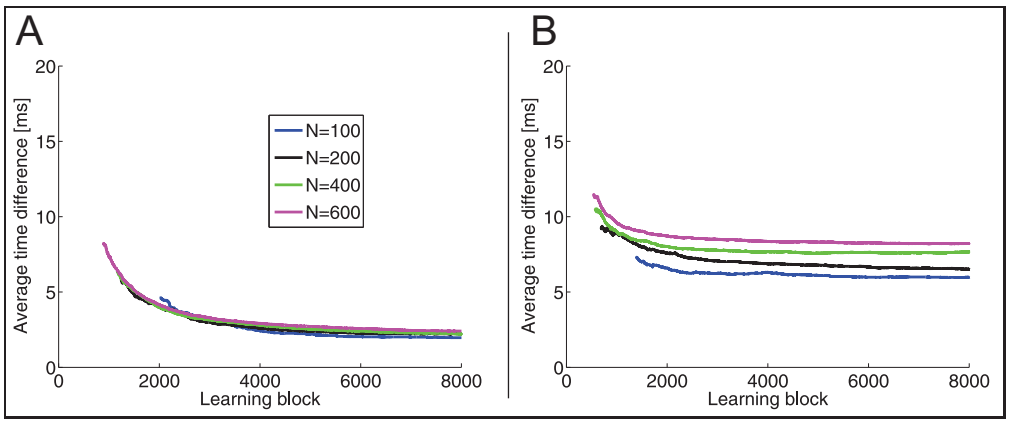

Figure 1: Examples of average differences in time of spike produced during recall and the teacher spike. **A** shows the time differences for a low load of $\alpha = 0.01$. Here, regardless of N the difference converges to 2 ms. **B** shows the same for a load of $\alpha = 0.04$. Shown are only the time differences for successful recall. The average difference converges to a higher value around 10 ms. The gaps at the beginning are due to the fact that the initial weights are zero, and therefore there are no spikes during recall.

Chapter 4

Learning of Precise Spike Times with Homeostatic Membrane Potential Dependent Synaptic Plasticity

4.1 Abstract

Precise spatio-temporal patterns of neuronal action potentials underly e.g. sensory representations and control of muscle activities. However, it is not known how the synaptic efficacies in the neuronal networks of the brain adapt such that they can reliably generate spikes at specific points in time. Existing activity-dependent plasticity rules like Spike-Timing-Dependent Plasticity are agnostic to the goal of learning spike times. On the other hand, the existing formal and supervised learning algorithms perform a temporally precise comparison of projected activity with the target, but there is no known biologically plausible implementation of this comparison. Here, we propose a simple and local unsupervised synaptic plasticity mechanism that is derived from the requirement of a balanced membrane potential. Since the relevant signal for synaptic change is the postsynaptic voltage rather than spike times, we call the plasticity rule Membrane Potential Dependent Plasticity (MPDP). Combining our plasticity mechanism with spike after-hyperpolarization causes a sensitivity of synaptic change to pre- and postsynaptic spike times which can reproduce Hebbian spike timing dependent plasticity for inhibitory synapses as was found in experiments. In addition, the sensitivity of MPDP to the time course of the voltage when generating a spike allows MPDP to distinguish between weak (spurious) and strong (teacher) spikes, which therefore provides a neuronal basis for the comparison of actual and target activity. For spatio-temporal input spike patterns our conceptually simple plasticity rule achieves a surprisingly high storage capacity for spike associations. The sensitivity of the MPDP to the subthreshold membrane potential during training allows robust memory retrieval after learning even in the presence of activity corrupted by noise. We propose that MPDP represents a biologically

realistic mechanism to learn temporal target activity patterns.

4.2 Introduction

Precise and recurring spatio-temporal patterns of action potentials are observed in various biological neuronal networks. In zebra finches, precise sequences of activations in region HVC are found during singing and listening to the own song [84]. Also, when spike times of sensory neurons are measured, the variability of latencies relative to the onset of a externally induced stimulus is often higher than if the latencies are measured relative to other sensory neurons [85, 86]; spike times covary. Therefore, information about the stimulus is coded in spatio-temporal spike patterns. Theoretical considerations show that in some situations spike-time coding is superior to rate coding [87]. Xu and colleagues demonstrated that through associative training it is possible to imprint new sequences of activations in visual cortex [88], which shows that there are plasticity mechanisms which are used to learn precise sequences.
These observations suggest that spatio-temporal patterns of spike activities underlie coding and processing of information in many networks of the brain. However, it is not known which synaptic plasticity mechanisms enable neuronal networks to learn, generate, and read out precise action potential patterns. A theoretical framework to investigate this question is the chronotron, where the postsynaptic neuron is trained to fire a spike at predefined times relative to the onset of a fixed input pattern [81]. A natural candidate plasticity rule for chronotron training is Spike-Timing Dependent Plasticity (STDP) [49] in combination with a supervisor who enforces spikes at the desired times. Legenstein and colleagues [89] investigated the capabilities of supervised STDP in the chronotron task and identified a key problem: STDP has no means to distinguish between desired spikes caused by the supervisor and spurious spikes resulting from the neuronal dynamics. As a result every spike gets reinforced, and plasticity does not terminate when the correct output is achieved, which eventually unlearns the desired synaptic state. The failings of STDP hint at the requirements of a working learning algorithm. Information about the type of a spike (desired or spurious) has to be available to each synapse, where it modulates spike time based synaptic plasticity. Synapses evoking undesired spikes should be weakened, synapses that contribute to desired spikes should be strengthened, but only until the self-generated output activity matches the desired one. Plasticity should cease if the output neurons generate the desired spikes without supervisor intervention. In other words, at the core of a learning algorithm has to be a comparison of actual and target activity, and synaptic changes have to be computed based on the difference between the two.
In recent years, a number of supervised learning rules have been proposed to train to fire temporally precise output spikes in response to recurring spatio-temporal input patterns [39, 81, 90]. They compare the target spike train to the self-generated (actual) output and devise synaptic changes to transform the latter into the former. However, because spikes are discrete events in time that influence the future dy-

namics of the neuron, the comparison is necessarily non-local in time, which might be difficult to implement for a biological neuron and synapse. Another group of algorithms performs a comparison of actual and target firing rate instead of spike times [38, 78, 79, 82]. Because they work with the instaneous firing rate, they do not rely on sampling of discrete spikes and therefore the comparison is local in time. It is interesting to note that these learning algorithms are implicitely sensitive to the current membrane potential, of which the firing rate is a monotonous function. However, two important questions remain unanswered: How is the desired activity communicated to a biological neuron and how does the synapse compute the difference?

In this study, we investigate the learning capabilities of a plasticity rule which relies only on postsynaptic membrane potential and presynaptic spikes as signals. To distinguish it from spike times based rules, we call it Membrane Potential Dependent Plasticity (MPDP). We derive MPDP from a homeostatic requirement on the voltage and show that in combination with spike after-hyperpolarisation (SAHP) it is compatible with experimentally observed STDP of inhibitory synapses [20]. Despite its Anti-Hebbian nature, MPDP combined with SAHP can be used to train a neuron to generate desired temporally structured spiking output in an associative manner. During learning, the supervisor or teacher induces spikes at the desired times by a strong input. Because of the differences in the time course of the voltage, a synapse can sense the difference between spurious spikes caused by weak inputs and teacher spikes caused by strong inputs. As a consequence, weight changes are matched to the respective spike type. Therefore, our learning algorithm provides a biologically plausible answer for the open question presented above. Additionally, the sensitivity of MPDP to subthreshold voltage leads to a noise-tolerant network after training with noise free examples. For a quantitative analysis, we simplify the neuron model and apply our learning mechanism to train a chronotron [81]. We find that the attainable memory capacity is comparable to that of a range of existing learning rules [39, 81, 82], however the noise tolerance after training is superior in networks trained with MPDP in comparison to those trained with the other learning algorithms.

4.3 Results

In the following, we start with presenting our Membrane Potential Dependent Plasticity rule (MPDP). We constructed a simple yet biologically plausible feed-forward network and show that MPDP, when tested with spike pairs, is equivalent to inhibitory Hebbian STDP as reported by Haas and colleagues [20]. We then show that with MPDP the output neuron of this example can be trained to generate spikes at specific times. Lastly, we turn to a simplified model to evaluate and compare with other rules the attainable memory capacity with MPDP, as well as its noise tolerance.

4.3.1 Membrane Potential Dependent Plasticity

We formulated a basic homeostatic requirement on the membrane potential of a neuron. The neuron should stay in a sensible working regime; in other words, its voltage should be confined to moderate values. We formalized this by introducing two thresholds on the voltage. In this study, ϑ_D lies between the firing threshold and resting potential and ϑ_P is equal to the resting potential. With these thresholds, we formulated an error function (see Eq. 4.5 in Methods). Using it and a simple LIF neuron model with linear dynamics below the firing threshold, we computed an update rule for the weights, Eq. 4.7. Weight changes with this rule "bend" the voltage at the times of non-zero error towards the region between the two thresholds. Fig. 4.1 B shows how MPDP effects the voltage for recurring input activity.

4.3.2 Homeostatic MPDP on inhibitory synapses is compatible with STDP

We first investigated the biological plausibility of a network with MPDP. Experimental studies on plasticity of cortical excitatory neurons often find Hebbian plasticity rules like Hebbian Spike Timing Dependent Plasticity (STDP; see [16, 25, 26, 47, 91] for examples). Reports on Anti-Hebbian plasticity or sensitivity to subthreshold voltage in excitatory cortical neurons are scarce [23, 52, 92, 93]. However, it has been reported that plasticity in (certain) inhibitory synapses onto excitatory cells has a Hebbian characteristic [20], i.e. synapses active before a postsynaptic spike become stronger, those active after the spike become weaker. The net effect of this rule on the postsynaptic neuron is *Anti-Hebbian*, because weight increases tend to suppress output spikes.

In experimental investigations of STDP, neurons are tested with pairs of pre- and postsynaptic spikes. We mimicked this procedure in a simple network consisting of one pre- and one postsynaptic neuron, and one "experimentator neuron" . The postsynaptic neuron was modelled as a conductance based LIF neuron. The experimentator neuron has a fixed strong excitatory synaptic weight onto the postsynaptic neuron, so that a spike of the experimentator neuron causes a postsynaptic spike. We used it to control the postsynaptic spike times. The presynaptic neuron is inhibitory and its weight is small compared to the experimentator, so that it has negligible influence on the postsynaptic spike time. We probed synaptic plasticity by inducing a pair of a pre- and a postsynaptic spike at times t_{pre} and t_{post}, and vary t_{pre} while keeping t_{post} fixed. The resulting weight change of the inhibitory neuron as a function of timing difference is shown in Fig. 4.1 C. The shape of the function is in qualitative agreement with experimental results [20].

It is necessary to assume the presence of an "experimentator neuron". The reason is that the shape of the STDP curve explicitely depends on the specifics of spike induction since the MPDP rule is sensitive only to subthreshold voltage. For example, using a delta-shaped input current would lead to a LTD-only STDP curve, since the time the voltage needs to cross the firing threshold starting from equilibrium is infinitely short.

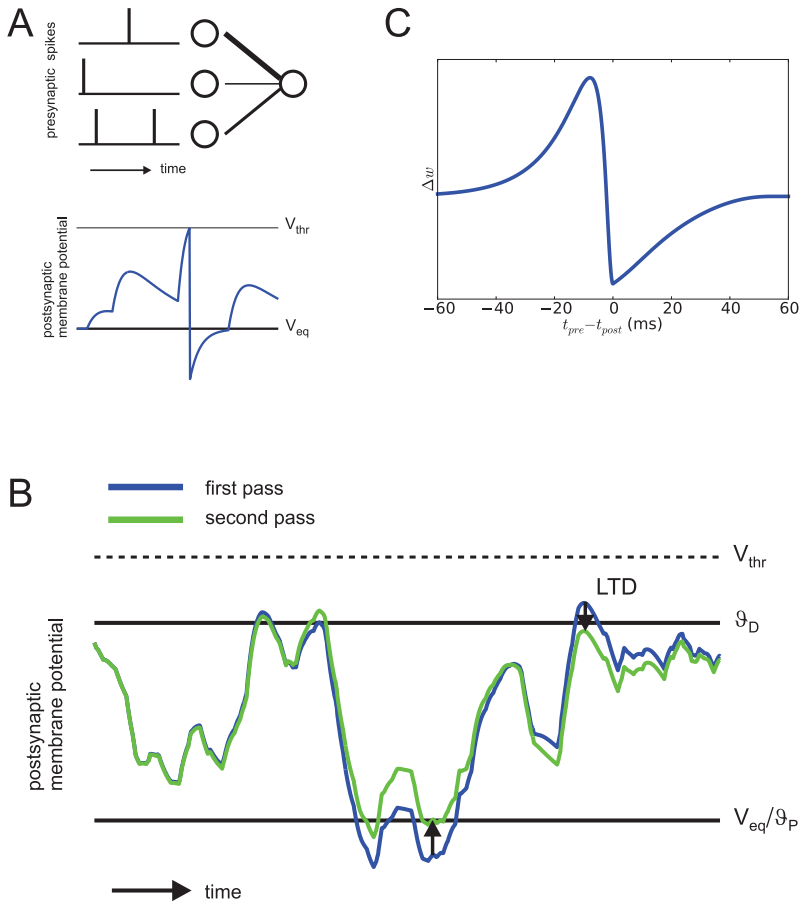

Figure 4.1: **A:** The model network has a simple feed-forward structure. The top picture shows three pre- and one postsynaptic neurons, connected by synapses. Line Width in this example corresponds to synaptic strength. Bottom picture shows the postsynaptic membrane potential in response to the input. **B:** Illustration of Anti-Hebbian Membrane Potential Dependent Plasticity (MPDP). A LIF neuron is presented twice with the same presynaptic input pattern. Excitation never exceeds V_{thr}. MPDP changes synapses to counteract hyperpolarization and depolarization occuring in the first presentation (blue trace), reducing (arrows) them on the second presentation (green trace). **C:** Homeostatic MPDP on inhibitory synapses is compatible with STDP as found in experiments. Plasticity is tested for different temporal distances between pre- and postsynaptic spiking; the resulting spike timing characteristic is in agreement with experimental data on STDP of inhibitory synapses [20].

4.3.3 Homeostatic MPDP allows associative learning

At first glance, it might seem unlikely that a homeostatic plasticity mechanism can implement associative learning. It is Anti-Hebbian in nature, because if the membrane potential is close to firing threshold it gets suppressed, and if is below the

resting potential it gets lifted up. However, the neuronal dynamics shows somewhat stereotypic behavior before, during and after each spike. To induce a spike, the neuron needs to be depolarized up to V_{thr}, where active feed-back processes kick in. These processes cause a very short and strong depolarization and a subsequent undershoot of the membrane potential (hyperpolarization), from where it relaxes back to equilibrium.

To demonstrate the capability of MPDP for learning of exact spike times, we constructed a simple yet plausible feed-forward network of N_i inhibitory and N_e excitatory neurons. Synaptic weights were initialized randomly. Both populations projected onto one conductance based LIF neuron. We presented this network frozen poissonian noise as the sole presynaptic firing pattern (Fig. 4.2, top). Excitatory synapses were kept fixed and inhibitory synapses changed according to MPDP. First we let the network learn to balance all inputs from the excitatory population such that the membrane potential mostly stays between the thresholds ϑ_P^I and ϑ_D^I. We then introduced the teacher input as a strong synaptic input from a different source (e.g. a different neuron population, Fig. 4.2, second to top). After repeated presentations of the input pattern with the teacher input, inhibition around the teacher spike is released such that after learning the output neuron will spike close to the desired spike time even without the teacher input (Fig. 4.2, third and fourth to top). At the same time, due to the balance requirement of the learning rule, inhibitory and excitatory conductances covary and thus their influence on the membrane potential mostly cancels out (Fig. 4.2 bottom). Due to the sterotypical shape of the membrane potential around the teacher spike, a homeostatic learning rule is able to perform associative learning by release of inhibition.

To further investigate the learning process, we simplified the setup. All synapses were subject to MPDP and were allowed to change their sign. A population of N presynaptic neurons fires one spike in each neuron at equidistant times. They project onto a single postsynaptic LIF neuron and all weights are zero initially. In each training trial an external delta-shaped suprathreshold current is induced at the postsynaptic neuron at a fixed time relative to the onset of the input pattern (teacher spike). The postsynaptic neuron reaches its firing threshold instantaneously, spikes and undergoes reset into a hyperpolarized state (blue trace on the left in Fig. 4.3). This is mathematically equivalent to adding a reset kernel at the time of the external current [39]. Because we set $\vartheta_P = V_{eq} = 0$, potentiation is induced in all synapses which have temporal overlap of their PSP-kernel with the hyperpolarization. Probing the neuron a second time without the external spike shows a small bump in the membrane potential around the time of the teacher spike. We continued to present the same input pattern, alternating between teaching trials (with teacher spike) and recall trials without teacher and with synaptic plasticity switched off. Plasticity is Hebbian until the weights are strong enough such that there is considerable depolarization before the teacher spike, inducing synaptic depression. Also, spike after-hyperpolarization is partially compensated by excitation, which reduces the window for potentiation. Continuation of learning after the spike association has been achieved (second to right plot) shrinks the windows for depression and po-

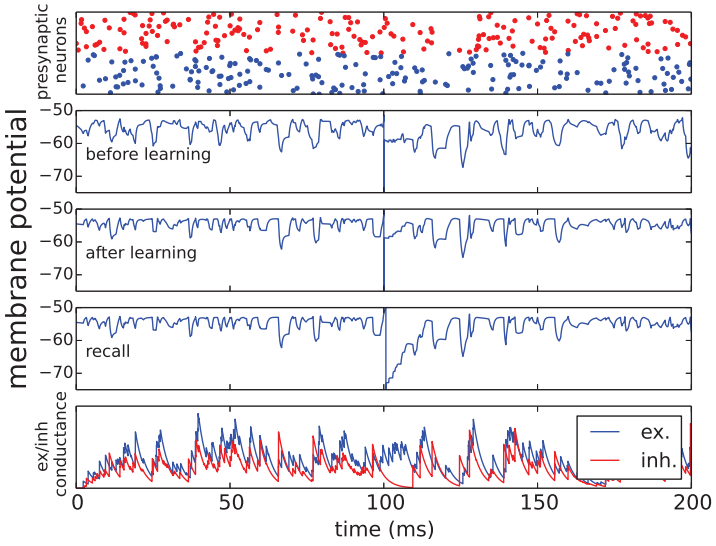

Figure 4.2: **Hebbian learning with homeostatic MPDP on inhibitory synapses.** A conductance based integrate-and-fire neuron is repeatedly presented with a fixed input pattern of activity in presynaptic inhibitory or excitatory neuron populations (top row - blue is excitatory, red inhibitory). Before learning, the neuron is allowed to adapt it's inhibitory weights according to homeostatic MPDP, such that the membrane potential mostly stays between the two learning thresholds. Then a strong excitatory input is given concurrently with the pattern to induce a spike at $t = 100ms$ (second row). Learning is restricted to inhibitory weights. By release of inhibition, the net input after the teacher spike is increased (third row). After learning has converged, the neuron is presented the input pattern without the teacher input and reproduces the spike close to the target time (4th row) . At all other times, excitatory and inhibitory conductances are balanced (bottom row).

tentiation, until they are very narrow and very close to each other in time. Because synaptic plasticity is determined by the integral over the normalized PSP during periods of depolarization and hyperpolarization, depression and potentiation become very similar in magnitude for each synapse and synaptic plasticity slows down nearly to a stop. Furthermore, the output spike has become stable. The time course of the membrane potential during teaching and recall trials is almost the same (Fig. 4.3 right).

4.3.4 Quantitative evaluation of MPDP

Memory capacity. We numerically evaluated the capacity of MPDP to train a network to produce precise spike times using the simplified feed-forward network described above. We constructed input patterns and desired output using the chronotron framework [81]. During training, we monitored the success of recall

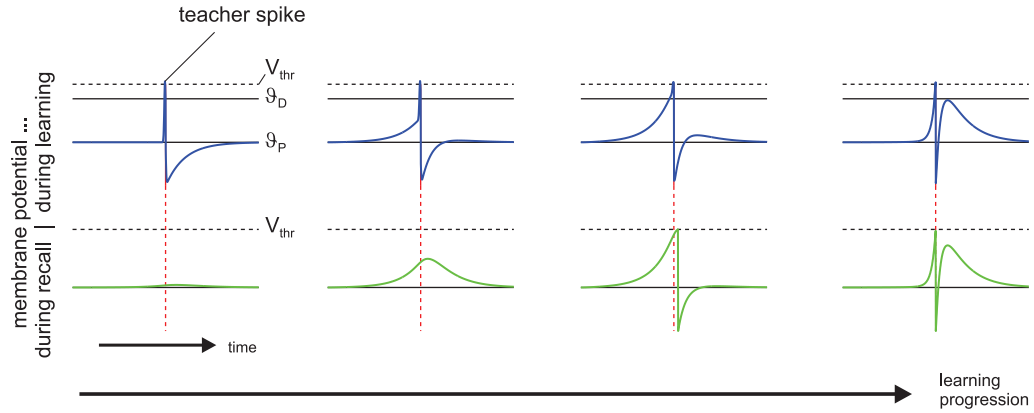

Figure 4.3: **Hebbian learning with homeostatic MPDP**. A postsynaptic neuron is presented the same input pattern multiple times, alternating between teaching trials with teacher spike (blue trace) and recall trials (green trace) to test the output. Initially, all weights are zero (left). Learning is Hebbian initially until strong depolarization occurs (second to left). When the spike first appears during recall, it is still not at the exact location of the teacher spike (second to right). Continued learning moves it closer to the desired location. Also, the time windows of the voltage being above ϑ_D and below ϑ_P shrink and move closer in time (right). Synaptic plasticity almost stops. The number of learning trials before each state is 1, 16, 53, and 1600 from left to right.

over time. The network of size $N = 1000$ generates the desired output spikes within the window of tolerance after 600 learning blocks (Fig. 4.4 A). However, weights are still changed by training, and continuation of it reduces the difference of actual and desired output spike time (see Fig. 4.4 B). After around 2000 learning blocks the average temporal error of all recalled spikes stays constant for the remainder of training. For $\alpha \leq 0.1$ the self-generated output spike is on average less than 0.5 ms away from the desired time. The final fraction of recalled spikes and average distance are shown in Fig. 4.4 C and D. The smallest network ($N = 200$) never reaches perfect recall, but has a capacity of $\alpha_{90} = 0.095$ (for the definition of capacity, see Materials and Methods). All other networks achieve perfect recall up to a load of $\alpha = 0.1$ and a capacity of $\alpha_{90} \approx 0.135$. The average distance of spikes from teacher grows with the load, but stays below 0.5 ms.

To put these results into perspective, we trained chronotrons again using three other learning rules and computed the respective memory capacity. Fig. 4.5 shows the capacity of all plasticity rules. The upper bound established by FP-Learning is $\alpha_{90} \approx 0.26$. MPDP is capable of storing half of the maximal possible number of associations in the weights.

Training and recall with noise on the membrane potential. Next, we turned to an evaluation of memory under the influence of noise. Having a noise free network

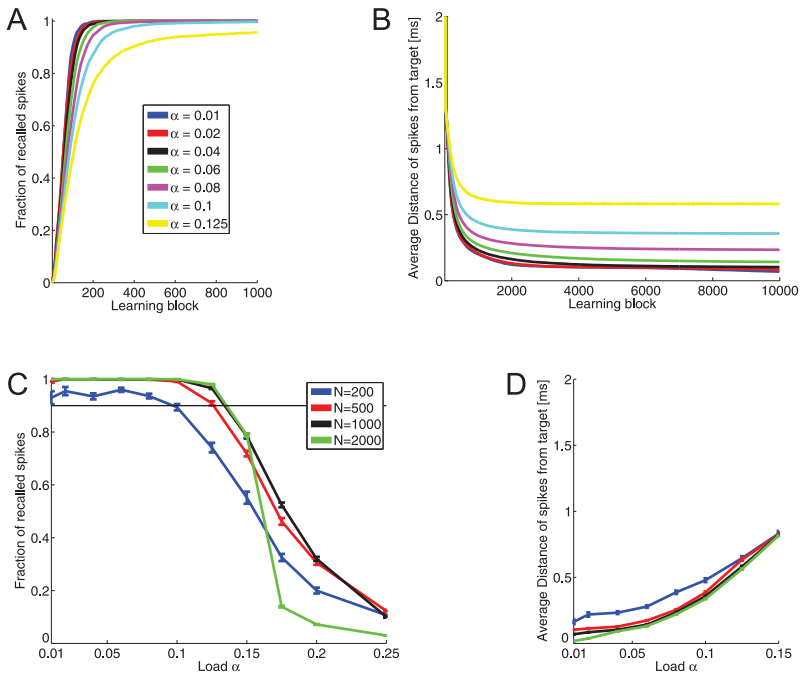

Figure 4.4: **Capacity of networks with MPDP. A:** Fraction of pattern where the network generates an output spike within 2 ms distance of target time t_d^μ, and no spurious spikes. Network size is $N = 1000$. The desired spikes are learned within ≈ 600 steps. **B:** Average distance of output spikes to target for the same network size. Training continues even though the desired spikes are generated; however, they are pushed closer to the desired time. **C:** Average fraction of recalled spikes after 10000 learning blocks for all network sizes as a function of the load. Networks with $N = 200$ have a high probability to not be able to recall all spikes even for low loads. Otherwise, recall gets better with network size. The thin black line lies at fraction of recall equal to 90 %. The critical load α_{90} is the point where the graph crosses this line. **D:** Average distance of recalled spikes as a function of the load. The lower the loads, the closer the output spike are to their desired location.

is a highly idealized situation and neurons in the brain are more likely to be subject to noise, be it because of inherent stochasticity of spike generation or the fact that sensory inputs are almost never "pure", but likely to arrive with additional more or less random inputs. First, we tested training and recall of spike times using an additional random input of a given variance σ_{input} on the postsynaptic neuron. The random input is a gaussian white noise process with zero mean, and because inputs decay with the membrane time constant, this results in a additional random walk with a restoring force. We trained the chronotron with additional noise of width $\sigma_{input} \in \{0, 0.2, 0.5, 1, 2, 5\}mV$. The width is the standard deviation of the random walk. Afterwards, we evaluated the critical load of networks of size $N = 200, 500, 1000$ depending on the noise level during training and during recall. The results are shown in Fig. 4.6.

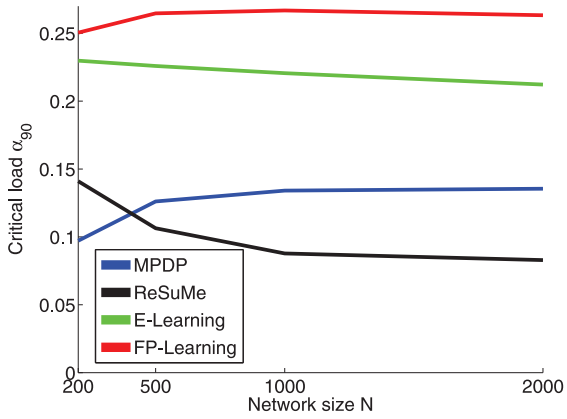

Figure 4.5: Critical load as a function of network size for all four learning rules. MPDP reaches approximately half of the maximal capacity.

With MPDP, the network trained without noise can perfectly recall patterns up to a load of $\alpha = 0.1$ even with additional noise input of $\sigma_{input} = 0.5mV$. Adding noise during training decreases the capacity, but at the same time recall robustness against noise is improved. This is contrasted by the network trained with FP-Learning. Here, noise-free training results in a network with imperfect recall under noise. However, noise during training alleviates this problem. Training with a given noise width σ_{input} makes recall with the same and less noise width perfect. One interesting observation is that unlike with MPDP, with FP-Learning the memory capacity for noise-free recall stays constant regardless of noise during training. This is explained by the variance of the weights after training. With FP-Learning, the variance increases approximately linearly with noise width, while the mean of the weights decreases linearly into negative values. The resulting membrane potential is strongly biased towards hyperpolarized states. What FP-Learning effectively does during training is to scale down the noise relative to the weights. This reduces the influence of noise, but also leads to a membrane potential that stays below resting potential most of the time during input activity. Because of the threshold for LTP, MPDP can not scale the weights freely, therefore it suffers from a declining memory capacity.

Training and recall with input spike time jitter. As a second noise condition we tested training and recall in the case that the input spike times are not fixed. In each pattern presentation, we added to each presynaptic spike time some random number drawn from a gaussian distribution with mean zero and some given variance. The input is not frozen noise anymore, but a jittered version of the underlying input pattern $\{t_i^\mu\}$. Similarly to the condition of a stochastic input current, we tested the capacity of the network if during recall the input pattern are jittered or if during training the input is jittered (but noise free during recall).
Fig. 4.7 A ($N = 1000$) and B ($N = 2000$) shows the recall of networks trained noise

free with MPDP if during recall the spike times of the input patterns are jittered. For jitter with a small variance ($\sigma_{jitter} < 0.5ms$), the recall is almost unaffected. For stronger jitter, recall deteriorates. A rather strange feature of the recall is that for intermediate loads $\alpha \approx 0.05$ the recall is worse than for loads close to the maximal capacity ($\alpha_{90} \approx 0.125$). This observation is counter-intuitive and calls for explanation, because recall usually becomes worse for memory systems if their load is close to the capacity. However, fluctiations of the membrane potential due to jitter in the input spike times are scaled by the weights. This seperates this noise condition from the one with stochastic input current. A comparison of the weight statistics of networks trained with MPDP after training shows that the slump in the recall covaries with the weight variance (Fig. 4.7 C and D). For $N = 1000$ the minimum of the slump lies at $\alpha = 0.06$, which coincides with the maximum of the weight variance. For $N = 2000$, both lie at $\alpha = 0.04$ instead. The mean of the weights does have little to no influence on that; it stays almost constant as a function of load. E-Learning and FP-Learning do not have the same characteristics (data not shown). For example, with FP-Learning weight average and variance stay basically constant until a load of $\alpha \approx 0.2$, rather close to the capacity. Only then the mean decreases and variance increases (see for example Fig. 4.6 F, right plot for $\sigma_{input} = 0$ during training).

Networks trained without noise and tested with jittered input show a similar behavior to noise induced by an external stochastic current (Fig. 4.6 E, blue lines, versus Fig. 4.7 E). Networks trained with MPDP tolerate noise up to a certain degree without showing a deterioration of recall. With the other learning rules, the recall gets worse with arbitrary small noise levels. On the other hand, training a network with FP-Learning while injecting stochastic currents (the previous noise condition) led to almost unharmed capacity. The reason is that FP-Learning "downscales" the noise by scaling up the weight variance. This is not a viable path for jitter of input spike times. Therefore, E-Learning and FP-Learning as well as MPDP show a decrease of capacity if during training the input spike times are jittered. An interesting outlier is ReSuMe. The networks trained noise free with ReSuMe have low capacity and unstable recall. Even with slight jitter the recall does not reach 90 % anymore. Therefore, we do not include ReSuMe in Fig. 4.7 E. However, training the network with jitter leads to an increase of capacity (Fig. 4.7 F).

4.4 Discussion

We introduced a synaptic plasticity mechanism that is based on the requirement to balance the membrane potential and therefore uses the postsynaptic membrane potential rather than postsynaptic spike times as the relevant signal for synaptic changes (Membrane Potential Dependent Plasticity, MPDP). We have shown that this simple rule allows the somewhat paradoxical temporal association of enforced output spikes with arbitrary frozen noise input spike patterns (chronotron). Before, this task could only be achieved with supervised learning rules that provided knowledge not only about the desired spike times, but also about the type of each

postsynaptic spike (desired or spurious). With MPDP, the supervisor only has to provide the desired spike, while the synapse endowed with MPDP distinguishes between desired and spurios spikes exploiting the time course of the voltage around the spike. Additionally, the sensitivity of MPDP to subthreshold membrane potential allows for robustness against noise.

4.4.1 Biological plausibility of MPDP

Spike-Timing-Dependent Plasticity (STDP) is experimentally well established and simple to formalize, which made it a widely used plasticity mechanism in modelling. It is therefore important to note that MPDP is compatible with experimental results on STDP, in particular with those of Hebbian STDP on inhibitory synapses. The reason is that spikes come with a stereotypic trace in the membrane potential. The voltage rises to the threshold, the spike itself is a short and strong depolarization, and afterwards the neuron undergoes reset, all of which are signals for MPDP. Pairing a postsynaptic spike with presynaptic spikes at different timings gives rise to a plasticity window which shares its main features with the STDP window: The magnitude of weight change drops with the temporal distance between both spikes and the sign switches close to concurrent spiking.
It is known that the somatic membrane potential plays a role in synaptic plasticity. Many studies investigated the effect of prolonged voltage deflections by clamping the voltage for an extended time while repeatedly exciting presynaptic neurons (e.g. see [94]). However, MPDP predicts that synaptic plasticity is sensitive to the exact time course of the membrane potential, as well as the timing of presynaptic spikes. This necessitates that dendrites and spines reproduce the time course of somatic voltage without substantial attenuation. Morphologically the dendritic spines form a compartement separated from the dendrite, which, for example, keeps calcium localized in the spine. It has been a topic under investigation whether the spine neck dampens invading currents. Despite experimental difficulties in measuring spine voltage, recent studies found that backpropagating action potentials indeed invade spines almost unhindered [95]. Furthermore, independently of spine morphology and proximity to soma, the time course of a somatic hyperpolarizing current step is well reproduced in dendrites [96] and spines [97]. This shows that at least in principle the somatic voltage trace can be available at the synapse. In turn, voltage-dependent calcium channels can transform subthreshold voltage deflections into an influx of calcium, the major messenger for synaptic plasticity. A few studies found that short depolarization events act as signals for synaptic plasticity [52, 93], with a dependence of sign and magnitude of weight change on the timing of presynaptic spikes.
Another important point is the sign of synaptic change. “Membrane Potential Dependent Plasticity” per se is a very general term which potentially could include many different rules [28,98]. In this study, MPDP serves as a mechanism that keeps the membrane potential bounded. For inhibitory synapses this requirement results in a Hebbian plasticity rule, which has been reported previously [20]. Inhibitory

neurons in cortex have been implied to precisely balance excitatory inputs [99]. MPDP on excitatory synapses is necessarily "Anti-Hebbian". Lamsa et al [92] found that pairing presynaptic spikes with postsynaptic hyperpolarization can lead to synaptic potentiation. This was caused by calcium permeable AMPA receptors (CP-AMPARs) present in these synapses. However, Anti-Hebbian plasticity does not rely on CP-AMPARs alone. Verhoog et al. [23], for example, found Anti-Hebbian STDP in human cortex, which depends on dendritic voltage-dependent calcium channels. Taken together, these findings demonstrate the existence of cellular machinery which could implement homeostatic MPDP, either on excitatory or inhibitory synapses.

4.4.2 Properties and capabilities of Homeostatic MPDP

We derived homeostatic MPDP from a balance requirement: Synapses change in order to prevent hyperpolarization and strong depolarization for recurring input activity. This kind of balance reduces metabolic costs of a neuron and keeps it at a sensible and sensitive point of operation [100]. The resulting plasticity rule is Anti-Hebbian in nature because synapses change to decrease net input when the postsynaptic neuron is excited and to increase net input when it is inhibited. However, spike after-hyperpolarization turns homeostatic MPDP effectively into Hebbian plasticity. Every postsynaptic spike causes a voltage reset into a hyperpolarized state. Therefore synapses of presynaptic neurons which fired close in time to the postsynaptic spike will change to increase net input if the same spatio-temporal input pattern re-occurs. The total change summed over all synapses depends on the duration and magnitude of hyperpolarization. Because the induced synaptic change reduces this duration, total synaptic change is also reduced. The same is true for total synaptic change to decrease net input, which depends on the duration where the membrane potential stays above ϑ_D (resp. ϑ_P^I for inhibitory synapses) and which reduces this duration in future occurances. If the rise time of the voltage before the spike and residual spike after-hyperpolarization are both short and close in time, potentiation and depression will become approximately cancelled around a spike.

In this view, associative synaptic plasticity or "learning" is the consequence of imbalance. A spike is stable if the time course of the voltage in its proximity leads to balanced weight changes. For example, if input is just sufficient to cause a spike, the voltage slope just before the spike is shallow and synaptic depression outweighs potentiation. On the other hand, the delta-pulse shaped currents used to excite the postsynaptic neuron during chronotron training are very strong inputs. They are not unlearned. Instead, the weights potentiate until the membrane potential is in a balanced state, and the neuron fires the teacher spike on its own when left alone.

Another interesting aspect of MPDP is the emergence of robustness against noise. Most obviously, with the choice of the threshold for depression the neuron sets a minimal distance of the voltage to the firing threshold for known input patterns. This allows to have perfect recall in the case of noisy input in the chronotron. The

second effect of the depression threshold is more subtle. Not only does it prevent spurious spikes, but through learning the slope of the membrane potential just before the desired spike tends to become steep. This is necessary to prevent spike extinction by noise. To see how this influences noise robustness, consider an output spike with a flat slope of the voltage. Increasing the voltage slightly around the spike time moves the intersection of the voltage with the firing threshold forward in time by a proportionally large margin. Decreasing voltage moves it backwards in time or could even extinguish the spike; a flat slope implies a low peak of the "virtual" membrane potential. MPDP in contrast achieves a state which is robust against spike extinction as well as the generation of spurious spikes. On the downside, keeping the voltage away from the firing threshold as well as imposing steepness on the slope just before spikes puts additional constraints on the weights. Robustness comes at the cost of capacity.

4.4.3 Relation of MPDP to other learning rules

There are many supervised learning algorithms that are used to train neuronal networks to generate desired spatio-temporal activity patterns. All of them involve a comparison of the self-generated output to the desired target activity. They can be broadly put into three different classes. E-Learning and FP-Learning [39, 81] are examples of algorithms of the first class which are used to train a neuron to generate spikes at exactly defined times. They first observe the complete output and then evaluate it against the target. E-Learning performs a gradient descent on the Victor-Purpura distance [83] between both spike trains. This means that the weight changes associated to one particular spike (actual or desired) can depend on distant output spikes. In FP-Learning, the training trial is interrupted if the algorithm encounters an output error. Subsequent spikes are not evaluated anymore. Thereby these algorithms are non-local in time and very artificial.
Another class of learning algorithms emerged recently with the examples PBSNLR [101] and HTP [39]. They take an entirely different route. The postsynaptic membrane potential is treated as a static sum of PSP kernels weighted by the respective synaptic weight, similar to the SRM_0 model of the LIF neuron. The firing threshold is moved towards infinity to prevent output spikes and voltage resets are added at the target spike times. Then the algorithms perform a perceptron classification on discretely sampled time points of the voltage, with the aim to keep it below the actual firing threshold for all non-spike times and to make sure a threshold crossing at the desired spike times. These algorithms were devised as purely technical solutions and are highly artificial. However, MPDP bears some similarity to the described procedure: Except close to teacher inputs, at every point in time recently active synapses get depressed if the voltage is above the threshold for depression. This is comparable to a perceptron classification on a continuous set of points.
A third class of algorithms compares actual and target activity locally in time. In contrast to the algorithms mentioned above, they are usually not used to learn exact spike times, but rather continuous time dependent firing rates. The ur-example is

the Widrow-Hoff rule [42, 82]. More recently, similar rules were developed by Xie and Seung [79], Brea et al. [38] and Urbanzcik and Senn [78]. In contrast to the Widrow-Hoff rule, the more recent rules are defined for spiking LIF neurons with a "soft" firing threshold, i.e. spike generation is stochastic and the probability of firing a spike is a monotonous function of the current voltage. In these rules, at every point in time the synaptic change is proportional to the difference of the current firing rate and a target firing rate specified by an external supervisor. When it comes to biological implementation, the central problem of Widrow-Hoff type rules is the comparison of self-generated and target activity. It is derived from the abstract goal to imprint the target activity into the network. This target needs to be communicated to the neuron and synaptic plasticity has to be sensitive to the difference of the neurons' own current acticity state (implicitely represented by its membrane potential) and the desired target activity. Usually, no plausible biological implementation for this comparison is given. The combination of homeostatic MPDP, hyperpolarization and a teacher now offers a solution to both problems. The teacher provides information about the target activity through temporally confined, strong input currents which cause a spike. Spike after-hyperpolarization (SAHP) allows to compare the actual input to the target without inducing spurious spikes detrimental to learning. The more SAHP is compensated by synaptic inputs, the closer the self-generated activity is to the target and the less synapses need to be potentiated. This is implemented naturally in MPDP, where potentiation is proportional to the magnitude and duration of hyperpolarization. On the other hand, strong subthreshold depolarization implies that self-generated spurious spikes are highly probable, and weights need to be depressed to prevent spurious spikes in future presentations.

A further solution for the problem of how information about the target is provided was given by Urbanczik and Senn [78]. Here, the neuron is modelled with soma and dendrite as seperate compartements instead of point neurons as used in this study. The teacher is emulated by synaptic input projecting directly onto the soma, which causes a specfic time course of the somatic membrane potential. The voltage in the dendrite is determined by a different set of synaptic inputs, but not influenced by the somatic voltage; however, the soma gets input from the dendrites. The weight change rule then acts to minimize the difference of somatic (teacher) spiking and the activity as it would be caused by the current dendritic voltage. This model represents a natural way to introduce an otherwise abstract teacher into the neuron. Nonetheless, the neuron still has to estimate a firing rate from its current dendritic voltage, for which no explicit synaptic mechanism is provided. Also, it is worth noting that the model of Urbanczik and Senn requires a one-way barrier to prevent somatic voltage invading the dendrites; in contrast, MPDP requires a strong two-way coupling between somatic and dendritic/synaptic voltage.

Another putative mechanism for a biolgical implementation of the δ-rule was provided by D'Souza et al. [102]. In this model, a neuron recieves early auditory and late visual input. By the combination of spike frequency adaptation (SFA) and STDP, the visual input acts as the teacher that imprints the desired response to a

given auditory input in an associative manner. However, the model is quite specific to the barn owl setting; for example, parameters have to be tuned to the delay between auditory and visual input.
Applying rules of the Widrow-Hoff type to fully deterministic neurons can lead to unsatisfactory results. ReSuMe is an example of such a rule [82]. Its memory capacity is low, but it increases sharply if the input is noisy during training (see Fig. 4.7). A propable reason is that in a fully deterministic setting, the actual spike times do not allow a good estimation of the expected activity. This sounds paradoxial. But if we consider a deterministic neuron with noise-free inputs the membrane potential can be arbitrarily close to the firing threshold without crossing it. But even the slightest perturbation can cause spurious spikes at those times. This leads to bad convergence in chronotron training, since the perturbations caused by weight changes for one pattern can easily destroy previously learned correct output for another pattern [39]. The problem of these rules is the sensing of the activity via the instantaneous firing rate. Therefore, the explicit sensitivity to subthreshold voltages of MPDP is advantageous if training examples are noise free.
We conclude that our MPDP rule with hyperpolarization and teacher input represents a biologically plausible implementation of the comparison of actual and target activity that is key to all supervised learning algorithms. Also, because MPDP is explicitely sensitive to the membrane potential and not the firing rate, it is fully applicable to deterministic neurons. Additionally, the training procedure leads to networks whose output is robust against input noise, similar to what learning algorithms of the Widrow-Hoff type achieve.

4.4.4 Outlook

We derived the synaptic plasticity rule from the objective to keep the membrane potential within bounds, which is a homeostatic principle that at first sight would primarily serve the stability of network dynamics. In particular, this principle might explain the strikingly detailed balance of excitation and inhibition as observed in cortex [103–105] (compare also Fig. 4.2, bottom row). In fact, such homeostatic plasticity has been found e.g. for parvalbumin expressing interneurons which selectively adapt their synaptic strength in an activity dependent manner to match the excitatory inputs to target cells [99]. Being an anti-hebbian mechanism homeostatic plasticity might even appear to contradict associative learning. Therefore we find it particularly intriguing that -when combined with the ubiquitous spike after-hyperpolarizarion- it can paradoxically entail robust spike-based associative learning. We think this fact suggests that the balance in cortex could rather reflect a powerful learning principle at work.

4.5 Materials and Methods

In this section, we present the models used. We start with the simpler leaky integrate-and-fire neuron model (LIF neuron) and use it to derive the MPDP rule.

We then show how MPDP can be applied to a more realistic conductance based integrate-and-fire neuron. Last, we describe the chronotron setup we use for quantitatively assessing the memory capacity of MPDP.

4.5.1 The LIF neuron and derivation of MPDP

We investigated plasticity processes in a simple single-layered feed-forward network with N (presynaptic) input neurons and one (postsynaptic) output neuron (see Fig. 4.1 A). For the input population we stochastically generate spatio-temporal spike patterns which are kept fixed throughout training (frozen noise). We denote the time of the k-th spike of presynaptic neuron with index i as t_i^k.
The postsynaptic neuron is modelled as a LIF neuron. The evolution of the voltage $V(t)$ over time is given by

$$\tau_m \dot{V} = -V + I_{syn} + I_{ext} \ . \tag{4.1}$$

I_{syn} and I_{ext} are synaptic and external currents, respectively, and τ_m is the membrane time constant of the neuron. If the voltage reaches the firing threshold V_{thr} at time t_{post}, the neuron generates a spike and undergoes immediate reset to the reset potential $V_{reset} < 0$. In the absence of any input currents, the neuron relaxes to an equilibrium potential of $V_{eq} = 0$. Synaptic currents are given by

$$\tau_s \dot{I}_{syn} = -I_{syn} + \sum_i w_i \sum_k \delta\left(t - t_i^k\right) \ . \tag{4.2}$$

τ_s is the decay time constant of synaptic currents and w_i is the synaptic weight of presynaptic neuron i. For ease of derivation of MPDP, we reformulated the LIF model. Because of the linearity of Eq. 4.1, we can write the voltage as the sum of kernels for postsynaptic potentials (PSPs) $\varepsilon(s)$ and resets $R(s)$:

$$V(t) = \sum_i w_i \sum_k \varepsilon(t - t_k^i) + \sum_{t_{post}} R(t - t_{post}) + \int_0^\infty \kappa(t-s) I_{ext}(s) ds \ . \tag{4.3}$$

$\kappa = \exp\left(-(t-s)/\tau_m\right)$ is the passive response kernel by which external currents are filtered. The other kernels are

$$\begin{aligned} \varepsilon(s) &= \Theta(s) \frac{1}{\tau_m - \tau_s} \left(\exp(-s/\tau_m) - \exp(-s/\tau_s)\right) \\ R(s) &= \Theta(s)(V_{reset} - V_{thr}) \exp(-s/\tau_m) \ . \end{aligned} \tag{4.4}$$

$\Theta(s)$ is the Heaviside step function. This formulation is also known as the simple Spike Response Model (SRM_0, [41]).
We next derive the plasticity rule from the naive demand of a balanced membrane potential: The neuron should not be hyperpolarized nor too strongly depolarized. This is a sensible demand for the dynamics of a neuronal network, because it holds the neurons at sensitive working points and also keeps metabolic costs down. For

the formalization of the objective, we introduce an error function which assigns a value to the current voltage:

$$2E(t) = \gamma \left([V(t) - \vartheta_D]_+ \right)^2 + \left([\vartheta_P - V(t)]_+ \right)^2 \ , \tag{4.5}$$

where $\vartheta_{D,P}$ are thresholds for plasticity, and γ is a factor that scales synaptic long-term depression (LTD) and long-term potentiation (LTP) relative to each other. Whenever $V(t) > \vartheta_D$ or $V(t) < \vartheta_P$, the error function is greater than zero. Therefore, to minimize the error, the voltage must stay between both thresholds. In this study, we choose $\vartheta_P = V_{eq}$. ϑ_D is set between the firing threshold and V_{eq}. From the error function, a weight change rule can be obtained by computing the partial derivative of $E(t)$ with respect to weight w_i:

$$\begin{aligned} \frac{\partial E(t)}{\partial w_i} &= \gamma \left[V(t) - \vartheta_D \right]_+ \frac{\partial V(t)}{\partial w_i} - \left[\vartheta_P - V(t) \right]_+ \frac{\partial V(t)}{\partial w_i} \\ &= \left(\gamma \left[V(t) - \vartheta_D \right]_+ - \left[\vartheta_P - V(t) \right]_+ \right) \sum_k \varepsilon \left(t - t_i^k \right) \ . \end{aligned} \tag{4.6}$$

The MPDP rule then reads

$$\dot{w}_i = -\eta \frac{\partial E(t)}{\partial w_i} = \eta \left(-\gamma \left[V(t) - \vartheta_D \right]_+ + \left[\vartheta_P - V(t) \right]_+ \right) \sum_k \varepsilon \left(t - t_i^k \right) \ . \tag{4.7}$$

η is the learning rate. The weights change along the gradient of the error function, i.e. MPDP is a gradient descent rule that minimizes the error resulting from a given input pattern.

4.5.2 The conductance based LIF neuron

The simple model above suffers from the fact MPDP is agnostic to the type of synapse. In principle, MPDP can turn excitatory synapses into inhibitory ones by changing the sign of any weight w_i. Since this is a violation of Dale's law, we present a more biologically realistic scenario involving MPDP. We split the presynaptic population into N_e excitatory and N_i inhibitory neurons. The postsynaptic neuron is modelled as a conductance based LIF neuron governed by

$$C_m \frac{\mathrm{d}V}{\mathrm{d}t} = -g_L(V - V_L) - (g_s + g_f)(V - V_h) - g_{ex}(V - V_{ex}) - g_{in}(V - Vin) \ , \tag{4.8}$$

where V denotes the membrane potential, C_m the membrane capacitance, V_L the resting potential, g_L the leak conductance, V_i and V_{ex} the reversal potential of inhibition and excitation, respectively and g_{in} and g_{ex} their respective conductances. The spike after-hyperpolarisation is modeled to be biphasic consisting of a fast and a slow part, described by conductances g_f and g_s that keep the membrane potential close to the hyperpolarisation potential V_h. When the membrane potential surpasses

the spiking threshhold V_{thr} at time t_{post}, a spike is registered and the membrane potential is reset to $V_{reset} = V_h$. All conductances are modeled as step and decay functions. The reset conductances are given by

$$\tau_{f,s}\dot{g}_{f,s} = -g_{f,s} + \Delta g_{f,s} \sum_{t_{post}} \delta\left(t - t_{post}\right) \ , \tag{4.9}$$

where $\Delta g_{f,s}$ is the increase of the fast and slow conductance at the time of each postsynaptic spike, respectively. They decay back with time constants $\tau_f < \tau_s$. The input conductances g_{ex} and g_{in} are step and decay functions as well, that are increased by w_i when presynaptic neuron i spikes and decay with time constant τ_s. w_i denotes the strength of synapse i.
In this model, we employ MPDP as defined by Eq. 4.7 with the following restrictions:

- Technically, there is no fixed PSP kernel for the conductance based model, since the amplitude of a single PSP depends on the current voltage. Still, we use the same rule by keeping track of "virtual PSPs" for each synapse that do not affect the neuronal dynamics.
- MPDP affects only inhibitory synapses. Excitatory ones are kept fixed.
- Because inhibitory synapses have negative impact on the neuron, we exchange LTP and LTD in the MPDP rule to account for that. Formally, we introduce thresholds ϑ_D^I and ϑ_P^I.

ϑ_D^I lies below the equilibrium potential V_L, and an inhibitory synapse depresses whenever it is active and $V(t) < \vartheta_D^I$. Similarly, when $V(t) > \vartheta_P^I$, any active inhibitory synapse gets potentiated. Note that the qualitative effect on the membrane potential remains unchanged to the example in Fig. 4.1 B.

4.5.3 Evaluation of memory capacity

The memory capacity of a typical neuronal network in a given task crucially depends on the learning rules applied (for an example in spiking networks see [81]). Recently, it was shown that the maximal number of spiking input-output associations learnable by a postsynaptic neuron lies in the range of 0.1 to 0.3 per presynaptic input neuron [39]. The exact number mostly depends on the shape of the PSP (determined by τ_m and τ_s) and to a lesser extent on average pre- and postsynaptic firing rates. Here, we evaluate the memory capacity attainable with MPDP and compare it with ReSuMe [82], E-Learning [81] and FP-Learning [39], with the latter learning rule being optimal in terms of memory capacity. For ease of comparison, we adapt the chronotron setting introduced by Florian [81], use the simple neuron model of the LIF neuron and let synapses change their sign. The definitions of patterns, associations and memory capacity is similar to the ones used in tempotron and perceptron training [42, 75]. We provide a short description of ReSuMe, E-Learning and FP-Learning below.

Chronotron setting. The goal of the chronotron is to imprint input-output associations into the weights. One input pattern consists of spatio-temporal spiking activity of the N input neurons with duration $T = 200ms$. In each pattern, each input neuron spikes exactly once, with spike times t_i^μ drawn i.i.d. from the interval $[0, T]$. $\mu \in 1, \ldots, P$ indexes the patterns. For each input pattern we draw one desired output spike time t_d^μ i.i.d. from the interval $[\Delta_{edge}, T - \Delta_{edge}]$, with $\Delta_{edge} = 20ms$. We reduce the length of the output interval to ensure that each output spike in principle can be generated by the input. If the desired output spike time is too early there might be no input spikes earlier than t_d, which makes it impossible for the postsynaptic neuron to generate the desired output. After all P patterns have been generated, we keep them fixed for the duration of network training and recall testing. Training is organized in learning trials and learning blocks. A learning trial in MPDP consists of the presentation of one of the input patterns and concurrent induction of a teacher spike at time t_d^μ by injection of a supratheshold delta-pulse current by the supervisor. In all other learning rules, the supervisor passively observes the output activity and changes weights afterwards based on the actual output. A learning block consists of P learning trials, with each of the different input patterns presented exactly once in randomized order. After each learning trial, synaptic weights are updated. After each learning block, we present the input patterns again to test the recall quality. Supervisor intervention and synaptic plasticity are switched off for recall trials.

Computing the capacity. We test the capacity of each learning rule (MPDP, ReSuMe, E-Learning and FP-Learning) by training networks of different sizes, $N \in \{200, 500, 1000, 2000\}$. Because we assume that the number of patterns or input-output associations that can be learned scales with N [39,81], we introduce the load parameter α with $P = \alpha N$. We pick discrete $\alpha \in [0.01, 0.3]$. For each combination of α and N, we generate 50 different realizations of P patterns and N initial weights, which are drawn from a gaussian distribution with mean and standard deviation $T \cdot 30mV/N$. For a non-spiking neuron (i.e. Eq. 4.1 with $V_{thr} \gg 1$) this would result in an average membrane potential of $30mV$ before learning. As a result initially the postsynaptic neuron fires several spurious spikes. This way we test the ability of a learning rule to extinguish them.
After each learning block, the recall is tested. Recall is counted as a success if the postsynaptic neuron fires exactly one output spike in a window of length $4ms$ centered around t_d^μ, and no additional spike at any time. We define success loosely, because MPDP and FP-Learning do not converge onto generating the output spike exactly at t_d^μ.
We train each network for a fixed number of learning blocks (10000 in the case of MPDP, 20000 for the others). Because we evaluate recall after each learning block, we can check whether the system has converged. We define capacity as the "critical load" α_{90}, where on average 90 % of the spikes are recalled after training. To approximate it, we plot the fraction of patterns correctly learned as a function of the load α. The critical load is defined as the point where a horizontal line at 90

% correct recall meets the graph.

Testing noise tolerance. The threshold for LTD, ϑ_D, is not only a way to impose homeostasis on the synaptic weights. It is also a safeguard against spurious spikes that could be caused by fluctuations in the input or membrane potential. The reason is that after convergence of weight changes for known input patterns the voltage mostly stays below ϑ_D for all non spike times due to the repulsion of the membrane potential away from threshold. This leaves room for the voltage to fluctuate without causing spurious spikes.
We apply noise in two conditions. First we want to know if a trained network is able to recall the learned input-output associations in the presence of noise, i.e. we train the network first and apply noise only during the recall trials. Second we test if a learning rule can be used to train the network in the presence of noise. In this condition, we test recall noise free.
We induce noise in two different ways. One way is to add a stochastic external current

$$I_{ext}(t) = \frac{\sigma_{input}}{\sqrt{\tau_m}}\eta(t) \ . \tag{4.10}$$

$\eta(t)$ is a gaussian white noise process with zero mean and unit variance. The factor makes sure that the actual noise on the membrane potential has standard deviation σ_{input}.

The other way is to jitter the input spike times. Instead of using presynaptic spike times t_i^μ, we let the neurons spike at times

$$\hat{t}_i^\mu = t_i^\mu + \mathcal{N}(0, \sigma_{jitter}) \ , \tag{4.11}$$

where $\mathcal{N}(0, \sigma)$ is a random number drawn from a gaussian distribution with standard deviation σ.
If we apply noise only during recall, we use the weights after the final learning block and for each noise level $\sigma_{input,jitter}$ we average the recall over 50 seperate noise realizations and all training realizations.
Although both procedures lead to random fluctuations of the membrane potential in each pattern presentation, they lead to different results. The reason is that by using jitter on the input spike times, the statistics of the weights impact on the actual amount of fluctuations of the voltage. This has noticable consequences for the different learning rules.

4.5.4 Learning algorithms used for quantitative comparison

Our goal is a quantitative analysis of the memory capacity of MPDP in the chronotron task. We feel this necessitates a comparison to other learning rules. We chose ReSuMe [82], which is a prototypical learning rule for spiking output, E-Learning [81] as a powerful extension, and FP-Learning [39], which was shown to achieve optimal memory capacity in the task. Here, we provide a short description of all three rules.

The δ-rule and ReSuMe. The δ-rule, also called the Widrow-Hoff-rule [42], lies at the core of a whole class of learning rules used to teach a neuronal network some target activity pattern. Synaptic changes are driven by the difference of desired and actual output, weighted by the presynaptic activity:

$$\Delta w(t) \propto f_{pre}(t) \left(f_{post}^{target}(t) - f_{post}^{actual}(t) \right) \ . \tag{4.12}$$

We denote pre- and postsynaptic firing rate with $f_{pre,post}$. The target activity $f_{post}^{target}(t)$ is some arbitrary time dependent firing rate. The actual self-generated activity $f_{post}^{actual}(t)$ is given by the current input or voltage of the postsynaptic neuron (depending on the formulation), transformed by the input-output function $g(h)$ of the neuron.

ReSuMe (short for Remote Supervised Method) is a supervised spike-based learning rule first proposed in 2005 [82]. It is derived from the Widrow-Hoff rule for rate-based neurons, applied to deterministic spiking neurons. Therefore, continuous time dependent firing rates get replaced with discrete spiking events in time, expressed as sums of delta-functions. Because these functions have zero width in time, it is necessary to temporally spread out presynaptic spikes by convolving the presynaptic spike train with a temporal kernel. Although the choice of the kernel is free, usually a causal exponential kernel works best. We also used ReSuMe with a PSP kernel to train chronotron, but the results were worse than with the exponential kernel (data not shown). The weight change is given by

$$\dot{w}(t) \propto [S_d(t) - S_o(t)] \left[a_d + \int_0^\infty \exp(-s/\tau_{plas}) S_i(t-s) ds \right] \ , \tag{4.13}$$

where $S_d(t)$ is the desired, $S_o(t)$ is the self-generated and $S_i(t)$ the input spike train at synapse i. τ_{plas} is the decay time constant of the exponential kernel. a_d is a constant which makes sure that the actual and target firing rates match; learning also works without, therefore we choose $a_d = 0$ in our study. ReSuMe converges when both actual and desired spike lie at the same time, because in this case the weight changes cancel exactly.

In recent years, several rules for spiking neurons have been devised which are similar to the δ-rule [38, 78, 79]. With the "PSP sum"

$$\lambda_i = \sum_k \varepsilon(t - t_i^k) \ , \tag{4.14}$$

the weight change takes the form

$$\dot{w}_i \propto [S_{teacher}(t) - \rho(V(t))] \, f(\rho(V(t))) \lambda_i(t) \ . \tag{4.15}$$

$S_{teacher}$ is a stochastic realization of a given desired time dependent target firing rate, $\rho(V(t))$ is the instantaneous firing rate, which depends on the current membrane potential, and $f(\rho)$ is a function which additionally scales the weight changes depending on the current firing rate. Although the rule of Xie and Seung [79] was defined in a reward learning framework, it is equivalent to the formulation above if the output neuron is forced to fire a teacher spike train and reward is kept constant.

E-Learning. E-Learning was conceived as an improved learning algorithm for spike time learning [81]. It is derived from the Victor-Pupura distance (VP distance) between spike trains [83]. The VP-distance is used to compare the similarity between two different spike trains. Basically, spikes can be shifted, deleted or inserted in order to transform one spike train into the other. Each action is assigned a cost, and the VP distance is the minimum transformation cost. The cost of shifting a spike is proportional to the distance it is shifted and weighted with a parameter τ_q. If the shift is too far, it gets cheaper to delete and re-insert that spike.
E-Learning is a gradient descent on the VP distance and has smoother convergence than ReSuMe. In this rule, first the actual output spike train is compared to the desired spike train. With the VP algorithm it is determined if output spikes must be shifted or erased or if some desired output spike has no close actual spike so a new spike has to be inserted. Based on this evaluation, actual and desired spikes are put in three categories:

- Actual output spikes are "paired" if they have a pendant, i.e. a desired spike close in time and no other actual output spike closer (and vice versa). These spikes are put into a set S.
- Unpaired actual output spike that need to be deleted are put into the set D.
- Unpaired desired output spike times are put into the set J, i.e. the set of spikes that have to be inserted.

To clarify, S contains pairs of "paired" actual and desired spike times, D contains the times of all unpaired actual spikes, and J the times of unpaired desired spike times. With the PSP sum as above, the E-Learning rule is then

$$\Delta w_i = \gamma \left[\sum_{t_{ins} \in J} \lambda_i(t^{ins}) - \sum_{t^{del} \in D} \lambda_i(t^{del}) + \frac{\gamma_r}{\tau_q^2} \sum_{(t^{act}, t^{des}) \in S} (t^{act} - t^{des}) \lambda_i(t^{act}) \right] . \quad (4.16)$$

γ is the learning rate, and γ_r is a factor to scale spike shifting relative to deletion and insertion.
The former two terms of the rule correspond to ReSuMe, except the kernel is not a simple exponential decay. The advantage of E-Learning is that the weight changes for spikes close to their desired location are scaled with the distance, which improves convergence and consequentially memory capacity.

FP-Learning. FP-Learning [39] was devised to remedy a central problem in learning rules like ReSuMe and others. Any erroneous or missing spike "distorts" the time course of the membrane potential behind it compared to the desired final state. This creates a wrong environment for the learning rule, and weight changes can potentially be wrong. Therefore, the FP-Learning algorithm stops the learning trial as soon as it encounters any spike output error. Additionally, FP-Learning introduces a margin of tolerable error for the desired output spikes. An actual output spike should be generated in the window of tolerance $[t_d - \epsilon, t_d + \epsilon]$ with the adjustable margin ϵ. Weights are changed on two occasions:

1. If a spike occurs outside the window of tolerance for any t_d at time t_{err}, then weights are depressed by $\Delta w_i \propto -\lambda_i(t_{err})$. This also applies if the spike in question is the second one within a given tolerance window.

2. If $t = t_d + \varepsilon$ and no spike has occured in the window of tolerance, then $t_{err} = t_d + \varepsilon$ and $\Delta w_i \propto \lambda_i(t_{err})$.

In both cases, the learning trial immediately ends, to prevent that the "distorted" membrane potential leads to spurious weight changes. Because of this property, this rule is also referred to as "First Error Learning".

4.5.5 Parameters of the simulations

Conductance based neuron. The parameters used are as follows: $C_m = 0.25nF$, $g_L = 20nS$, $V_L = -55mV$, $V_{thr} = -50$ $V_{ex} = -40mV$, $V_h = V_{reset} = V_{in} = -75mV$, $\Delta g_s = 0.001$, $\Delta g_f = 0.04$, $\tau_f = 3ms$, $\tau_s = 12.5ms$, and $\tau_s = 3ms$. For the MPDP rule, the parameters are: $\vartheta_D^I = -58mV$, $\vartheta_P^I = -53mV$, $\gamma = 100$, $\eta = 5 \cdot 10^{-8}$ and $\tau_m = C_m/g_L = 12.5ms$.

Simple LIF neuron. The neurons' parameters are $\tau_s = 3ms$, $\tau_m = 10ms$ and $V_{thr} = 20mV$. The reset potential is $V_{reset} = -5mV$ with MPDP and $V_{reset} = 0mV$ for the other learning rules. For MPDP we use $\vartheta_D = 18mV$, $\vartheta_P = 0mV$, $\gamma = 14$, and $\eta = 5 * 10^{-4}$. With ReSuMe, we find $\tau_{plas} = 10ms$, and $\eta = \{10, 4, 2, 1\} \cdot 10^{-10}$ for 200, 500, 1000 and 2000 neurons as good parameters. FP-Learning has only a single free parameter, the learning rate $\eta = 10^{-9}$.

Numerical procedures. All networks with MPDP were numerically integrated using a simple Euler integration scheme. The simulations for the conductance based LIF neuron were written in Python and used a step size of 0.01 ms. The neurons parameters are set to values that are both biologically realistic and similar to those of the quantitative analysis. For reference, we put them into the Supporting Informations.
The simulations of the simple neuron and scripts for analysis were written in Matlab (Mathworks, Natick, MA). Here, we used a step size of 0.1 ms.
The networks that were trained with ReSuMe, E-Learning and FP-Learning were simulated using an event-based scheme [106], since in these rules the subthreshold voltage is not important.
The parameters like learning rates and thresholds we use are set by hand for all plasticity rules. Before doing the final simulations, we did a search in parameter space by hand to find combinations which yield high performance in the chronotron task.
The error we report in Fig. 4.4 C and D, Fig. 4.6 A to D and Fig. 4.7 A and B is the standard error of the mean (SEM) over all 50 realizations.

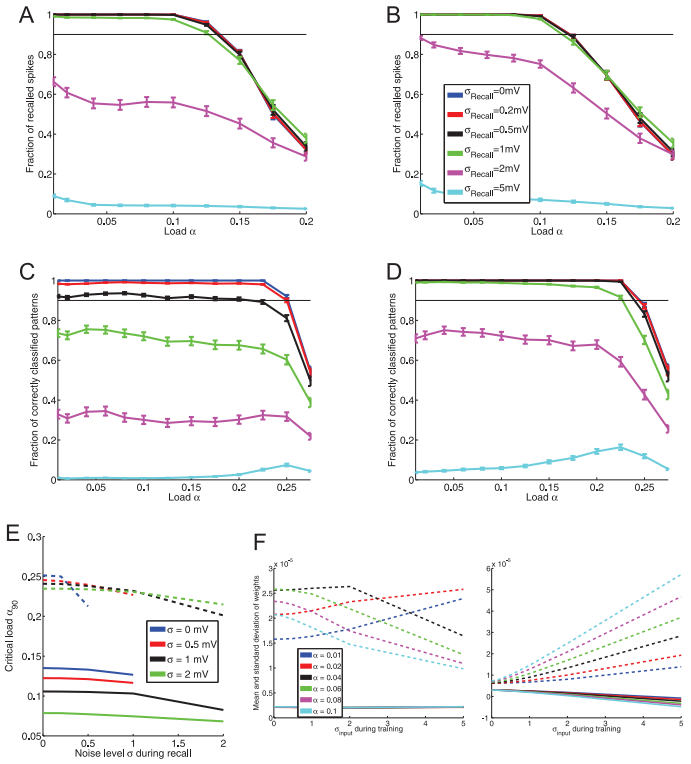

Figure 4.6: **Capacity of networks under input noise. A:** Recall as a function of the load for different levels of noise during recall. Noise is imposed as an additional stochstastic external current. Networks were trained with MPDP. Up to a noise level $\sigma input = 1mV$ during recall, there is almost no degradation of capacity. **B:** Same as A, but with stochastic input noise of width $0.5mV$ during network training. The capacity is slightly reduced, but resistance against noise is slightly better. **C** and **D:** Same as A and B, but the network was trained with FP-Learning. The capacity is doubled. However, the network trained without noise shows an immediate degradation of recall with noise. If the network is trained with noisy examples (D, $\sigma_{input} = 0.5mV$), also recall with noise of the same magnitude is perfect. **E:** Comparison of capacity of networks trained with MPDP and FP-Learning depending on input noise during training and recall. Solid lines: MPDP, dashed lines: FP-Learning. Lines that are cut off indicate that the network failed to reach 90 % recall for higher noise. x-axis is noise level during recall. Different colors indicate noise level during training. Curiously, although FP-Learning suffers more from higher noise during recall than during training, the capacity drops less than with MPDP. **F:** Comparison of weight statistics of MPDP (left) and FP-Learning (right) after learning. Solid lines are mean, dashed lines are standard deviation. With MPDP, the weigths stay within a bounded regime, the mean is independent of noise or load during training; the cyan line for $\alpha = 0.1$ occludes the others. FP-Learning rescales the weights during training with noise: The mean becomes negative, and the standard deviation grows linearly with noise level. This effectively scales down the noise by stochastic input.

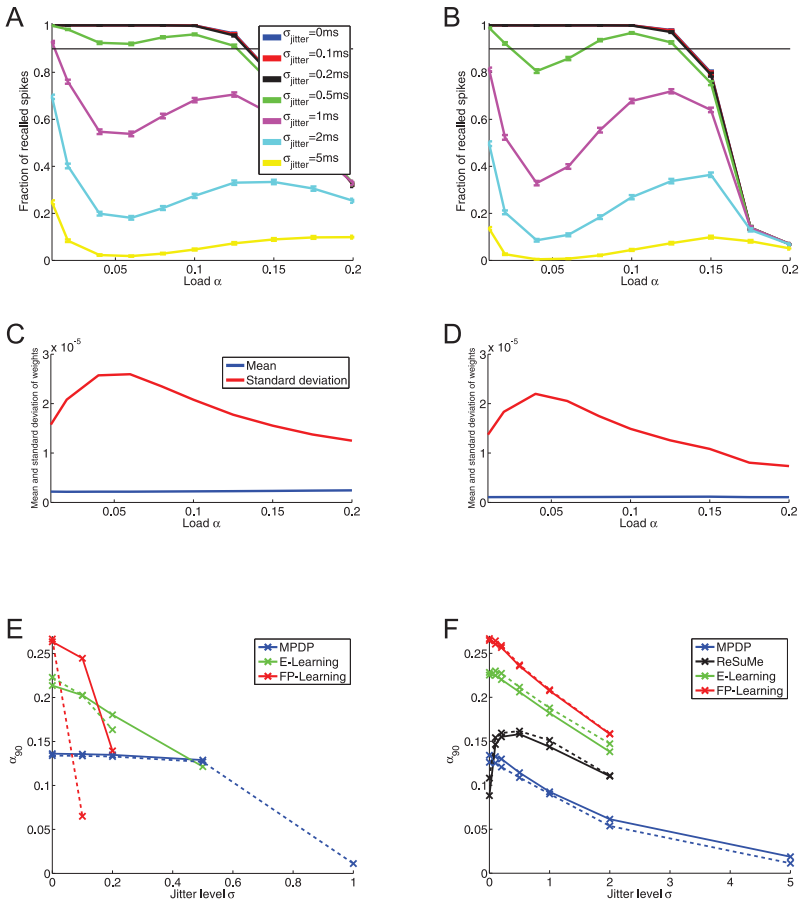

Figure 4.7: **Recall and capacity with input jitter. A:** Recall of networks trained noise-free with MPDP if during recall the input patterns are jittered ($N = 1000$). The black line lies on top of the blue and red ones (same in B). Up to $\sigma_{jitter} = 0.5ms$, the recall is unhindered. A curious feature is a "slump" in the recall for strong input jitter and intermediate loads. This slump is even more visible for the larger network with $N = 2000$ (**B**). The slump strongly correlates with the variance of the weights as a function of network load (**C** for $N = 1000$, **D** for $N = 2000$). The mean of the weights stays almost constant. **E:** Critical load as a function of input jitter during recall. The networks are trained noise free with different learning rules. Solid lines show $N = 2000$, dashed lines $N = 1000$. Crosses show sampling points. If a line is discontinued, this means that for this input jitter the networks do not reach 90 % recall anymore. Recall for MPDP stays almost constant until $\sigma_{jitter} = 0.5$, while for the other learning rules a considerable drop-off of recall is visible. **F:** Noise free recall of networks trained with noisy input. For MPFP, E-Learning and FP-Learning alike the capacity drops with increasing training noise. The exception is ReSuMe. Here, the capacity strongly *increases* if the noise is small.

Chapter 5

Discussion

5.1 Summary

The topic of this thesis is synaptic plasticity and its functional implications for learning. In publication I, the Contribution Dynamics model for spike-timing dependent plasticity was developed. It incorporates novel contributions to model the interactions between multiple spikes, and over a range of diverse data sets achieves better fit errors over contemporary plasticity models while being at the same level of complexity. Also, it was shown that there is a possible link between synaptic plasticity and the importance of theta-band oscillations for memory formation. The simple spSTDP model shows a susceptibility to firing rate modulations around 6 Hz, in the theta range. Among the higher order models, the CD model best retains this susceptibility and phase dependence of weight changes. This represents a robust mechanism for synaptic plasticity to take advantage of firing rate modulations without the need for precise spike time locking. In other words, this sensitivity allows learning even with highly stochastic neuronal firing if theta oscillations are enforced externally.
Publication II and chapter 4 deal with a different model of synaptic plasticity. The plasticity rule in publication II is motivated by reports of STDP in inhibitory synapses. Haas and colleagues [20] found Hebbian STDP for synapses of inhibitory interneurons onto excitatory neurons in the entorhinal cortex. However, this plasticity rule is Hebbian *only* regarding the weights; i.e. pre- before postsynaptic spiking potentiates the synapse, and reversing the order depresses the synapse. The actual effect on the postsynaptic neuron is sign-reversed: Potentation of the synapse leads to suppression of postsynaptic activity. In other words, causal spiking is suppressed, anti-causal spiking is reinforced. This kind of plasticity is usually thought to be detrimental for learning. However, if we consider additional spike after-hyperpolarization, anti-Hebbian STDP allows for associative learning using a simple teacher. Spike after-hyperpolarization desensitizes the neuron to excitation. This way, the neuron can sum up input to safely "compare" it to the firing threshold. The exact mechanism is demonstrated in publication II using tempotron learning, which also shows that it is beneficial to have synaptic depression which does not de-

pend on postsynaptic spiking. Instead, a second threshold below the firing threshold was introduced. When the voltage crosses this threshold from below, it triggers a spike-like signal which, however, does not influence the neuronal voltage dynamics. Instead, when the signal arrives at the synapses they depress proportional to the trace of the presynaptic activity. The combination of this subthreshold synaptic depression, anti-causal potentiation and spike after-hyperpolarization can be exactly mapped to the classical Perceptron Learning Rule (PLR). Because of the locality of the learning algorithm presented in publication II, it represents a biologically plausible implementation of the PLR. In chapter 4, the idea of a membrane potential dependent plasticity rule is fully explored. MPDP retains the Anti-Hebbian characteristic of the Anti-STDP rule from publication II. With this plasticity rule, additional spike after-hyperpolarization and a teacher who enforces spikes at the desired times, a postsynaptic neuron can be trained to spike at these times just by the presynaptic input. The performance of the learning algorithm compares well to several artificial learning rules.

5.2 Discussion

The modelling of STDP and theta susceptibility

Despite the best efforts over the past decades, the rules underlying synaptic plasticity are still not well understood. One reason is the difficulty in obtaining quantitative data of plasticity processes and weight changes. This is made worse by the huge diversity of synapse types and experimental protocols. Experiments have been performed in thick-tufted cells in layer 5 of [16, 47], pyramidal cells in layer 2/3 [25] in the visual cortex or somatosensory cortex of rats [48, 91], others have been done in hippocampal cells in slices [64] or in culture [19, 26], in living *Xenopus* tadpoles [21] or in the olfactory system of locusts [22], just to name a few. Electrical stimulation of presynaptic neurons is done either by patching them [47] or by placing a bipolar electrode close to the dendritic tree of the postsynaptic neuron and exciting synapses extracellularly [48, 107]. The specifics of the STDP window also depend on dendritic location of the examined synapse [108, 109]. It is no surprise that the phenomenology of STDP is very diverse [49]. Sometimes seemingly minor details in the experimental procedure change the outcome of the experiment drastically. An interesting example was provided by Wittenberg and Wang [64]. They recreated STDP experiments performed by Nishiyama and colleagues [110] at excitatory synapses projecting from the CA3 region to CA1 in the hippocampus of rats. The earlier work found classical STDP, i.e. potentiation for a pre-post spike pair, at this synapse type. However, Wittenberg and Wang observed no synaptic change. Instead, the postsynaptic neuron additionally has to fire at an elevated rate, or fire two spikes after the presynaptic one (a pre-post-post triplet) for the synapse to potentiate. The difference to the experiments of Nishiyama and colleagues was that the latter group used cesium instead of potassium in their intracellular solution in the patch pipette; everything else was the same. After Wittenberg and Wang used

cesium, they reproduced the ealier results. Cesium leads to a slight depolarization and a broadening of bAPs, which was enough to retrieve classical STDP.
Despite this diversity of findings, spSTDP is by far the most commonly used plasticity model in theoretical studies. There are several reasons for its widespread use:

- spSTDP faithfully recreates the STDP window with the minimal amount of parameters, compare figures 2.2 and 2.3.
- The causal LTP part of the STDP window is very appealing from a theoretical point of view. In supervised learning rules often causal LTP is derived from an abstract objective [18, 38, 80].
- spSTDP is a very simple model, which allows for analytical tractability and low computational cost in network simulations.

However, there are severe caveats concerning the use of spSTDP. In neuronal network models it is an inherently unstable plasticity rule that has to be augmented with some kind of stop condition, like synaptic scaling or bounded weights [24, 89]. Experiments that probe spike patterns beyond simple spike pairs reveal that spSTDP is a poor fit to the results [25, 26, 47, 48, 107]. Given the shortcomings of spSTDP on this data, the widespread use can be troubling, because it is rarely investigated how higher-order contributions to synaptic plasticity change the theoretical results obtained with spSTDP. However, this requires using higher-order models that capture the effects of spikes (or voltage) on synaptic plasticity beyond spike pairs. But modellers constructing this kind of model run into a problem: They have to be constrained by data. Every model consists of two parts, the mathematical formulation and the set of parameters. In chapter 2 and publication I we have seen a vast range of different model formulations. They get constrained to data by fitting the model parameters such that the fit error, i.e. the deviation between model predictions and experimental data, is minimized. The minimal models presented in chapter 2 have 8 (Triplet model), 11 (CD model, Uramoto model) or 13 parameters (Graupner model). The big problem is that the data sets which can be used to constrain the models usually have around 10 to 18 different data points. This makes fitting the models prone to overfitting; a model with many parameters likely fits the data well, but it will not generalize well to additional data points obtained in the same experimental setting. The problem can be alleviated to some extent by fitting the same model (using different parameters) to diverse data sets. Each data set displays different features of synaptic plasticity, which should be captured by a general model of synaptic plasticity. In this respect, of the three models considered the CD model displays the best fit to all data sets. The other models especially struggle to capture the adaptation effects in the data set of Froemke and colleagues [107]. Excluding either pre- or postsynaptic adaptation in the CD model leads to an increase of the fit error by a factor of ten. In the other data sets, including adaptation most of the time improves fit error, but not as much.
Modelling attempts to explain the role of theta oscillations in learning processes

usually involve the precise locking of spike times induced by the externally induced oscillations [111–114]. While there is evidence for spike time locking by theta oscillations in hippocampus, it is desireable to find a more general principle for the influence of oscillatory activity on synaptic plasticity. The investigation of the susceptibility of synapses for periodic firing rate modulations in publication I showed that indeed such a principle might exist in the mammalian brain. Even the basic spSTDP model shows a pronounced dependence of synaptic changes on oscillation frequency and relative phase of the connected neurons. The characteristics of the weight change match the properties of the STDP window, namely having potentiation if the postsynaptic phase trails by between $\pi/4$ in the theta range and $\approx \pi/2$ for higher and lower oscillation frequencies, i.e. potentiation for presynaptic activity before postsynaptic activity and depression if the order is reversed. This susceptibility is to some extend retained in the CD model; however, the maximum of LTP is in general shifted towards zero phase difference, which has been observed in experiments.

The relation between MPDP and supervised learning rules

The Perceptron Learning Rule and the δ-rule are both very basic supervised learning rules, conceived for simplicistic neuronal networks of rate-based neurons. The supervisor postulated in these learning rules has full knowledge about the target and current output activity, and can manipulate each synapse in order to transform the latter into the former. This raises three question concerning the biological plausibility of supervised learning:

- Where is the supervisor located, and how does it know what the desired (or target) output is?
- How does the supervisor compute the difference between target and actual output?
- How are the weight changes relayed to the synapse?

From physiological experiments we know that synaptic plasticity is sensitive to the activity of the neurons connected by the synapse. There are hints that plasticity rules are modulated by dopamine or other neuromodulators, which could act as a general reward signal [115]. However, reward signals are spatially unspecific. The brain area responsible for computing reward just observes the outcome of an action and translates it into a reward. For example the amount of food yielded by hunting determines how good the hunter feels afterwards. Also, reward signals are too slow for supervised spike-timing based learning rules. By the time a reward signal arrives at the synapse, the trace of presynaptic activity is likely already gone. Weight changes by supervised learning rules in spiking networks need to be very specific in time. The notion of a supervisor that lies outside of the learning neuron conflicts with this requirement, because it has to send the information to each synapse on a separate channel. The problem of this concept are highlighted in a quote from the article introducing the tempotron by Gütig and Sompolinsky [75]:

> Such learning nexessarily requires supervisory signals, which instruct the neuron about the correct decision. An important question concerning the biological feasibility of tempotron learning is through which pathways supervisory signals arrive at the site of plasticity and how they are translated into the appropriate synaptic changes.

We therefore conclude that a hypothetical supervisor mechanism located in the neuron is beneficial, where it can generate supervisory signals that arrive quickly enough to induce timing specific weight changes.
When we take a closer look at the learning rules for spiking networks, we can roughly separate them into two classes. The tempotron Learning Rule, E-Learning and FP-Learning are examples of the first class. Similarly to the PLR and δ-rule, they are very artificial, since all three are non-local in time. The tempotron Learning Rule observes the output of the neuron and looks for the time of the maximum of the voltage t_{max} after the trial is over. Only then weight changes are assigned proportional to the presynaptic activity at time t_{max}. In E-Learning and FP-Learning, weight changes specific to a given output spike depend on the proximity to desired output spikes. In none of these rules the location or biological implementation of the supervisor is specified, nor do they provide plausible synaptic plasticity mechanisms with which could realize the learning rules. However, they are very useful to examine memory capacities of spiking neuronal networks [39, 75]. The second class of learning rules are the ones by Pfister and colleagues [80], Brea and colleagues [38] and Urbanczik and Senn [78]. In the following I will collectively refer to them as the Pfister rule, since Pfister and colleagues provided the earliest formulation in a supervised learning setting. In contrast to the learning rules in the first class, this rule is defined for stochastic output neurons. The strong non-linearity of spike generation is replaced it with a smooth activation function. Additionally, the Pfister rule is local in time, and it provides a concrete hypothesis for the supervisory mechanism. The desired activity is communicated by the activation of the neuron by a teacher. It induces spikes using strong and short input currents corresponding to a stochastic realization of the target firing rate. The signals for synaptic plasticity are bAPs that travel from the soma into the dendritic tree. The supervisory mechanism itself is defined by the synaptic plasticity rules. The synapses are directly sensitive to the difference of teacher induced target activity $S(t)$ and the input-driven instantaneous firing rate $r(V(t))$, where $V(t)$ is the membrane potential resulting from the "student input", i.e. the input from presynaptic neurons weighted by the synapses to be trained:

$$\frac{dw_i}{dt} \propto [S(t) - r(V(t))]\, \lambda_i(t) \ . \tag{5.1}$$

λ_i is the PSP sum, which is multiplied with the difference of teacher spike train and intrinsic activity. In order to investigate the consequences of this learning rule, let us examine the resulting synaptic plasticity phenomena. In general, the synaptic weight becomes stable and changes cease on average if the intrinsic activity $r(V(t))$ matches the spike trains induced by the teacher. In the case that there is a teacher

spike at time t_d, but the current firing rate is low ($r(V(t_d)) \approx 0$), then

$$\Delta w_i \propto \lambda_i(t_d) \ . \tag{5.2}$$

If we probe this weight change with pairs of a presynaptic spike and a teacher spike at different relative timings, the resulting weight change as a function of the timing is very similar to the LTP part of the STDP window; the LTD part is not reproduced. In the opposite case where there are no teacher spikes but the input-driven firing rate is high the weight change is

$$\Delta w_i \propto -r(V(t))\lambda_i(t) \ . \tag{5.3}$$

This means that synapses which contribute to a period of high activity without teacher spiking will be depressed.

With this synaptic plasticity rule, Pfister and colleagues give an answer to the questions posed above. However, new questions concerning the plausibility are raised. The Pfister rule crucially relies on the fact that teacher spikes and student activity enter differently into equation (5.1). The spikes from the teacher provide a bAP-like signal which upon arrival at the synapse prompt timing-dependent potentiation. In contrast, the activity resulting from the synapses that have to be trained (the student synapses) is given by the instantaneous firing rate, which is a continuous signal. It is not clear how actual output spikes caused by this synaptic input should be treated. Adding them to the teacher spike train $S(t)$ is detrimental, since the resulting reinforcement of these spikes would lead to runaway potentiation. In this context, a minor question is how the synapse could precisely sense the instantaneous firing rate $r(V(t))$. If we exclude adaptation effects, a possible answer to the question is that the firing rate is a monotonous function of the membrane potential. Experiments have shown that synapses can be sensitive to the voltage, which could explain how they sense the firing rate. A last caveat is that the shift from causal (Hebbian) LTP, equation (5.2), to Anti-Hebbian LTD, equation (5.3), has not been observed (yet) in experiments. This likely is due to how they are conducted. In typical plasticity experiments two neurons connected by a synapse are patched and spikes at specific times are induced similarly to how the teacher produces the teacher spikes. The resulting activity is extremely sparse; typically, spike pairs are repeated every 5 seconds. In contrast, in the living brain the activity of many neurons contributes to the output. Because of their sparse activity, pairwise spike time experiments are likely unsuited to investigate the feasibility of supervised learning rules.

Let us now turn to MPDP; for brevity I will refer to the combination of the Membrane Potential Dependent Plasticity rule and spike after-hyperpolarization as MPDP in the following. Its predecessor, the plasticity rule presented in publication II, was originally devised to train a neuron to associate two different inputs, one of which was time-delayed. This necessitates the Anti-Hebbian STDP rule introduced in publication II. To prevent spurious spiking by the student input during training, a threshold below the firing threshold was introduced. If the membrane potential crosses this threshold from below, a spike like signal is generated which

induces synaptic depression. Also, this type of depression provides a stop condition for learning, as shown in the example of the Perceptron Learning Rule. The full MPDP rule is the logical evolution of this earlier rule. When compared to the Pfister rule, one of its conceptual advantages is the fact that teacher spikes and actual output spikes are not artificially seperated into different signals. Instead, teacher spikes differ from spurious spikes in the time course of the membrane potential. Teacher spikes have a very fast rise of the voltage to the firing threshold. In contrast, the voltage rises slower before spurious spikes. Therefore, voltage dependent depression outweighs potentiation induced by the reset, and spurious spikes are extinguished eventually. The model using the conductance based neuron with teacher input provided by strong synapses demonstrates that this principle even works in a biologically more plausible setting, where the teacher input does cause an instantaneous rise of the voltage. Furthermore, MPDP avoids using the instantaneous firing rate by directly implementing a threshold on the membrane potential for synaptic depression. The effect is the same, as demonstrated by equation (5.3). In absence of any spiking (teacher or spurious), synapses that contribute to periods of high depolarization are depressed. Teacher spikes "punch holes" into this threshold by resetting the neuron. This leads to potentiation by spike after-hyperpolarization (SAHP), but also for the duration of the reset kernel the neuron is hold at an relatively unresponsive state. Inputs that are just sufficient to drive the relaxed neuron to fire a spike will not cause a spike during the reset period. An additional benefit of this threshold is a "dead zone" of no synaptic change when the voltage stays between both thresholds for plasticity. This is different to the Pfister rule, where the neuron is usually modelled as a LIF neuron (SRM_0 model) with exponential escape noise. Technically, the firing rate is never zero and therefore every teaching trial will induce weight changes. A side effect of using thresholds for synaptic plasticity is that MPDP is suitable for deterministic neurons as well as for stochastic neuron models. The Pfister rule will have problems if the output neuron is deterministic. This is highlighted by the performance of ReSuMe, which is derived from the δ-rule that uses a comparison of target and actual output activity similar to the Pfister rule. ReSuMe has a low memory capacity that increases if the output neuron is stochastic.

Similar to the Pfister rule, there is no direct experimental evidence for MPDP in a single synapse type. However, there are reports of synaptic potentiation when the postsynaptic neuron is hyperpolarized [92], albeit in excitatory synapses onto inhibitory interneurons. Also, a synaptic depression only rule has been reported for presynaptic spikes that are paired with postsynaptic subthreshold depolarization [52]. However, MPDP avoids two of the problems of the Pfister rule. It does not need an artificial separation of teacher and student induced activity and it uses the voltage directly for synaptic plasticity instead of the instantaneous firing rate. Additionally, it can be used for stochastic neurons as well as for deterministic neurons.

5.3 Future work

MPDP as developed in chapter 4 is a heuristic learning algorithm. It was devised as learning rule for associative learning of two time-delayed inputs. Some of its features, especially the usage of the relative refractoriness of the output neuron after a teacher spike and the Anti-Hebbian voltage dependent depression are quite unique. As shown in the previous section, there are some convergent properties of MPDP and the Pfister rule. An interesting question for future investigations is to work out a formal connection between the two. As shown in the previous section, there are some similarities: The voltage-dependent synaptic depression is very similar to depression given by equation (5.3), and the teacher mechanism is the same in both learning rules. If such a connection can be derived, MPDP is an alternative and more biological feasible implementation for supervised learning. Additionally, it proposes a concrete mechanism how synaptic plasticity rules can distinguish between teacher spikes and self-generated activity by using the temporal profile of the membrane potential around each spike.

Another question concerns the stability of weights under the MPDP rule. The example of a single output spike to be learned shows that after a sufficient number of learning rules, the temporal profile of the voltage in teaching trials and recall trials is very similar (see figure 4.3). It is likely that withdrawing the teacher input does not lead to unlearning of this spike, but that weight changes will be the same regardless of the presence of the teacher. However, there is a caveat. Weight changes in the example of a single spike do not cease. Instead, synapses of input neurons active just before the desired spike times continue to depress. This eventually leads to a hyperpolarized state just before the output spike, which in turn induces synaptic potentiation that is expressed *before* the hyperpolarization. After many learning trials, this causes a wavelike appearence of the temporal profile of the voltage. It is likely that the magnitude of this effect depends on the load of the system. Figure 4.4 shows that for low loads the temporal distance of output spike and teacher has not converged at the end of training. In contrast, for high loads the changes have ceased. The effect of high loads is a relatively high level of noise on the synaptic weights that interferes with learning.

If a single spike becomes stable, i.e. removing the teacher does not affect the weight changes, it is worth investigating if the same is true if several spikes are learned at the same time. If yes, this suggests that memories are maintained by recall, i.e. presenting one particular input pattern causes weight changes similar to training trials. It is clear that such a mechanism is highly beneficial for memory maintenance.

A last question is wether MPDP or a derivative learning rule can be used for the training of recurrent networks. This is a notoriously difficult problem [39]. Memmesheimer and colleagues tried to train recurrent networks to fire cyclic sequences of spikes using their exact HTP method. Interestingly, despite using a network simulation method with adjustable precision, the activity was not stable. Numerical errors accumulated quickly up to the point where neurons missed their spikes and the sequence died out [39]. In contrast, training with the FP-Learning

rule lead to stable activity. The difference is that with this rule the network during training is subject to the noise induced by weight changes, which causes the learning algorithm to over-learn slightly as a safe-guard against noise. This safe-guard is a crucial part of MPDP, therefore it is likely that MPDP or a derivative learning rule can be used in training of recurrent networks.

Appendices

Appendix A

List of published articles

Publications in journals with peer review

- Joscha T. Schmiedt, Christian Albers, Klaus Pawelzik. Spike timing-dependent plasticity as dynamic filter. Advances in Neural Information Processing Systems 23 (2010)
- Christian Albers, Joscha T. Schmiedt, Klaus Pawelzik. Theta-specific susceptibility in a model of adaptive synaptic plasticity. Frontiers in computational neuroscience (7) (2013)
- Christian Albers, Maren Westkott, Klaus Pawelzik. Perfect Associative Learning with Spike-Timing-Dependent Plasticity. Advances in Neural Information Processing Systems 26 (2013)

Publications on pre-print servers without peer review

- Christian Albers, Maren Westkott, Klaus Pawelzik. Learning of Precise Spike Times with Homeostatic Membrane Potential Dependent Synaptic Plasticity. arXiv:1407.6525v2 [q-bio.NC] (2015)

Appendix B

Overview over contributions to the publications

Publication I

The contribution dynamics model is derived from the model developed in the NIPS article from 2010. Christian Albers added the q-dynamics. The fitting procedure for the CD model was planned by Joscha Schmiedt and Christian Albers. Christian Albers implemented the fitting procedure for the CD model and the Triplet model. Christian Albers performed the comparison to the Uramoto model and the cross-model survey of the response properties of synaptic plasticity to oscillatory activity. Joscha Schmiedt helped interpreting the results. The manuscript was written by all three authors with main contributions by Christian Albers.

Publication II

The development of the plasticity rule was sparked by previous work by Maren Westkott and Klaus Pawelzik. Klaus Pawelzik worked out the original proof of equivalence to the perceptron learning rule. Maren Westkott and Christian Albers found an error, and all three authors worked out the corrected proof. Christian Albers performed the numerical simulations for the Tempotron and the Chronotron. The manuscript was written equally by all three authors.

Overview over contributions to manuscript in chapter 4

The idea of subthreshold membrane potential dependent plasticity was worked out by all three authors. Maren Westkott performed the simulations of the biological setting (conductance based LIF neuron). Christian Albers performed the simulations of the simplified model with the LIF neuron for memory capacity and noise robustness. Maren Westkott helped analysing the data. The manuscript was written by all three authors with main contributions by Christian Albers.

Bibliography

[1] Bear MF, Connors BW, Paradiso MA (2007) Neuroscience: Exploring the Brain. Philadelphi, PA: Lippincott Williams & Wilkins, 857 pp.

[2] Hodgkin AL, Huxley AF (1952) A quantitative description of membrane current and its application to conduction and excitation in nerve. The Journal of Physiology 117: 500–544.

[3] Jolivet R, Schürmann F, Berger TK, Naud R, Gerstner W, et al. (2008) The quantitative single-neuron modeling competition. Biological Cybernetics 99: 417–426.

[4] Kunkel S, Schmidt M, Eppler JM, Plesser HE, Masumoto G, et al. (2014) Spiking network simulation code for petascale computers. Frontiers in Neuroinformatics 8.

[5] Herculano-Houzel S, Lent R (2005) Isotropic fractionator: a simple, rapid method for the quantification of total cell and neuron numbers in the brain. The Journal of Neuroscience 25: 2518–2521.

[6] White J, Southgate E, Thomson J, Brenner S (1986) The structure of the nervous system of the nematode caenorhabditis elegans: the mind of a worm. Phil Trans R Soc Lond 314: 1–340.

[7] Varshney LR, Chen BL, Paniagua E, Hall DH, Chklovskii DB (2011) Structural properties of the caenorhabditis elegans neuronal network. PLoS Computational Biology 7: e1001066.

[8] Palyanov A, Khayrulin S, Larson SD, Dibert A (2012) Towards a virtual C. elegans: A framework for simulation and visualization of the neuromuscular system in a 3D physical environment. In Silico Biology 11: 137–147.

[9] Ardiel EL, Rankin CH (2010) An elegant mind: learning and memory in Caenorhabditis elegans. Learning & Memory 17: 191–201.

[10] Roe AW, Pallas SL, Kwon YH, Sur M (1992) Visual projections routed to the auditory pathway in ferrets: receptive fields of visual neurons in primary auditory cortex. The Journal of Neuroscience 12: 3651–3664.

[11] Hebb DO (1949) The organization of behavior: A neuropsychological approach. John Wiley & Sons.

[12] Markram H, Gerstner W, Sjöström PJ (2011) A history of spike-timing-dependent plasticity. Frontiers in Synaptic Neuroscience 3.

[13] Bliss TV, Lømo T (1973) Long-lasting potentiation of synaptic transmission in the dentate area of the anaesthetized rabbit following stimulation of the perforant path. The Journal of Physiology 232: 331–356.

[14] Bienenstock EL, Cooper LN, Munro PW (1982) Theory for the development of neuron selectivity: orientation specificity and binocular interaction in visual cortex. The Journal of Neuroscience 2: 32–48.

[15] Dudek SM, Bear MF (1992) Homosynaptic long-term depression in area CA1 of hippocampus and effects of N-methyl-D-aspartate receptor blockade. Proceedings of the National Academy of Sciences 89: 4363–4367.

[16] Markram H, Lübke J, Frotscher M, Sakmann B (1997) Regulation of synaptic efficacy by coincidence of postsynaptic APs and EPSPs. Science 275: 213–215.

[17] Gerstner W, Ritz R, Van Hemmen JL (1993) Why spikes? Hebbian learning and retrieval of time-resolved excitation patterns. Biological Cybernetics 69: 503–515.

[18] Gerstner W, Kempter R, van Hemmen JL, Wagner H (1996) A neuronal learning rule for sub-millisecond temporal coding. Nature 383: 76–78.

[19] Bi Gq, Poo Mm (1998) Synaptic modifications in cultured hippocampal neurons: dependence on spike timing, synaptic strength, and postsynaptic cell type. The Journal of Neuroscience 18: 10464–10472.

[20] Haas JS, Nowotny T, Abarbanel HD (2006) Spike-timing-dependent plasticity of inhibitory synapses in the entorhinal cortex. Journal of Neurophysiology 96: 3305–3313.

[21] Zhang LI, Tao HW, Holt CE, Harris WA, Poo Mm (1998) A critical window for cooperation and competition among developing retinotectal synapses. Nature 395: 37–44.

[22] Cassenaer S, Laurent G (2007) Hebbian STDP in mushroom bodies facilitates the synchronous flow of olfactory information in locusts. Nature 448: 709–713.

[23] Verhoog MB, Goriounova NA, Obermayer J, Stroeder J, Hjorth JJ, et al. (2013) Mechanisms underlying the rules for associative plasticity at adult human neocortical synapses. The Journal of Neuroscience 33: 17197–17208.

[24] Song S, Miller KD, Abbott LF (2000) Competitive hebbian learning through spike-timing-dependent synaptic plasticity. Nature Neuroscience 3: 919–926.

[25] Froemke RC, Dan Y (2002) Spike-timing-dependent synaptic modification induced by natural spike trains. Nature 416: 433–438.

[26] Wang HX, Gerkin RC, Nauen DW, Bi GQ (2005) Coactivation and timing-dependent integration of synaptic potentiation and depression. Nature Neuroscience 8: 187–193.

[27] Pfister JP, Gerstner W (2006) Triplets of spikes in a model of spike timing-dependent plasticity. The Journal of Neuroscience 26: 9673–9682.

[28] Shouval HZ, Bear MF, Cooper LN (2002) A unified model of NMDA receptor-dependent bidirectional synaptic plasticity. Proceedings of the National Academy of Sciences 99: 10831–10836.

[29] Graupner M, Brunel N (2012) Calcium-based plasticity model explains sensitivity of synaptic changes to spike pattern, rate, and dendritic location. Proceedings of the National Academy of Sciences 109: 3991–3996.

[30] Nunez PL, Srinivasan R (2007) Electroencephalogram. Scholarpedia 2.

[31] Destexhe A, Bedard C (2013) Local field potential. Scholarpedia 8.

[32] Berry SD, Thompson RF (1978) Prediction of learning rate from the hippocampal electroencephalogram. Science 200: 1298–1300.

[33] Nokia MS, Penttonen M, Korhonen T, Wikgren J (2008) Hippocampal theta (3–8hz) activity during classical eyeblink conditioning in rabbits. Neurobiology of Learning and Memory 90: 62–70.

[34] Sederberg PB, Kahana MJ, Howard MW, Donner EJ, Madsen JR (2003) Theta and gamma oscillations during encoding predict subsequent recall. The Journal of Neuroscience 23: 10809–10814.

[35] Uramoto T, Torikai H (2013) A calcium-based simple model of multiple spike interactions in spike-timing-dependent plasticity. Neural Computation 25: 1853–1869.

[36] Zucker RS, Regehr WG (2002) Short-term synaptic plasticity. Annual Review of Physiology 64: 355–405.

[37] Turrigiano GG (2008) The self-tuning neuron: synaptic scaling of excitatory synapses. Cell 135: 422–435.

[38] Brea J, Senn W, Pfister JP (2013) Matching recall and storage in sequence learning with spiking neural networks. The Journal of Neuroscience 33: 9565–9575.

[39] Memmesheimer RM, Rubin R, Ölveczky BP, Sompolinsky H (2014) Learning precisely timed spikes. Neuron 82: 925–938.

[40] Dayan P, Abbott LF (2001) Theoretical Neuroscience. The MIT Press, 460 pp.

[41] Gerstner W, Kistler WM (2002) Spiking Neuron Models: Single Neurons, Populations, Plasticity. Cambridge university press, 494 pp.

[42] Hertz J, Krogh A, Palmer RG (1991) Introduction to the Theory of Neural Computation, volume 1. Santa Fe Institute Series (Addison-Wesley Longman, Boston), 327 pp.

[43] Mainen ZF, Sejnowski TJ (1995) Reliability of spike timing in neocortical neurons. Science 268: 1503–1506.

[44] Softky WR, Koch C (1993) The highly irregular firing of cortical cells is inconsistent with temporal integration of random EPSPs. The Journal of Neuroscience 13: 334–350.

[45] Maimon G, Assad JA (2009) Beyond poisson: increased spike-time regularity across primate parietal cortex. Neuron 62: 426–440.

[46] van Vreeswijk C, Sompolinsky H (1996) Chaos in neuronal networks with balanced excitatory and inhibitory activity. Science 274: 1724–1726.

[47] Sjöström PJ, Turrigiano GG, Nelson SB (2001) Rate, timing, and cooperativity jointly determine cortical synaptic plasticity. Neuron 32: 1149–1164.

[48] Nevian T, Sakmann B (2006) Spine Ca^{2+} signaling in spike-timing-dependent plasticity. The Journal of Neuroscience 26: 11001–11013.

[49] Caporale N, Dan Y (2008) Spike timing-dependent plasticity: A hebbian learning rule. Annu Rev Neurosci 31: 25–46.

[50] Lisman JE (2001) Three Ca^{2+} levels affect plasticity differently: the LTP zone, the LTD zone and no man's land. The Journal of Physiology 532: 285–285.

[51] Graupner M, Brunel N (2007) STDP in a bistable synapse model based on CaMKII and associated signaling pathways. PLoS computational biology 3: e221.

[52] Sjöström PJ, Turrigiano GG, Nelson SB (2004) Endocannabinoid-Dependent Neocortical Layer-5 LTD in the Absence of Postsynaptic Spiking. Journal of Neurophysiology 92: 3338–3343.

[53] Sjöström PJ, Turrigiano GG, Nelson SB (2007) Multiple forms of long-term plasticity at unitary neocortical layer 5 synapses. Neuropharmacology 52: 176–184.

[54] Burrone J, O'Byrne M, Murthy VN (2002) Multiple forms of synaptic plasticity triggered by selective suppression of activity in individual neurons. Nature 420: 414–418.

[55] Tsodyks MV, Markram H (1997) The neural code between neocortical pyramidal neurons depends on neurotransmitter release probability. Proceedings of the National Academy of Sciences 94: 719–723.

[56] Tsodyks M, Pawelzik K, Markram H (1998) Neural networks with dynamic synapses. Neural Computation 10: 821–835.

[57] Morrison A, Diesmann M, Gerstner W (2008) Phenomenological models of synaptic plasticity based on spike timing. Biological Cybernetics 98: 459–478.

[58] Jacob V, Brasier DJ, Erchova I, Feldman D, Shulz DE (2007) Spike timing-dependent synaptic depression in the *in vivo* barrel cortex of the rat. The Journal of Neuroscience 27: 1271–1284.

[59] Pawlak V, Greenberg DS, Sprekeler H, Gerstner W, Kerr JND (2013) Changing the responses of cortical neurons from sub- to suprathreshold using single spikes *in vivo*. Elife 2: 385–395.

[60] Hopfield JJ (1982) Neural networks and physical systems with emergent collective computational abilities. Proceedings of the National Academy of Sciences 79: 2554–2558.

[61] Hopfield JJ (2007) Hopfield network. Scholarpedia 2.

[62] Blais BS, Cooper L (2008) BCM theory. Scholarpedia 3.

[63] Cai Y, Gavornik JP, Cooper LN, Yeung LC, Shouval HZ (2007) Effect of stochastic synaptic and dendritic dynamics on synaptic plasticity in visual cortex and hippocampus. Journal of neurophysiology 97: 375–386.

[64] Wittenberg GM, Wang SSH (2006) Malleability of spike-timing-dependent plasticity at the CA3–CA1 synapse. The Journal of Neuroscience 26: 6610–6617.

[65] Schmajuk NA (2008) Classical conditioning. Scholarpedia 3.

[66] Asaka Y, Mauldin KN, Griffin AL, Seager MA, Shurell E, et al. (2005) Non-pharmacological amelioration of age-related learning deficits: The impact of hippocampal θ-triggered training. Proceedings of the National Academy of Sciences 102: 13284–13288.

[67] Guderian S, Schott BH, Richardson-Klavehn A, Düzel E (2009) Medial temporal theta state before an event predicts episodic encoding success in humans. Proceedings of the National Academy of Sciences 106: 5365–5370.

[68] Reiner M, Rozengurt R, Barnea A (2014) Better than sleep: Theta neurofeedback training accelerates memory consolidation. Biological Psychology 95: 45–53.

[69] Larson J, Wong D, Lynch G (1986) Patterned stimulation at the theta frequency is optimal for the induction of hippocampal long-term potentiation. Brain Research 368: 347–350.

[70] Greenstein YJ, Pavlides C, Winson J (1988) Long-term potentiation in the dentate gyrus is preferentially induced at theta rhythm periodicity. Brain Research 438: 331–334.

[71] Pavlides C, Greenstein YJ, Grudman M, Winson J (1988) Long-term potentiation in the dentate gyrus is induced preferentially on the positive phase of θ-rhythm. Brain Research 439: 383–387.

[72] Hyman JM, Wyble BP, Goyal V, Rossi CA, Hasselmo ME (2003) Stimulation in hippocampal region CA1 in behaving rats yields long-term potentiation when delivered to the peak of theta and long-term depression when delivered to the trough. The Journal of Neuroscience 23: 11725–11731.

[73] Fell J, Axmacher N (2011) The role of phase synchronization in memory processes. Nature Reviews Neuroscience 12: 105–118.

[74] Rosenblatt F (1958) The perceptron: a probabilistic model for information storage and organization in the brain. Psychological Review 65: 386.

[75] Gütig R, Sompolinsky H (2006) The tempotron: a neuron that learns spike timing–based decisions. Nature Neuroscience 9: 420–428.

[76] Rubin R, Monasson R, Sompolinsky H (2010) Theory of spike timing-based neural classifiers. Physical Review Letters 105: 218102.

[77] Seager MA, Johnson LD, Chabot ES, Asaka Y, Berry SD (2002) Oscillatory brain states and learning: Impact of hippocampal theta-contingent training. Proceedings of the National Academy of Sciences 99: 1616–1620.

[78] Urbanczik R, Senn W (2014) Learning by the dendritic prediction of somatic spiking. Neuron 81: 521–528.

[79] Xie X, Seung HS (2004) Learning in neural networks by reinforcement of irregular spiking. Physical Review E 69: 041909.

[80] Pfister J, Toyoizumi T, Barber D, Gerstner W (2006) Optimal spike-timing-dependent plasticity for precise action potential firing in supervised learning. Neural Computation 18: 1318–1348.

[81] Florian RV (2012) The chronotron: A neuron that learns to fire temporally precise spike patterns. PLoS One 7.

[82] Ponulak F, Kasinski A (2010) Supervised learning in spiking neural networks with ReSuMe: sequence learning, classification, and spike shifting. Neural Computation 22: 467–510.

[83] Victor J, Purpura KP (1996) Nature and precision of temporal coding in visual cortex: A metric-space analysis. Journal of Neurophysiology 76: 1310–1326.

[84] Hahnloser RHR, Kozhevnikov AA, Fee MS (2002) An ultra-sparse code underlies the generation of neural sequences in a songbird. Nature 419: 65–70.

[85] Gollisch T, Meister M (2008) Rapid neural coding in the retina with relative spike latencies. Science 319: 1108–1111.

[86] Masquelier T (2013) Neural variablility, or lack thereof. Frontiers in computational neuroscience 7.

[87] Van Rullen R, Thorpe SJ (2001) Rate coding versus temporal order coding: What the retional ganglion cells tell the visual cortex. Neural Computation 13: 1255–1283.

[88] Xu S, Jiang W, Poo Mm, Dan Y (2012) Activity recall in a visual cortical ensemble. Nature Neuroscience 15: 449–455.

[89] Legenstein R, Naeger C, Maass W (2005) What can a neuron learn with spike-timing-dependent plasticity? Neural Computation 17: 2337–2382.

[90] Bohte SM, Kok JN, La Poutre H (2002) Error-backpropagation in temporally encoded networks of spiking neurons. Neurocomputing 48: 17–37.

[91] Feldman DE (2000) Timing-based LTP and LTD at vertical inputs to layer II/III pyramidal cells in rat barrel cortex. Neuron 27: 45–56.

[92] Lamsa KP, Heeroma JH, Somogyi P, Rusakov DA, Kullmann DM (2007) Anti-Hebbian long-term potentiation in the hippocampal feedback inhibitory circuit. Science 315: 1262–1266.

[93] Fino E, Deniau JM, Venance L (2009) Brief subthreshold events can act as Hebbian signals for long-term plasticity. PLoS One 4.

[94] Artola A, Bröcher S, Singer W (1990) Different voltage-dependent thresholds for inducing long-term depression and long-term potentiation in slices of rat visual cortex. Nature 347: 69–72.

[95] Holthoff K, Zecevic D, Konnerth A (2010) Rapid time course of action potentials in spines and remote dendrites of mouse visual cortex neurons. The Journal of Physiology 588: 1085–1096.

[96] Palmer LM, Stuart GJ (2009) Membrane potential changes in dendritic spines during action potentials and synaptic input. The Journal of Neuroscience 29: 6897–6903.

[97] Popovic MA, Gao X, Carnevale NT, Zecevic D (2014) Cortical dendritic spine heads are not electrically isolated by the spine neck from membrane potential signals in parent dendrites. Cerebral Cortex 24: 385–395.

[98] Clopath C, Büsing L, Vasilaki E, Gerstner W (2010) Connectivity reflects coding: a model of voltage-based STDP with homeostasis. Nature Neuroscience 13: 344–352.

[99] Xue M, Atallah BV, Scanziani M (2014) Equalizing excitation–inhibition ratios across visual cortical neurons. Nature 511: 596–600.

[100] Attwell D, Laughlin SB (2001) An energy budget for signaling in the grey matter of the brain. Journal of Cerebral Blood Flow & Metabolism 21: 1133–1145.

[101] Xu Y, Zeng X, Zhong S (2013) A new supervised learning algorithm for spiking neurons. Neural Computation 25: 1472–1511.

[102] D'Souza P, Liu SC, Hahnloser RHR (2010) Perceptron learning rule derived from spike-frequency adaptation and spike-time-dependent plasticity. Proceedings of the National Academy of Sciences 107: 4722–4727.

[103] Wehr M, Zador AM (2003) Balanced inhibition underlies tuning and sharpens spike timing in auditory cortex. Nature 426: 442–446.

[104] Haider B, Duque A, Hasenstaub AR, McCormick DA (2006) Neocortical network activity *in vivo* is generated through a dynamic balance of excitation and inhibition. The Journal of Neuroscience 26: 4535–4545.

[105] Okun M, Lampl I (2008) Instantaneous correlation of excitation and inhibition during ongoing and sensory-evoked activities. Nature Neuroscience 11: 535–537.

[106] D'Haene M, Schrauwen B, Van Campenhout J, Stroobandt D (2009) Accelerating event-driven simulation of spiking neurons with multiple synaptic time constants. Neural Computation 21: 1068–1099.

[107] Froemke RC, Tsay IA, Raad M, Long JD, Dan Y (2006) Contribution of individual spikes in burst-induced long-term synaptic modification. Journal of Neurophysiology 95: 1620–1629.

[108] Froemke RC, Poo Mm, Dan Y (2005) Spike-timing-dependent synaptic plasticity depends on dendritic location. Nature 434: 221–225.

[109] Sjöström PJ, Häusser M (2006) A cooperative switch determines the sign of synaptic plasticity in distal dendrites of neocortical pyramidal neurons. Neuron 51: 227–238.

[110] Nishiyama M, Hong K, Mikoshiba K, Poo MM, Kato K (2000) Calcium stores regulate the polarity and input specificity of synaptic modification. Nature 408: 584–588.

[111] Moser EI, Kropff E, Moser MB (2008) Place cells, grid cells, and the brain's spatial representation system. Annu Rev Neurosci 31: 69–89.

[112] O'Keefe J, Recce ML (1993) Phase relationship between hippocampal place units and the EEG theta rhythm. Hippocampus 3: 317–330.

[113] Lengyel M, Szatmary Z, Érdi P (2003) Dynamically detuned oscillations account for the coupled rate and temporal code of place cell firing. Hippocampus 13: 700–714.

[114] Lengyel M, Kwag J, Paulsen O, Dayan P (2005) Matching storage and recall: hippocampal spike timing–dependent plasticity and phase response curves. Nature Neuroscience 8: 1677–1683.

[115] Pawlak V, Wickens JR, Kirkwood A, Kerr JN (2010) Timing is not everything: neuromodulation opens the STDP gate. Frontiers in Synaptic Neuroscience 2.

Danksagung

Ich möchte mich bei einer Reihe von Menschen bedanken, die mich auf dem Weg zu dieser Arbeit unterstützt und begleitet haben. Zuallererst bedanke ich mich bei Klaus Pawelzik. Er hat mir die Möglichkeit zu dieser Arbeit im Anschluss an meine Diplomarbeit gegeben. Ich werde auch nie die hübsche Studienarbeit vergessen - Sudokus lösen mit Hopfield-Netzen; eine Zeit lang war ich süchtig nach Sudokus. Er hat mir Freiheiten gelassen, meine Themen zu wählen, auf welche wir uns dann zusammen gestürzt haben. Er kann sehr fordernd sein und will immer die neuesten Ergebnisse und Plots sehen, was mir aber sehr geholfen hat. Ich denke zum Beispiel gerne an die Arbeit zum zweiten NIPS-Paper zurück, wo wir zu dritt (Klaus Pawelzik, Maren Westkott und ich) einen Monat fast manisch dran gesessen haben. Außerdem bin ich sehr dankbar für die Fahrten zu Tagungen, die er mir durch seine Arbeit ermöglicht hat. Ich bedanke mich bei Joscha Schmiedt, der mir in der ersten Zeit sehr geholfen hat. Ich werde nie vergessen, wie 2010 er und Klaus Pawelzik in meinem Krankenhauszimmer aufgetaucht sind und triumphierend das angenommene NIPS-Paper hochgehalten haben! Es war eine schöne Reise nach Vancouver zur NIPS. Ich danke Maren Westkott für die gemeinsame Arbeit mit vielen tollen Diskussionen. Außerdem kann sie Leute aufbauen, wenn es mal nicht so rund läuft. Ich bedanke mich bei David Rotermund für die technische Hilfe. Er hält hier die ganze Infrastruktur am Laufen. Er weiß alles und ist immer ansprechbar. Ein großer Dank geht auch an Udo Ernst. Er organisiert tolle Bernstein-Seminare auf Rügen und Darsz und Tagungen. Vor allem die CNS in Berlin war eine sehr interessante Erfahrung für mich! Außerdem hat er mir sehr geholfen bei der Benutzung des Clusters. Sein Shell-Skript von 2009 verwende ich im Wesentlichen noch heute. Vielen Dank auch an Agnes Janßen! Sie hilft bei allen bürokratischen Angelegenheit und hält uns damit den Rücken frei. Außerdem organisiert sie unsere (Weihnachts-)Feiern, Ausflüge, Kohltouren; sie ist das Herz unserer AG. Ich bedanke mich auch bei meinen Lieblings-Büromitbewohner Ingo Bathmann. Ich habe gerne mit dir gearbeitet! Ich bedanke mich auch bei Philipp Heyken, das Rennen war knapp! Ich saßimmer mit netten Leuten im Büro. Zu guter letzt möchte ich mich bei meinen Eltern Gertrud und Hans und dem Rest meiner Familie bedanken. Ohne ihre Unterstützung hätte ich diese Arbeit nicht abschliessen können.